Field Guide to Exhumed Major Faults in Southern California

Authors

Joseph R. Jacobs
Samuel B Howard
David Forand
Ory Dor
James P. Evans

Editors

Samuel B Howard
Joseph R. Jacobs

Updated September 10, 2005

SCEC

Table of Contents

Foreword

This field guide provides an overview of exposures and provides a field trip guide to localities of exhumed faults in southern California. We focus on exposures of faults that are documented or inferred to be exhumed from seismogenic depths. The goal of this guidebook is to provide geoscientists who are interested in fault zone mechanics and earthquake processes a summary of the results of the work on these sites.

Fault growth, evolution, and fault mechaics are of much interest to the seismological community because it is related to topics of earthquake mechanics, such as the width of the fault surface that slips during an earthquake (Kanamori and Heaton, 2000), fault zone structure (Rubin et al., 1999), and rupture propagation processes (Heaton, 1990; Andrews and Ben-Zion, 1997; Harris and Day, 1999). Characterization of fault zone structure and composition provides insight into these processes of fault nucleation, propagation, and termination.

The study of exhumed faults has been previously shown by such workers as Chester and Logan (1986, 1987), Chester et al. (1993), Schulz and Evans (2000), Pachell and Evans (2002), and Wilson et al. (2003) as a means to investigate active and inactive faults at the earth's surface that are representative of faults at depth. The direct study of faults at depth poses both logistical and economic challenges, although it certainly may be accomplished (i.e., the San Andreas Fault Observatory at Depth – SAFOD). Thus, studies of exhumed faults provide insight into aspects of fault composition and structure, and we can somtimes establish the history of the fault zone over time.

This field guide presents the initial effort to catalog fault exposures in southern California that are significant in understanding earthquake source and propagation processes. This work was conducted in a fault and rock mechanics (FARM) type of approach in order examine the rocks in a seismological context. The exhumed fault data sets provide interpretations on fault zone structure from depths of ~ 1 km to > 6 km predominantly in the San Gabriel and San Bernardino mountains (Figure 1). This field guide summarizes the following (when available) at each site:

- Location of site (UTM coordinates in meters in WGS 84 projection), including clear directions
- Basic geological and seismological context of site; rock type, exhumation amount, and fault/seismic history
- Current understanding of fault geometry and segmentation
- Summary of observations from the site, including:
  - –Physical characteristics of the fault zone (e.g., density of fractures, presence of subsidiary faults, and thicknesses of the fault core and damage zone)
  - –Chemical characterization, such as mineralogy, whole-rock geochemistry, and isotopic analyses
  - –Particle size distribution
- Seismological implications

This guidebook is the result of the efforts of Joe Jacobs, David Forand, and Sam Howard. Joe worked on this during part of his M.S. degree work at Utah State University, and Dave and Sam were SCEC summer interns. Most of the descriptions of how to get to sites, summaries of the work, and formatting of the guidebook are the results of their efforts.

This is a beta version of the guidebook. Suggestions and comments are welcome. We have established a format for this field guide, and we welcome contributions from other workers. We will edit for format, but will not change the content of any contribution, and we will acknowledge all other scientific works. We will work with SCEC to make this available online in the near future.

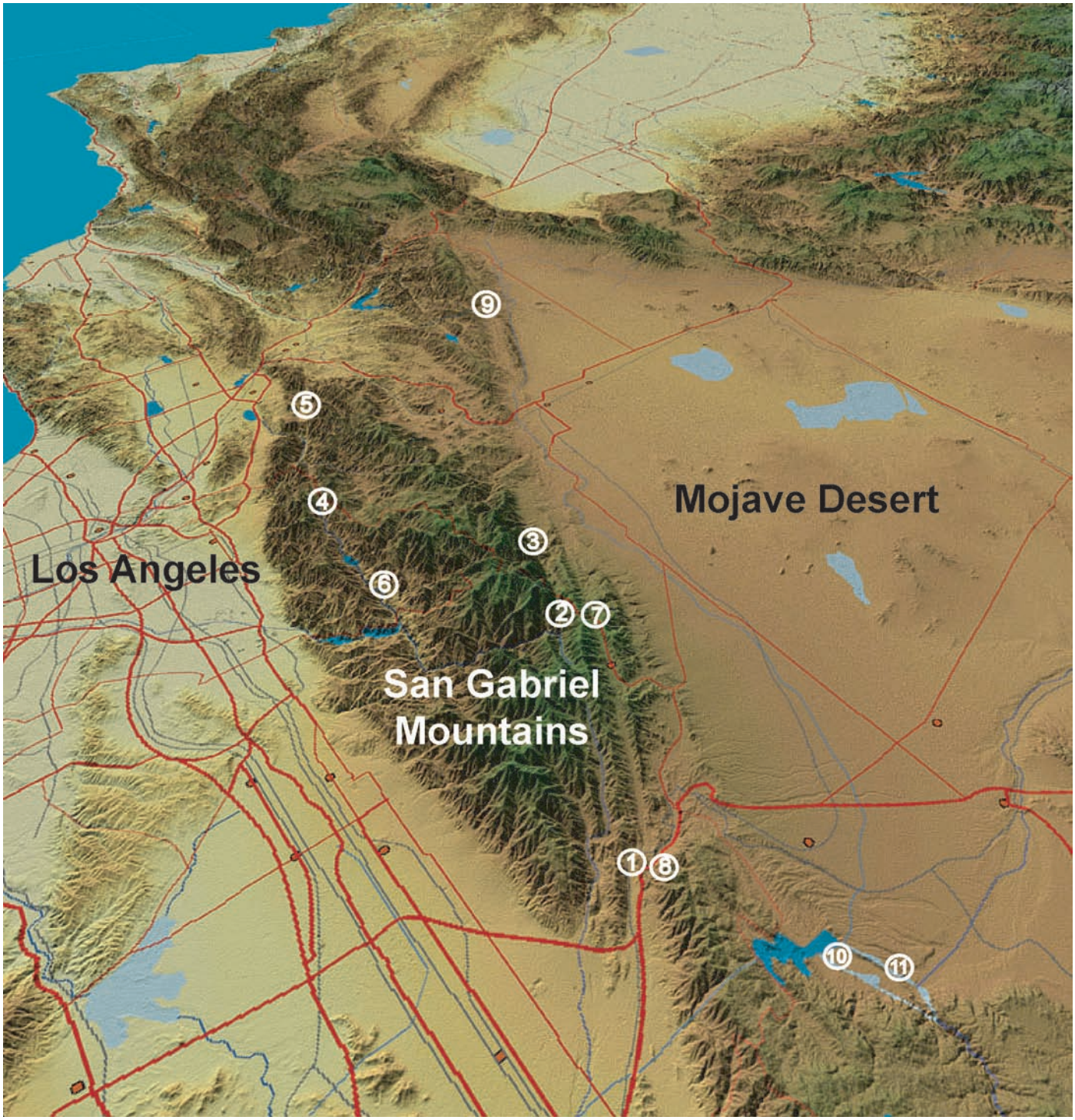

Figure 1. Oblique shaded relief map of southern California with the view to the northwest. Numbered circles show locations of sites. Punchbowl fault: 1-Blue Cut; 2-Lone Pine Canyon; 3-Devil's Punchbowl. San Gabriel fault: 4-Big Tujunga; 5-Little Tujunga; 6-Bear Creek. San Andreas fault: 7-Apple Valley and Wrightwood; 8-Cajon Pass; 9-Lake Hughes. Silverwood Lake area: 10-Eastwood fault; 11-Grass Valley fault. The site from the San Jacinto fault is off this malp. Original image from Bowen, 2003.

References

Andrews, D. J. and Y. Ben-Zion, Wrinkle-like pulse on a fault between different materials. *Journal of Geophysical Research*, 102, 553– 5571, 1997.

Bowen, W., Electronic Map Library. Department of Geography, California State University, Northridge, 2003. <http://130.166.124.2/library.html>

Chester F.M. and J.M. Logan, Implications for mechanical properties of brittle faults from observations of the Punchbowl fault zone, California, USA. *Pure and Applied Geophysics*, 124, 79-106, 1986.

Chester F.M. and J.M. Logan, Composite planar fabric of gouge from the Punchbowl fault, California. *Journal of Structural Geology*, 9, 621-634, 1987.

Chester, F.M., J.P. Evans, and R.L. Biegel, Internal structure and weakening mechanisms of the San Andreas fault. *Journal of Geophysical Research*, 98, B1, 771-786, 1993.
Kanamori, H. and T.H. Heaton, Microscopic and macroscopic physics of earthquakes. *American Geophysical Union Monographs*, 120, 147-161, 2000.

Harris, R.A., and S.M. Day, Dynamic 3D simulations of earthquakes on en echelon faults, *Geophysical Research Letters*, 26, 2089-2092, 1999.

Heaton, T.H., Evidence for and implication of self-healing pulses of slip in earthquake rupture. *Physics of The Earth and Planetary Interiors*, 64, 1-20, 1990.

Pachell, M. A., and Evans, J. P., Structural analysis of the Gemini strike-slip fault zone, Central Sierra Nevada, California. *Journal of Structural Geology*, 24, 1903-1924, 2002.

Rubin, C.M., S. Thompson, K. Abdrakhmatov, R.J. Weldon, Thrust fault paleoseismology in an intercontinental tectonic setting, Kyrgyz Tien Shan, central Asia. *Geological Society of America 1999 Annual Meeting*, 31, 376, 1999.

Schulz S.E., and J.P. Evans., Mesoscopic structure of the Punchbowl fault, southern California, and the geologic and geophysical structure of active strike slip faults. *Journal of Structural Geology*, 22, 913-930, 2000.

Wilson, J.E., J.S. Chester, and F.M. Chester, Microfracture analysis of fault growth and wear processes, Punchbowl Fault, San Andreas system, California. *Journal of Structural Geology*, 25, 1855-1873, 2003.

Chapter 1: Punchbowl Fault

Introduction

The Punchbowl fault is an inactive, exhumed fault of the San Andreas transform system that is located at the juncture of the San Gabriel Mountains and Mojave Desert, approximately 5 km southwest of the active strand of the San Andreas fault (Chester and Logan, 1987; Wilson et al., 2003) (Figure 1). The Punchbowl and San Andreas faults have

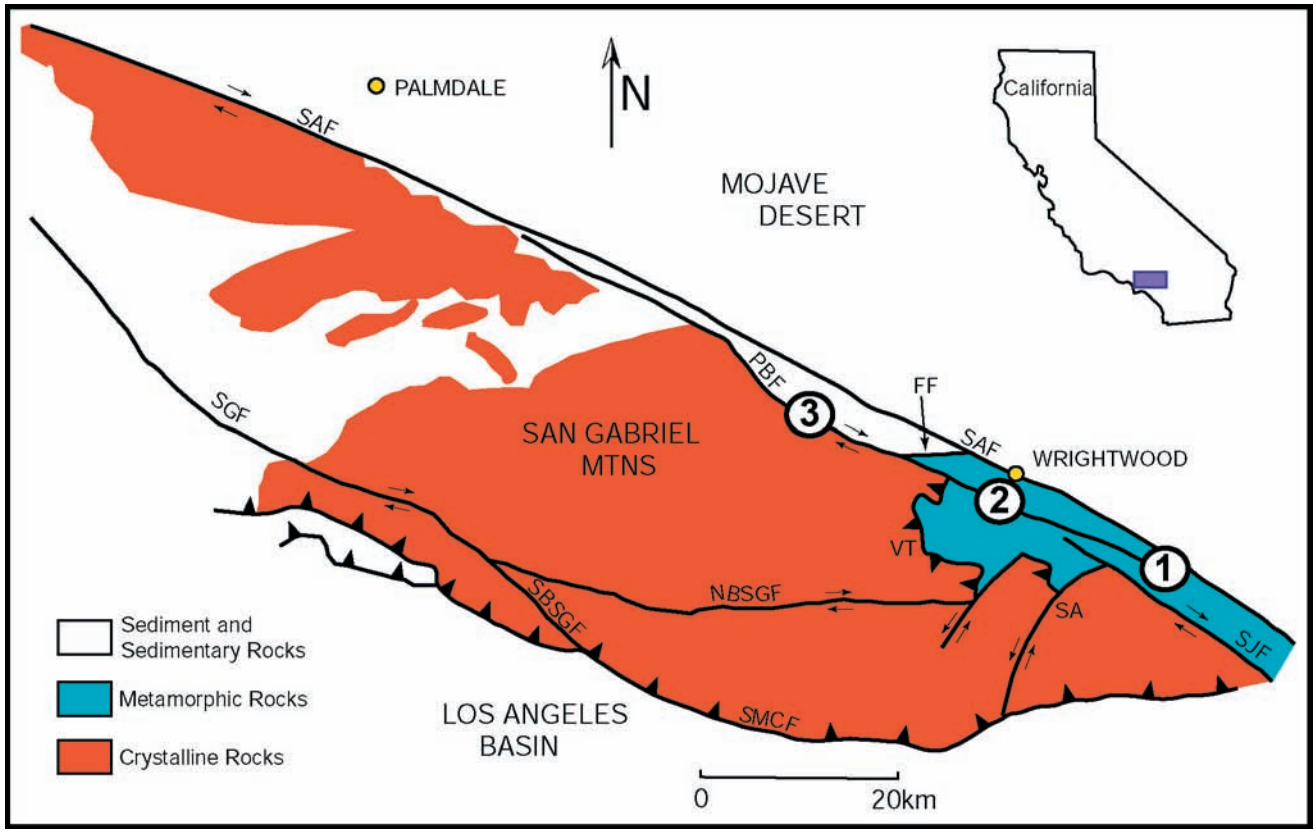

Figure 1. Simplified geologic map of the San Gabriel Mountains showing three sites along the Punchbowl fault: 1–Blue Cut; 2–Lone Pine Canyon; 3–Devil's Punchbowl. Other symbols include: FF–Fenner fault; PBF–Punchbowl fault; SAF–San Andreas fault; SA–San Antonio fault; SGF–San Gabriel fault (NBSGF–north branch; SBSGF–south branch); SJF–San Jacinto fault; SMCF–Sierra Madre-Cucamonga fault; VT–Vincent thrust. Adapted from Figure 3 of Schulz (1997).

roughly parallel strikes and join to the northwest and southeast (Dibblee, 1968). The Punchbowl fault is thought to be an abandoned strand of the San Andreas system that was active from 1-4 Ma (Dibblee, 1968, 1987; Weldon et al., 1993; Solum et al., 2003).

Correlation of stratigraphic units and structural features across the San Andreas and Punchbowl faults indicates that the Punchbowl fault accounts for 44 km of right-lateral separation during this time (Dibblee, 1968; Weldon et al., 1993; Wilson et al., 2003). The Punchbowl fault was subsequently exhumed from a depth of approximately 2-4 km, estimated from the overlying stratigraphic thickness (Chester and Logan, 1986, 1987). Therefore, the Punchbowl fault provides the opportunity to examine rocks that were faulted at depth, and is an analog for the modern San Andreas fault at shallow depths (Solum et al., 2003).

This field guide presents data from three different exposures of the Punchbowl fault (Figure 1). This allows for observation of along-strike variation within the fault zone. The localities presented are the Blue Cut exposure to the southeast, Lone Pine Canyon near Wrightwood, and the Devil's Punchbowl State Park to the northwest. Previous work on these fault exposures includes mesoscopic, microscopic, and geochemical analysis.

The Punchbowl fault exposures are among the most important study areas with respect to the study of the structure of seismogenic faults. The work of Chester and Logan (1986), Chester and Chester (1998), Chester et al. (2004), and Schulz and Evans (1998, 2000) presents detailed transect and map data on the structure and composition of these faults.

References

Chester, F.M. and J.S. Chester, Ultracataclasite structure and friction processes of the Punchbowl fault, San Andreas system, California. *Tectonophysics*, 295, 199-221, 1998.

Chester F.M. and J.M. Logan, Implications for mechanical properties of brittle faults from observations of the Punchbowl fault zone, California, USA. *Pure and Applied Geophysics*, 124, 79-106, 1986.

Chester F.M. and J.M. Logan, Composite planar fabric of gouge from the Punchbowl fault, California. *Journal of Structural Geology*, 9, 621-634, 1987.

Chester, F.M., J.M. Chester, D.L. Kirschner, S.E. Schulz, and J.P. Evans, Structure of large-displacement, strike-slip fault zones in the brittle continental crust. In: G.D. Karner, J.D. Morris, N.W. Driscoll, and E.A. Silver (editors), *Rheology and deformation of the lithosphere at continental margins*, 223-260, Columbia University Press, New York, NY, 2004.

Dibblee, T.W. Jr., Displacements on the San Andreas fault system in the San Gabriel, San Bernardino, and san Jacinto Mountains, southern California, in *Proc. Conf. on Geologic Problems of San Andreas Fault System*. Stanford University Publications of Geological Science, 11, 260-276, 1968.

Dibblee, T.W. Jr., Geology of the Devil's Punchbowl, Los Angeles County Park, California. *Geological Society of America Centennial Field guide—Cordilleran Section*, Published by the Geological Society of America, Inc., California, vol. 1, 193-198, 1987.

Schulz, S.E., Geochemical, petrologic, and structural characterization at multiple scales of deformation associated with the Punchbowl fault, southern California. M.S Thesis, *Utah State University*, Utah, 1997.

Schulz S.E., and J.P. Evans, Spatial variability in microscopic deformation and composition of the Punchbowl fault, southern California: Implications for mechanisms, fluid-rock interaction, and fault morphology. *Tectononphysics*, 295, 223-244, 1998.

Schulz S.E., and J.P. Evans., Mesoscopic structure of the Punchbowl fault, southern California, and the geologic and geophysical structure of active strike slip faults. *Journal of Structural Geology*, 22, 913-930, 2000.Solum, J.G., B.A. van der Pluijm, D.R. Pecor, and L.N. Warr, Influence of phyllosilicate mineral assemblages, fabrics, and fluids on the behavior of the Punchbowl fault, southern California. *Journal of Geophysical Research*, 108, B5, 2233, doi: 10.1029/2002JB001858, 2003.

Weldon, R.J. II, K.E. Meisling, and J. Alexander, A speculative history of the San Andreas fault in the central Transverse Ranges, California. In: R.E. Powell, R.J. Weldon, II and J.C. Matti (editors), The San Andreas Fault System: Displacement, Palinspastic Reconstruction, and Geologic Evolution. *Geological Society of America Memoir*, 178, 161-198, 1993.

Wilson, J.E., J.S. Chester, and F.M. Chester, Microfracture analysis of fault growth and wear processes, Punchbowl Fault, San Andreas system, California. *Journal of Structural Geology*, 25, 1855-1873, 2003.

Chapter 1: Punchbowl Fault

Site 1—Blue Cut

Directions

1. Heading southbound on I-15 through Cajon Pass, exit onto Cleghorn Road (Historic Route 66), 1.5 miles south of Cajon Junction (Hwy 138).
2. Continue for approximately 3 miles on Route 66. Exposure of the Punchbowl fault is on the southeast side of the road next to a large drainage pipe (Figure 1).

*To access the site from the northbound I-15 take the Kenwood exit off I-15 N, approximately 1 mile north of the I-215 merger. Drive north ~ 3.5 miles and park along the retaining wall on the southbound side of US-66.

UTM (WGS 84): 3791713 N, 0457251 E
Elevation: 2620 feet

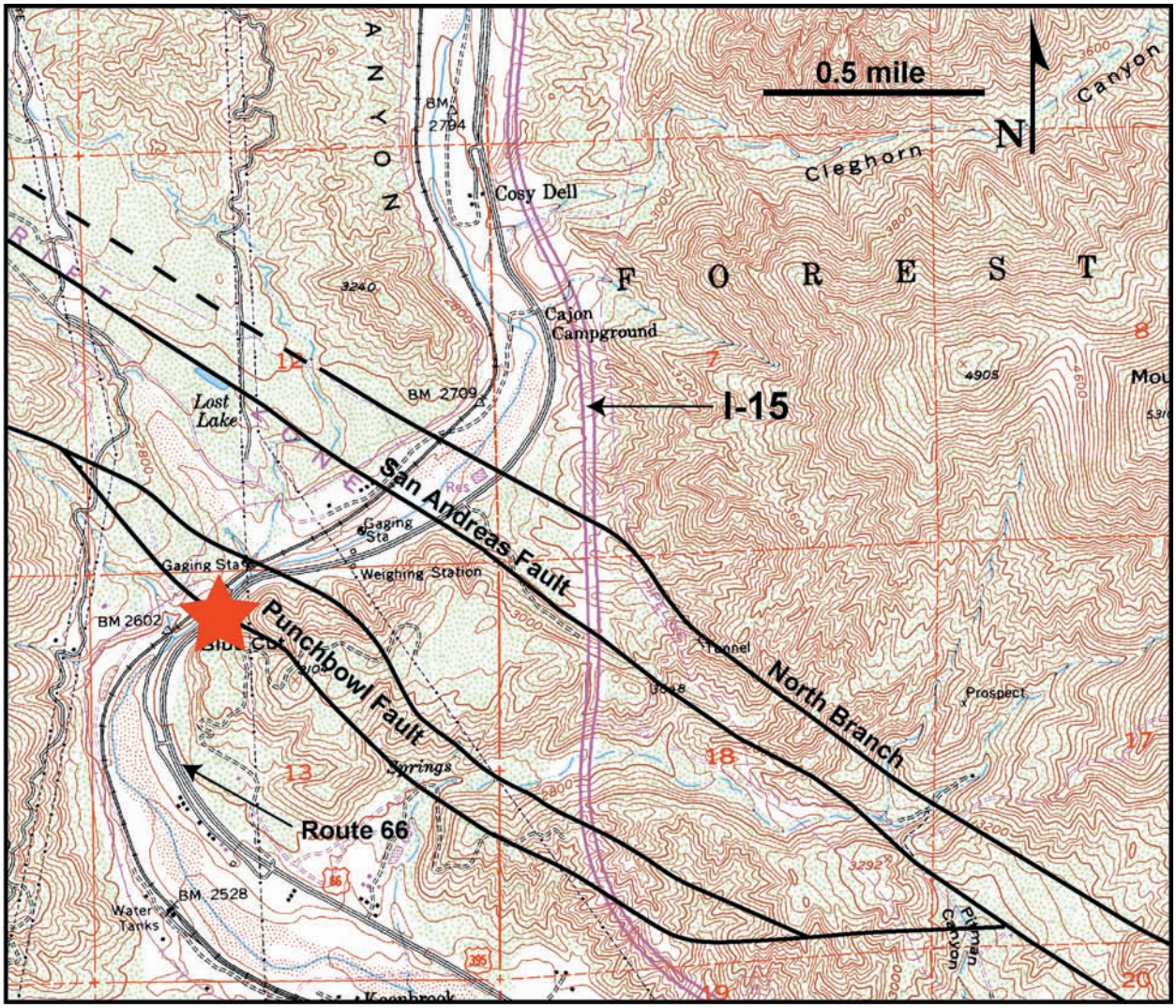

Figure 1. Topographic map of the Blue Cut area from the Cajon Pass Quadrangle. This map also shows fault traces from Weldon (1987). The red star marks the site location.

Geologic Setting

Blue Cut is a 1.5 km-long exposure along Route 66 that represents the near tip end of the 60 km-long fault block separating the Punchbowl and San Andreas faults (Weldon, 1987; Hazlett, 1995). Two strands of the San Andreas fault (SAF) and two strands of the Punchbowl fault are exposed in this cut (Figure 2).

The rocks surrounding the multiple strands are highly damaged. These four fault strands juxtapose various lithologies, such as the Pelona Schist, chloritized gneiss and tonalite, and Pelona Metabasalt. Cajon Creek has developed a right-stepping kink in the Blue Cut area due to dextral slip on the SAF (Hazlett, 1995), and a small sag pond, Lost Lake, lies along the active trace of the SAF.

Description

Near the western end of Blue Cut, adjacent to the drainage pipe on the south side of the road, the southern strand of the Punchbowl fault is exposed (Figure 3). The fault zone is approximately 30 m wide. At this location there is an increase in the density of slip surfaces and veins close to the fault core, which consists of a group of anastomosing gouge and cataclasite layers (Schulz, 1997). The gouge layers are typically less than 2 cm thick, are not foliated, and are bounded by slip planes that show slickenlines indicating strike-slip motion (Schulz, 1997). The schistose foliation of the Pelona Schist is oriented nearly vertical (i.e., subparallel to the fault) within 10 m of the south trace of the Punchbowl fault (Figure 4). Mesoscopic deformation associated with the Punchbowl fault begins to increase at about 50 m from the fault core (Figure 5) (Schulz and Evans, 2000).

The composition of the fault core and protolith at this site are similar, except for a small depletion in Al2O3, TiO2, and Na2O, an enrichment in MgO, and a higher LOI in the fault core (Schulz, 1997). The similarity between fault core and host rock geochemistry may suggest that the Punchbowl fault in the Blue Cut area has experienced less slip than other areas (e.g., Lone Pine Canyon and Devil's

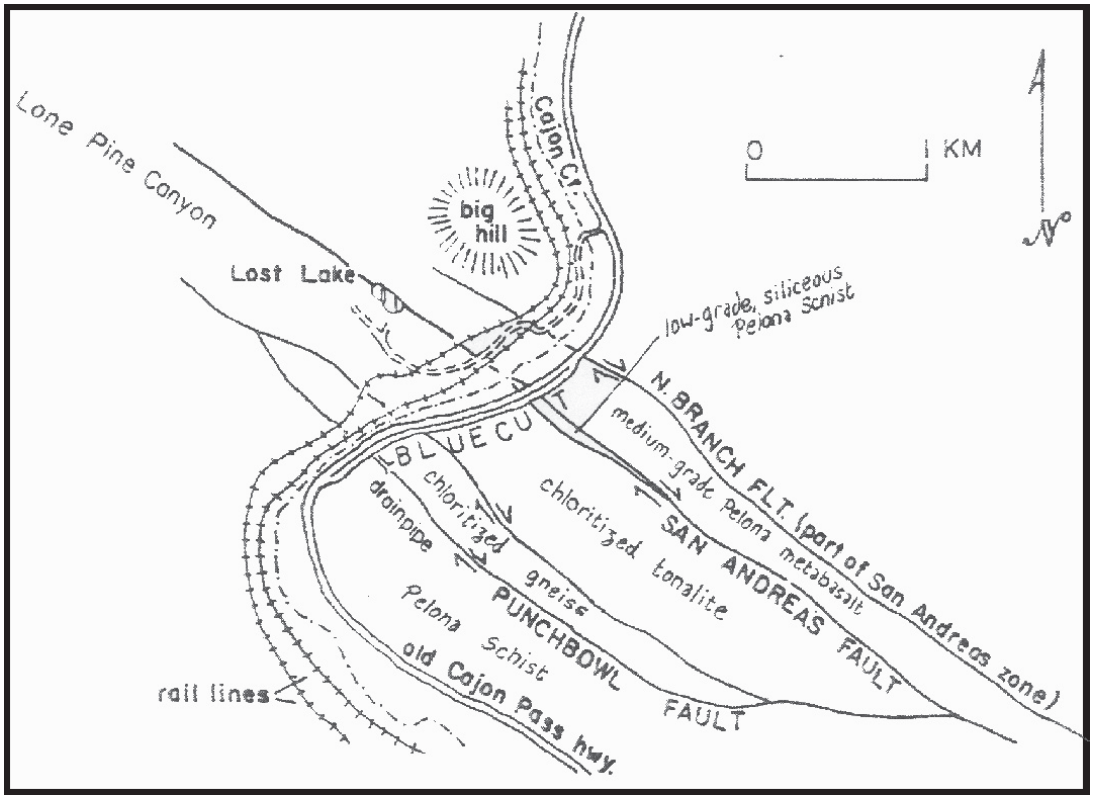

Figure 2. Geology of the Blue Cut area. [Figure 34 from Hazlett (1995), based on mapping by Weldon (1987).]

Figure 3. View to the southeast of the southern strand of the Punchbowl fault. Close-up view shows a cataclasite layer, possibly a major fault strand.

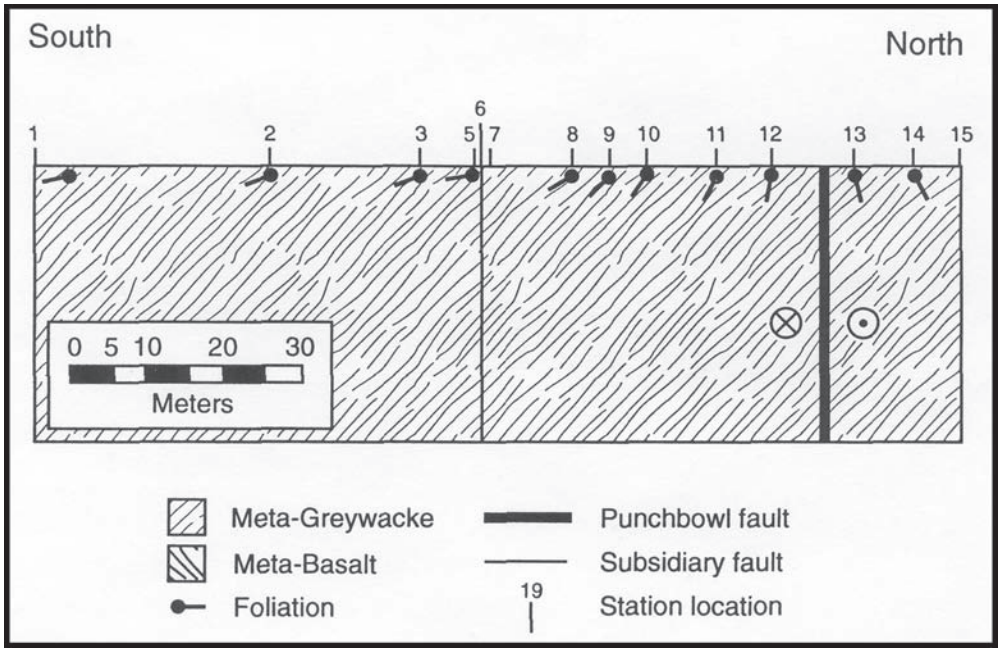

Figure 4. Generalized cross-section of traverse across the south branch of the Punchbowl fault at Blue Cut. Numbers indicate stations where measurements were collected. Tadpoles indicate the apparent dip of the foliation in the Pelona Schist. (Figure 7 from Schulz,1997.)

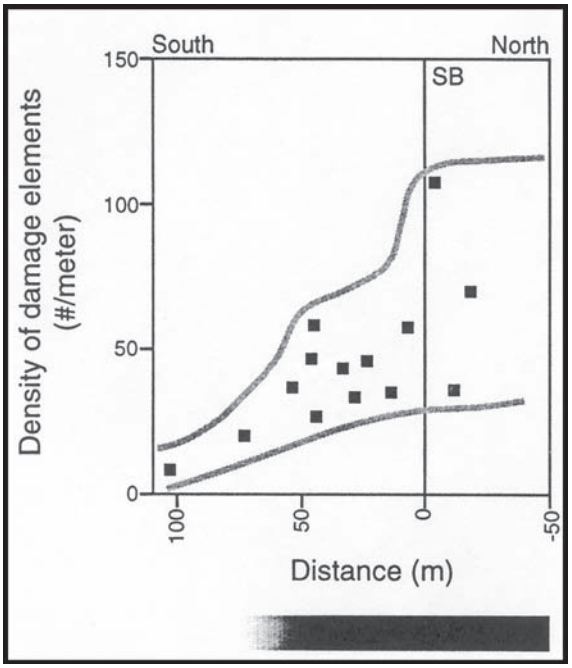

Figure 5. Density of mesoscopic damage elements plotted with respect to the distance from the fault core. Gray lines outline the range of deformation. The bar beneath the graph shows the extent of the damage zone. SB means the south branch of the Punchbowl fault. (Figure 15c from Schulz, 1997.)

Punchbowl), because the smaller amount of slip would place rocks of less variation in contact with the fault core (Schulz, 1997).

Seismological Implications

One of the key requirements of examining exhumed faults is to find sites with pre-existing planar structures (schistocity, dikes, etc.). We can measure the orientations of these plane structures as we approach the fault zone to get a sense of how shear-strain is accumulated. The exposures of the Punchbowl fault in the Pelona Schist typically show that the reorientation occurs over a narrower zone than when faults are in crystalline rocks.

The Blue Cut site is a good location to observe multiple strands of the San Andreas and Punchbowl faults. These strands create an "intrafault" damage zone characterized by predominantly brittle and semi-brittle deformation, with layered silicates deforming by fracturing, cataclasis, and slip; chemical alteration becomes more prevalent closer to the fault core (Schulz, 1997). The southern strand of the Punchbowl fault at Blue Cut is approximately 30 m thick, which is narrower than similar strike-slip faults (e.g., the San Gabriel fault) and even other portions of the Punchbowl fault.

Schulz (1997) proposes that the narrow fault zone is in part due to the schist lithology that the fault developed in, as opposed to the granitic gneisses at other locations (Chester et al., 1993). However, the fault core at Blue Cut is similar to other large displacement fault cores, which suggests that the processes that occur in the cores are similar, resulting in a foliated ultra cataclasite-dominated region of slip localization (Schulz, 1997).

The view of the outcrops along the edge of the railroad, where it cuts across the creek, helps give a sense of the nature of the intrafault damage. The narrow slip surfaces can be seen, and the damage zone rocks are characterized by the densely spaced fractures and alteration. We have not done any detailed work in this area, and we recommend that you do not attempt access to these sites, as the railroad companies discourage such actions.

References

Chester, F.M., J.P. Evans, and R.L. Biegel, Internal structure and weakening mechanisms of the San Andreas fault. J*ournal of Geophysical Research*, 98, B1, 771-786, 1993.

Hazlett, R., "Field Guide To the Geology of the Eastern San Gabriel Mountains & San Andreas Fault in the Cajon Pass Area." Southern California. California, 1995.

Schulz, S.E., Geochemical, petrologic, and structural characterization at multiple scales of deformation associated with the Punchbowl fault, southern California. M.S Thesis, *Utah State University*, Utah, 1997.

Schulz S.E., and J.P. Evans., Mesoscopic structure of the Punchbowl fault, southern California, and the geologic and geophysical structure of active strike slip faults. *Journal of Structural Geology*, 22, 913-930, 2000.

Weldon, Ray J., San Andreas fault, Cajon Pass, southern California. *Geological Society of America Centennial Field Guide—Cordilleran Section*. Published by the Geological Society of America, Inc., California, vol. 1, 193-198, 1987.

Chapter 1: Punchbowl Fault

Site 2—Lone Pine Canyon

Directions

1. From the town of Wrightwood, take Angeles Crest Highway west (State Highway 2) to the split with Big Pines Highway.
2. At the split, turn left and continue on Angeles Crest Highway (State Highway 2).
3. Follow Angeles Crest Highway for about 4 miles until you see a dirt road on your left (there may be sign mentioning Guffy Campground).
4. Turn left and follow the dirt road until you reach a gated jeep road.
5. Park at Guffy Campground (Figure 1).

Directions to Station A

1. Walking from the Guffy campground trailhead, follow the jeep road until a split occurs.
2. Take the right fork and continue for about 2 miles.
3. The fault exposure will be on your right (west) before the road makes a sharp turn (Figure 2).

UTM (WGS 84): 3799152 N, 0440107 E
Elevation: 7358 feet

Directions to Station B

1. From the Guffy campground trailhead, follow the jeep road until a split occurs.
2. Take the left fork and follow the jeep trail until it comes to a junction with a single track trail, which is marked by a sign.
3. Follow the trail south down the slope. The fault zone is exposed in the saddle (Figure 2).

UTM (WGS 84): 3798732 N, 0441381 E
Elevation: 8271 feet

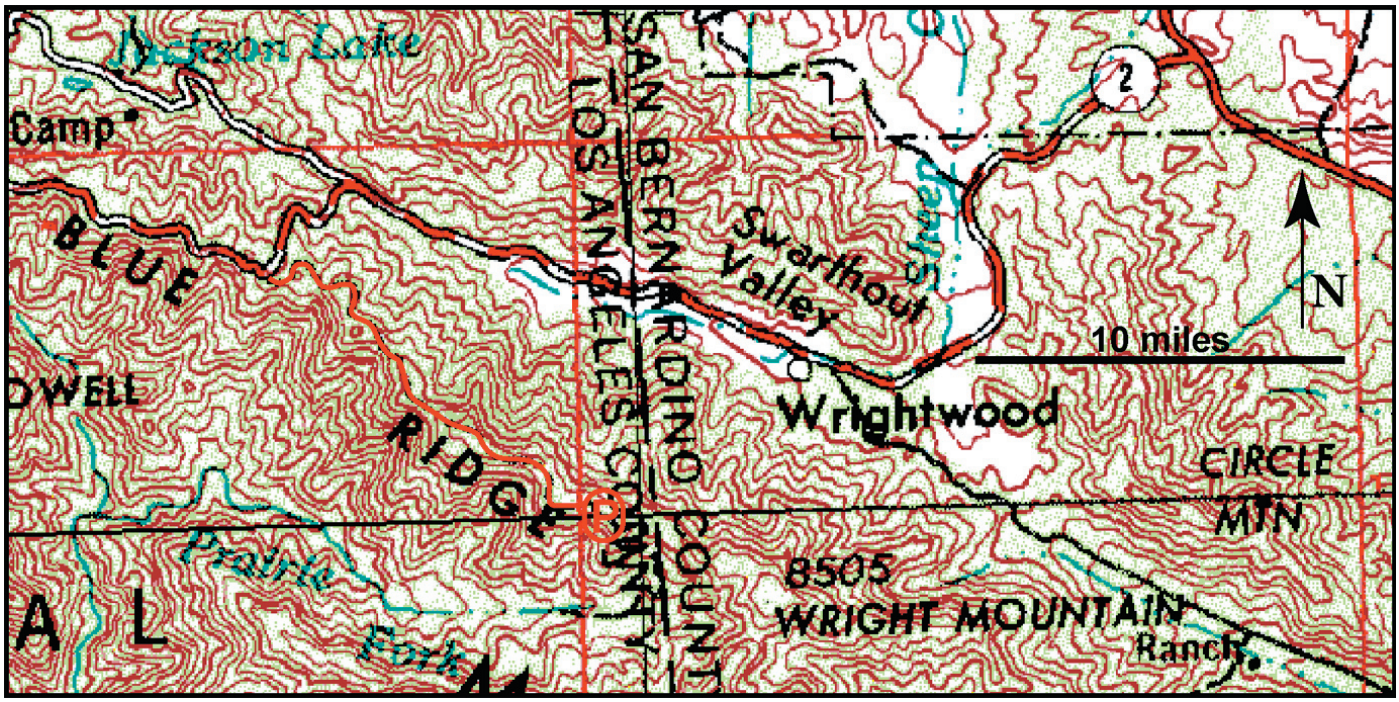

Figure 1. Topographic map of the Wrightwood area showing directions to Guffy Campground. The "P" outlined in red is the parking area.

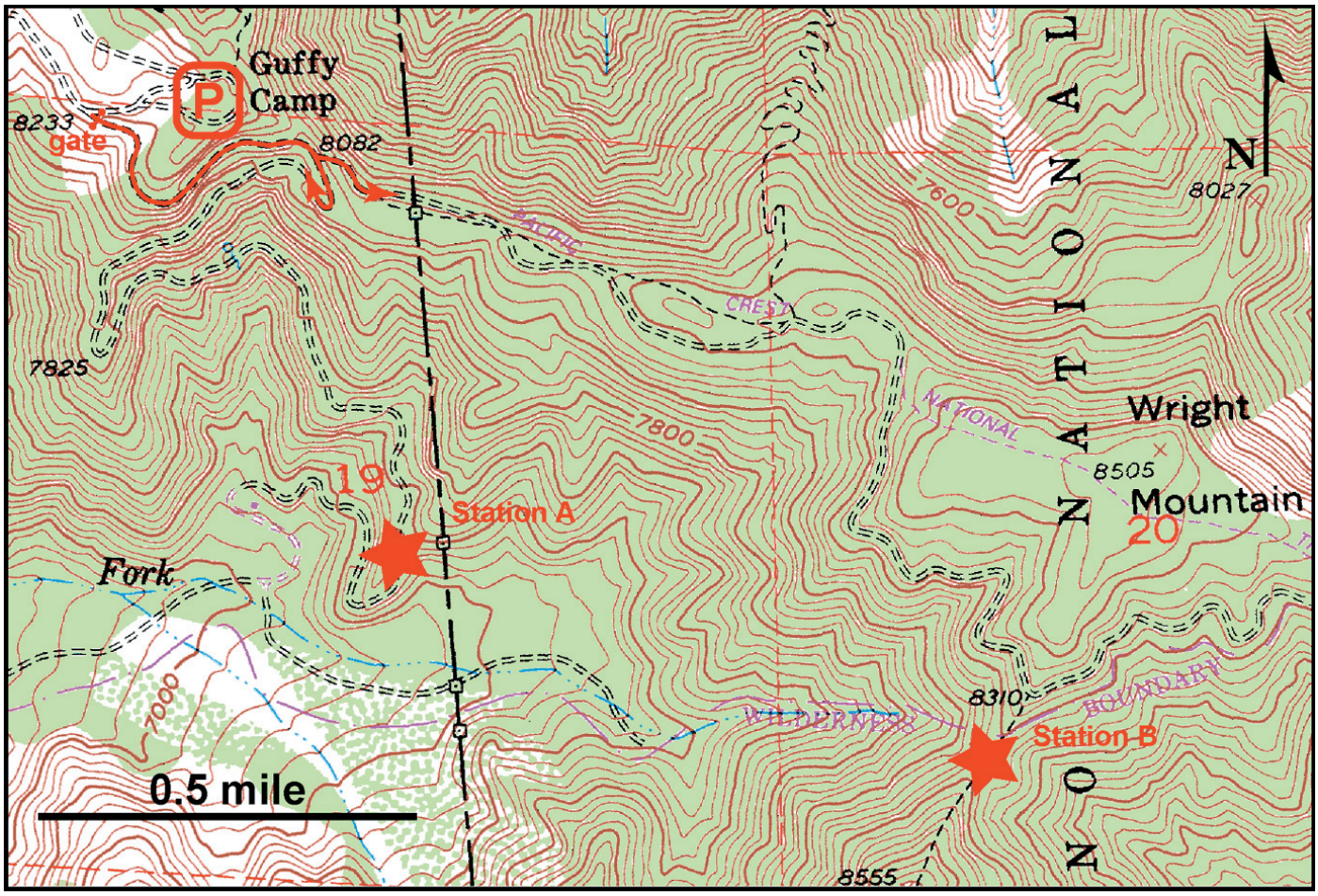

Figure 2. Topographic map from the Mt. San Antonio Quadrangle of Guffy Campground and locations of Stations A and B.

Geologic Setting

From 4 Ma until 1Ma, the Punchbowl fault was the active trace of the San Andreas fault system, with a cumulative displacement of 44 km. The Punchbowl fault has been exhumed 2-4 km due to the uplift of the San Gabriel Mountains (Chester and Logan, 1986; Schulz and Evans, 2000). The area surrounding the Lone Pine Canyon Site exhibits at least two traces of the Punchbowl fault (Schulz and Evans, 1998) and several other strands may be present (Weldon, pers. comm.).

Rock types in the area are predominantly Pelona Schist, as well as thin segments of an aplitic unit flanked by the two strands of the Punchbowl fault. The Pelona Schist is a late Cretaceous metagraywacke that is predominantly composed of quartz, albite, and muscovite (Schulz and Evans, 1998). The schistocity can be used as a strain marker in order to understand the nature of deformation of the Punchbowl fault in this area.

Two different sites provide fault exposure in the Lone Pine Canyon area (Figure 2). The northern branch of the Punchbowl fault is well exposed at Station A, which also has 130 m of deformed rock to the south (Schulz and Evans, 1998). Station B is 1.3 km southeast of Station A and has exposure of the entire Punchbowl fault zone. There is nearly continuous exposure between the two branches of the fault, which are roughly 130 m apart (Schulz and Evans, 1998).

Description of Station A

The Punchbowl fault at this site has been previously described by Schulz and Evans (2000) as follows:

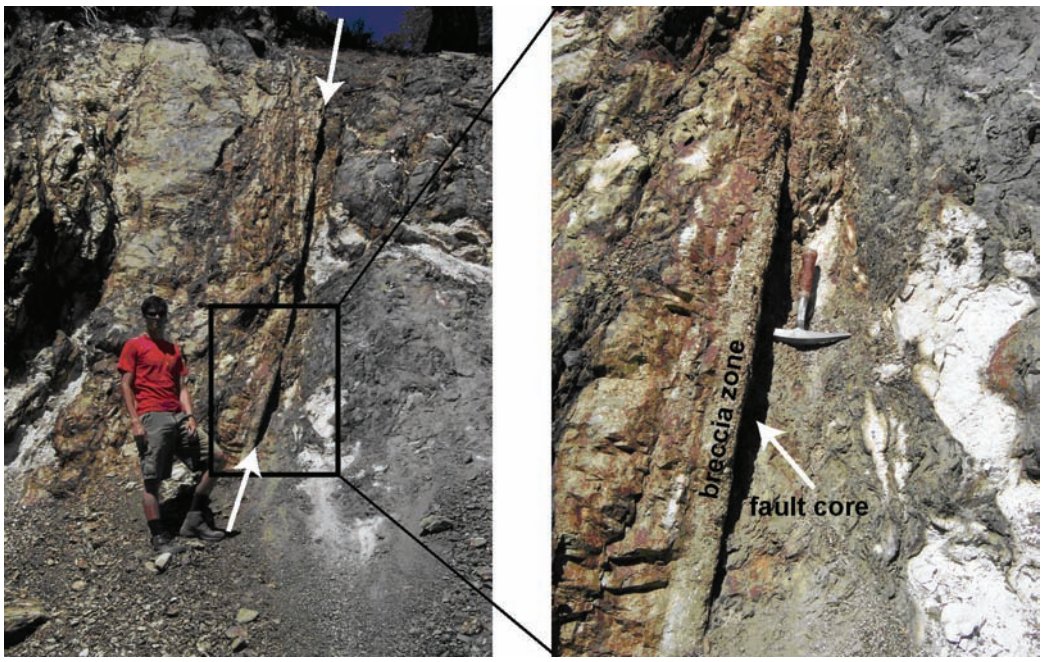

Figure 3. View to the west of the Punchbowl fault at Station A. White arrows indicate the location of the fault core.

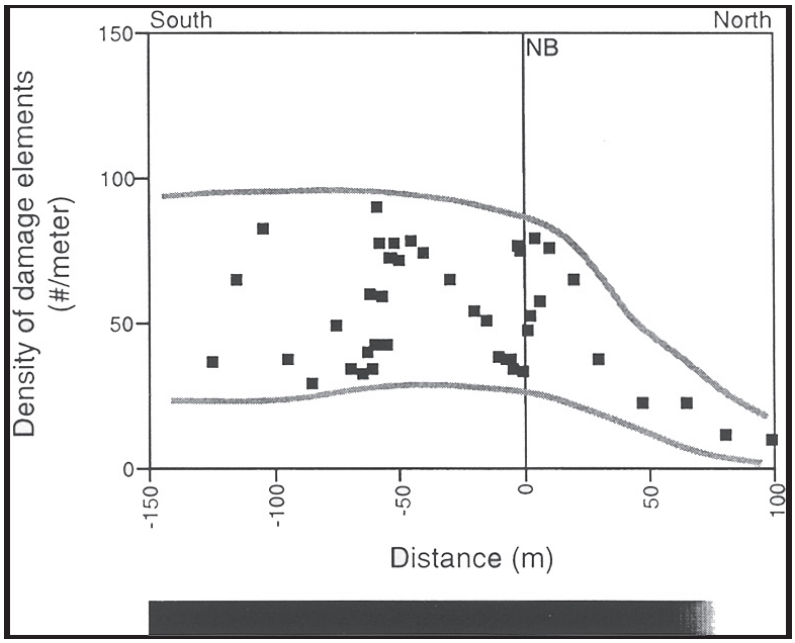

Figure 4. Densities of mesoscopic damage elements plotted with respect to the distance from the fault core at Station A. In the Pelona Schist, solid lines indicate the location of fault cores of the major strands of the Punchbowl fault. Grey lines outline the maximum and minimum deformation ranges measured. The bar beneath the graph shows the extent of the damage zone. (Figure 15a from Schulz, 1997.)

"The schist in traverse 1 [Station A] is relatively undeformed up to roughly 30 m from the fault trace, where the rock changes from a thinly foliated, grey, quartz-mica schist to a green-grey, highly fractured altered rock. The schist has a well-defined foliation north of the fault core and its orientation is unaffected by the Punchbowl fault. Beginning at 30 m north of the fault core,

foliation is difficult to distinguish. Within 8 m of the fault core, the rocks are extremely fractured and friable. South of the fault core at traverse 1 [Station A], between the two branches of the Punchbowl fault, the rocks are green-brown altered schists where fractures and slip surfaces are prevalent.

The fault core at all locations in this study is dark, fine grained and foliated to massive cataclasite. The fault core of the north branch of the Punchbowl fault at traverse 1 [Station A] is less than 10 cm thick, with a brecciated zone roughly 15 cm thick on the south side of the fault core that is continuous across much of the outcrop (Figure 3). This breccia zone is parallel to foliation but truncated by the fault core. The foliation surfaces are subparallel to the fault core, and they commonly contain slickenlines that plunge within 20° of horizontal."

Description of Station B

Both the north and south branches of the Punchbowl fault are exposed at Station B (Figure 5). However, the fault core of the north branch is not well exposed. Its location can be determined to within 5 m by a change in lithology (Schulz and Evans, 2000). The amount of alteration and deformation between the two branches at this site is irregular (Schulz and Evans, 2000). The fracture spacing is 2-5 cm at 15 m north of the north branch and the rocks have an increase in the density of slip surfaces and veins relative to the schist at 60 + m to the north (Schulz and Evans, 2000).

Seismological Implications

Schulz and Evans explain several important points associated with their study of the Punchbowl fault:

> "The type and spatial distribution of macroscopic and microscopic structures associated with the Punchbowl fault offer an indication of the fault-zone characteristics found at seismogenic depths along the SAF." (Schulz and Evans, 2000, pg. 914)

Figure 5. View to the southeast of Station B. Arrows denote approximate location of the north and south branches of the Punchbowl fault.

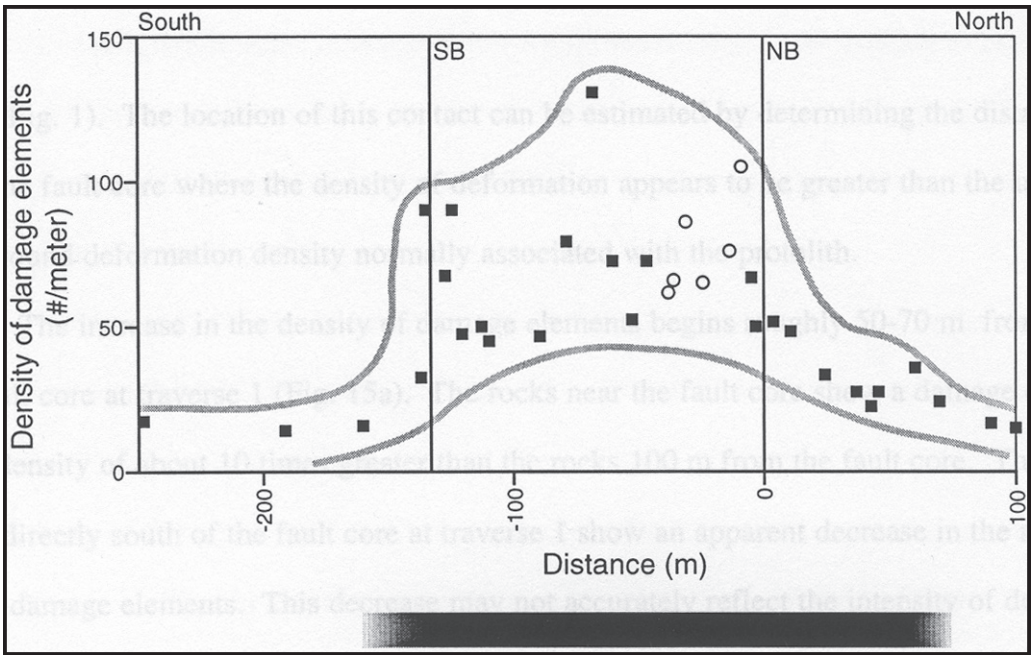

Figure 6. Densities of mesoscopic damage elements plotted with respect to the distance from the fault core at Station B. Open circles are in the aplite and closed squares in the Pelona Schist. Solid lines indicate the location of fault cores of the major strands of the Punchbowl fault. Grey lines outline the maximum and minimum deformation ranges measured. The bar beneath the graph shows the extent of the damage zone. (Figure 15b from Schulz, 1997.)

> "The Punchbowl Fault, exhumed from a depth of up to 4 km, is composed of a macroscopically identifiable damaged zone, which surrounds thin core zones of localized slip. The apparent thickness of the fault zone varies with the parameter that is measured. Increased fracture densities are noted up to 70 m away from the fault core, whereas foliation reorientation occurs in a zone ~30 m wide. Microscopic and compositional changes occur over even narrower zones (Schulz and Evans, 1998).
>
> Based on the distribution of microstructures, geochemical alteration, and changes in preexisting structures, the Punchbowl fault zone is narrower where it cuts the schist than are other strike-slip faults developed in granitic gneisses (Chester et al., 1993). The data from the Punchbowl fault show that the fault zone can be less than 200 m thick, with most of the deformation limited to an even thinner (20 m) zone of intense deformation and slip localization." (Schulz and Evans, 2000, pg. 927)

Schulz and Evans (2000) suggest the fault zone signature is different for singular measures of deformation. They also suggest these differences would cause different geophysical signatures within and around a fault.

References

Chester F.M. and J.M. Logan, Implications for mechanical properties of brittle faults from observations of the Punchbowl fault zone, California, USA. *Pure and Applied Geophysics*, 124, 79-106, 1986.

Schulz, S.E., Geochemical, petrologic, and structural characterization at multiple scales of deformation associated with the Punchbowl fault, southern California. M.S Thesis, *Utah State University*, 1997.

Schulz S.E., and J.P. Evans, Spatial variability in microscopic deformation and composition of the Punchbowl fault, southern California: Implications for mechanisms, fluid-rock interaction, and fault morphology. *Tectononphysics*, 295, 223-244, 1998.

Schulz S.E., and J.P. Evans., Mesoscopic structure of the Punchbowl fault, southern California, and the geologic and geophysical structure of active strike slip faults. *Journal of Structural Geology*, 22, 913-930, 2000.

Chapter 1: Punchbowl Fault

Site 3—Devil's Punchbowl

Directions

1. From the Los Angeles area, proceed north on Highway 14 towards Palmdale.
2. Exit Highway 14 onto Highway 138 and head southeast to Pearblossom.
3. At Pearblossom, turn right (south) onto Longview Rd. (131st Street).
4. Proceed ~ 2 miles on Longview Rd. and then take a left at the junction with Fort Tejon Rd.
5. Continue for ~ 0.5 mile and take the right fork onto Longview Rd.
6. After ~ 2 miles, turn left onto Tumbleweed Rd.
7. Take the right fork onto Devil's Punchbowl Rd. and follow it into the park.
8. Take the upper trail (Burkhart trail) from the park headquarters to Devil's Chair (Figure 1).

   *There is also an alternative approach from the southeast starting at South Fork Big Rock Creek Campground (Chester, 1999).

Geologic Setting

The Punchbowl fault is an inactive, exhumed fault of the San Andreas transform system. It is located at the juncture of the San Gabriel Mountains and Mojave Desert, approximately 5 km southwest of the active strand of the San Andreas fault (Chester

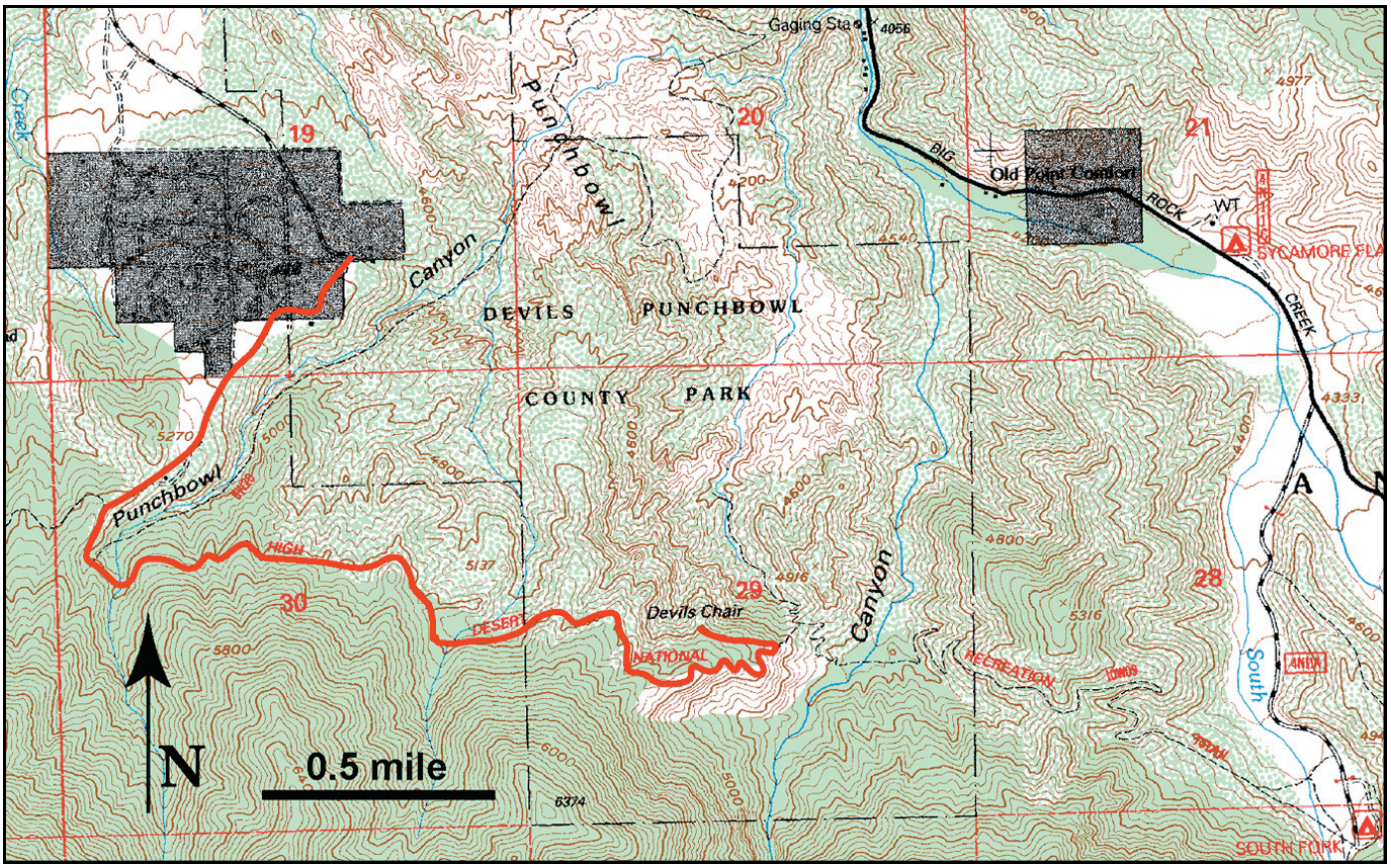

Figure 1. Topographic map from the Valyermo Quadrangle of Devil's Punchbowl County Park showing the hiking trail from the park office to Devil's Chair.

and Logan, 1987; Wilson et al., 2003). The Punchbowl fault is thought to be an abandoned strand of the San Andreas system that was active from 1-4 Ma (Dibblee, 1968, 1987; Weldon et al., 1993; Solum et al., 2003).

Correlation of stratigraphic units and structural features across the San Andreas and Punchbowl faults indicates that the Punchbowl fault accounts for 44 km of right-lateral separation during its period of activity. (Dibblee, 1968; Weldon et al., 1993; Wilson et al., 2003). The Punchbowl fault was subsequently exhumed from a depth of approximately 2-4 km, estimated from the overlying stratigraphic thickness (Chester and Logan, 1986, 1987).

In the Devil's Punchbowl area, the Punchbowl fault system consists of two fault strands that bind a slice of fractured crystalline basement rock up to 0.5 km thick (Noble, 1954; Chester and Chester, 1998). The northern strand of the Punchbowl fault juxtaposes crystalline basement rock and the Punchbowl Formation, a Miocene-Pliocene arkosic sandstone, along a continuous 0.3 m thick ultracataclasite layer (Chester and Chester, 1998). The southern fault strand juxtaposes similar rock types (Cox et al., 1983) and is often segmented and discontinuous (Chester and Chester, 1998).

Description

The Punchbowl fault is an oblique strike-slip fault dipping to the southwest which places crystalline basement above folded Tertiary sedimentary rocks (Figure 2). The intensity of deformation (i.e., folding, subsidiary faulting, and microfracturing) increases progressively towards the ultracataclasite layer in the fault core (Chester, 1999).

There are no obvious changes in orientation or character of the subsidiary faults with proximity to the fault core (Chester and Logan, 1987). Mesoscopic fracture density reaches background levels at approximately 20 m from the ultracataclasite layer, while microfracture density decreases to background levels at about 100 m from the layer (Chester, 1999) (Figure 3).

Numerous subsidiary faults are present in the damage zone of the Punchbowl fault. Slip and orientation measurements of subsidiary faults indicate that the slip direction during the latest stages of faulting was oriented with a plunge of 20 to 30° to the SE, which is consistent with the oblique reverse motion of the Punchbowl fault (Chester and Logan, 1987).

Microfractures have a systematic orientation relative to position in the fault zone (Wilson, 1998). Microfractures in the inner damage zone (within 2.5 m of the fault surface) display preferred orientations that are parallel and perpendicular to the fault surface (Wilson et al., 2003). A distinct microfracture set is present in the rest of the damage zone (i.e., middle and outer damage zone) that is perpendicular to the slip direction of the Punchbowl fault, which implies that the maximum principal compressive stress within the damage zone was approximately normal to the fault surface (Wilson et al., 2003).

Chester and Chester (1998) mapped the fault core at four different localities along the Punchbowl fault in the Devil's Punchbowl area. The following description of the fault core is from Chester (1999):

> "Several important features of the fault core are common to all of the mapped segments even though the map locations are spaced up to two kilometers apart. Most displacement on the fault occurred within a < 1-m wide zone of ultracataclasite. The boundaries between the ultracataclasite and surrounding proto-cataclasite are extremely sharp, but not parallel or planar on the meter-scale [Figure 4].
>
> On the basis of color, cohesion, fracture and vein fabric, and porphyroclast lithology, two main types of ultracataclasite are distinguished in the layer: an olive-black ultracataclasite in contact with the basement, and a dark yellow-brown ultracataclasite in contact with the sandstone. The two are juxtaposed along a continuous contact that is often coincident with a single, continuous, nearly planar, prominent fracture surface (pfs) that extends the length of the ultracataclasite layer in all exposures. No significant mixing of the brown and black ultracataclasites occurred by offset on anastamosing shear surfaces that cut the contact or by mobilization and injection of one ultracataclasite into the other. The ultracataclasites are cohesive

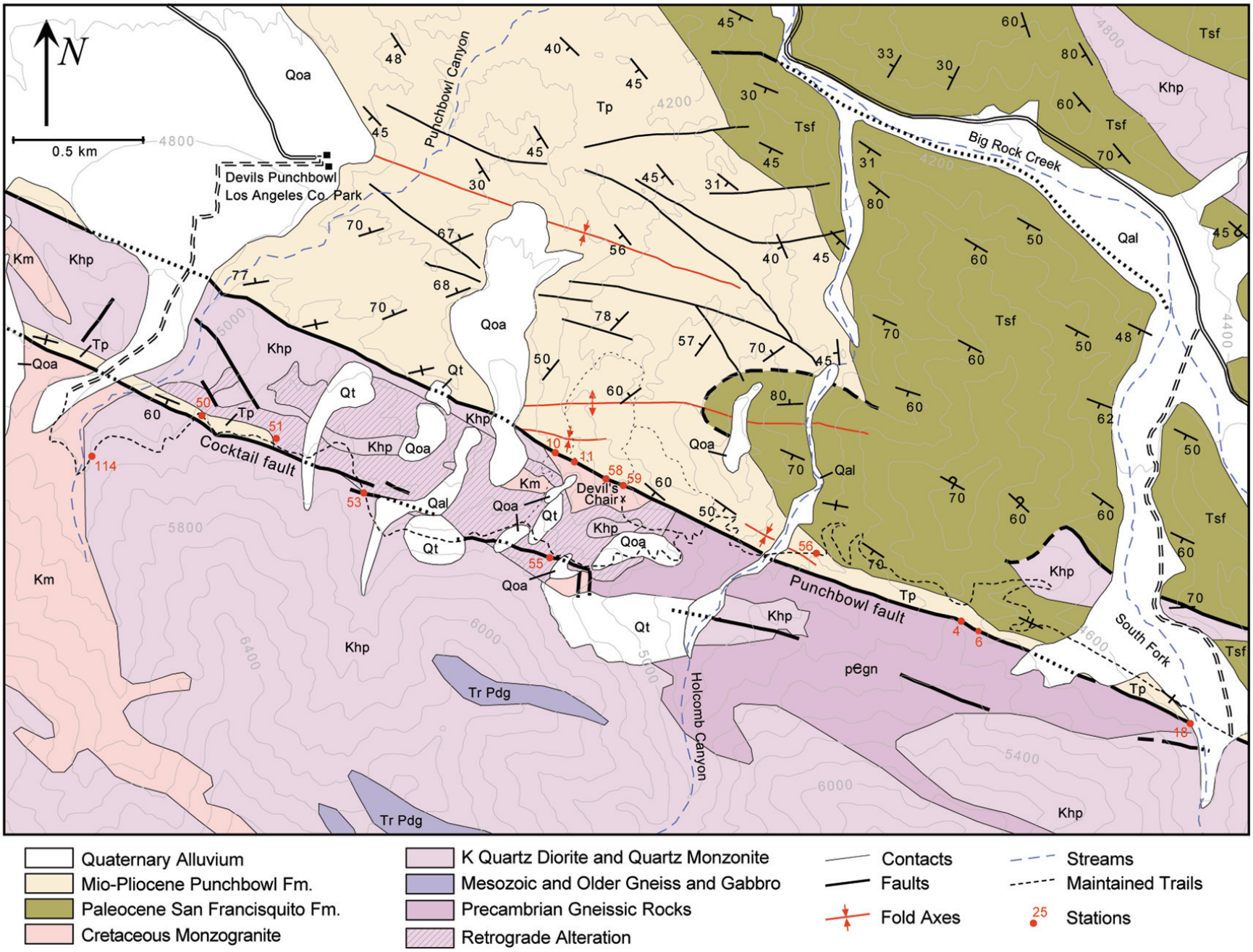

Figure 2. Geologic map of the Punchbowl fault zone in the Devil's Punchbowl Los Angeles County Park, CA (Figure 2 from Chester, 1999).

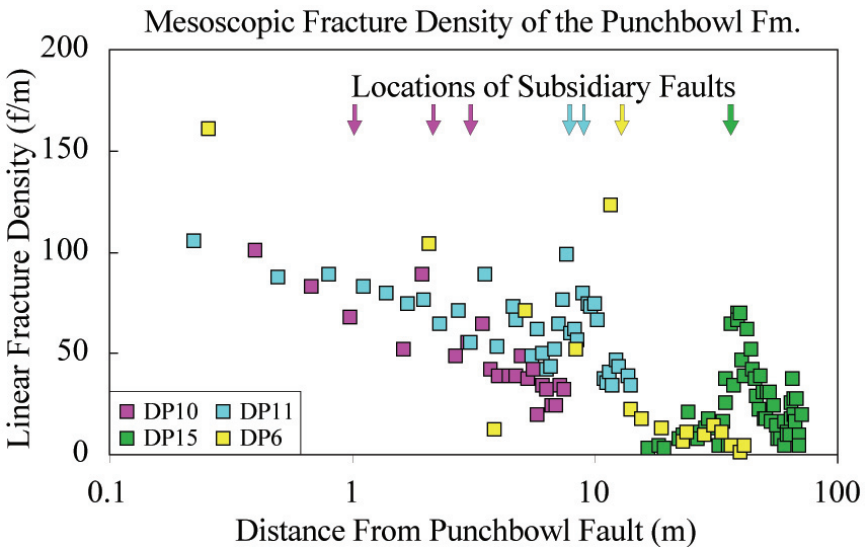

Figure 3. Density of mesoscopic scale fractures and subsidiary faults in the Punchbowl Formation sandstone as a function of distance from the Punchbowl fault. Linear density determined from the total number of fracture intercepts with two perpendicular line segments along four different traverses. Fracture density decreases with distance from the fault except locally near large subsidiary faults—shown by arrows coded to traverse by color (Figure 3 from Chester, 1999).

throughout except for thin accumulations of less cohesive, reworked ultracataclasite along the pfs.

Structural relations suggest that: 1) the black and brown ultracataclasites were derived from the basement and sandstone, respectively; 2) the black and brown ultracataclasites were juxtaposed along the pfs; 3) the subsequent, final several kilometers of slip on the Punchbowl fault occurred along the pfs; 4) earthquake ruptures followed the pfs without significant branching or jumping to other locations in the ultracataclasite."

Seismological Implications

The detailed fault zone work in the Devil's Punchbowl area has implications for earthquake mechanisms, which have been nicely summarized by Chester and Chester (1998):

"The internal structure of the Punchbowl fault implies that earthquake ruptures were not only confined to the ultracataclasite layer, but largely localized to the pfs [prominent fracture surface]. During the latest phase of deformation, the bulk of the ultracataclasite retained cohesion and layer contacts were relatively undisturbed. As such, the earthquake ruptures must have followed the pfs without significant branching or jumping to other locations in the ultracataclasite. By comparison with laboratory studies of rock friction, the localization of displacement in the Punchbowl ultracataclasite implies rate weakening behavior with small critical slip distance, and thus small nucleation and breakdown dimensions for ruptures.

Of the various mechanisms proposed to explain the low strength of the San Andreas and to produce dynamic weakening of faults, those that require or predict wide zones of less cohesive granular material that flows and mixes appear incompatible with our observations. Mechanisms that assume or are consistent with extreme localization of slip, such as thermal pressurization of pore fluids and possibly interface separation waves, are more consistent with structures produced during the final phase of movement on the Punchbowl fault."

References

Chester, F.M., Field Guide to the Punchbowl Fault Zone at Devil's Punchbowl Los Angeles County Park, California. *Texas A&M University*, Texas, vol. 2.1, 1999.

Chester, F.M. and J.S. Chester, Ultracataclasite structure and friction processes of the Punchbowl fault, San Andreas system, California. *Tectonophysics*, 295, 199-221, 1998.

Chester F.M. and J.M. Logan, Implications for mechanical properties of brittle faults from observations of the

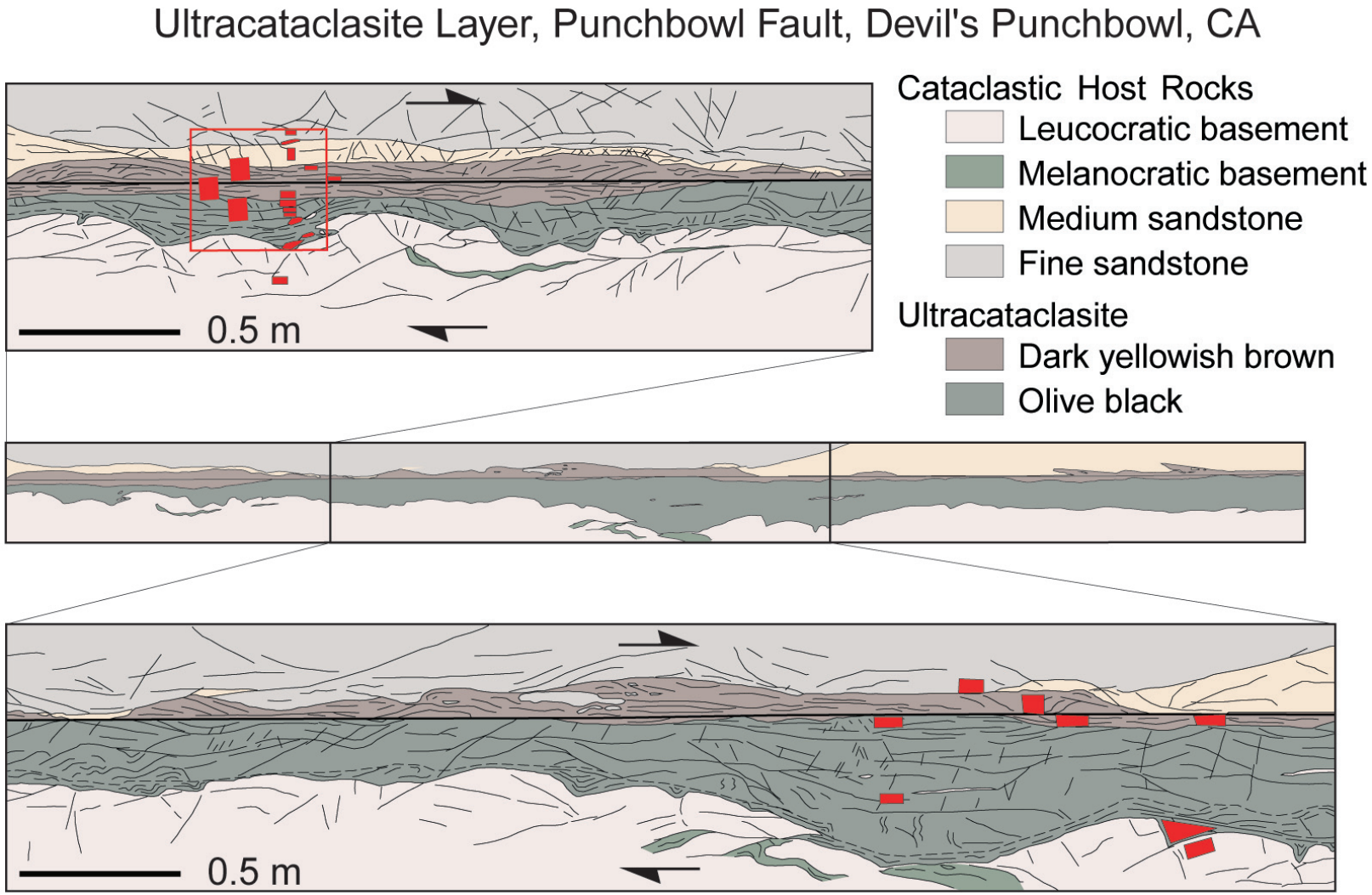

Figure 4. Portions of one of the four strip maps made of the ultracataclasite layer in the Punchbowl fault core. The orientation of the map is perpendicular to the layer and parallel to the slip direction. Thin black lines represent the location of contacts and fractures. Thick black line through the center of the layer is the prominent fracture surface. Size and location of the samples collected are shown by red filled areas. The maps document that the general structure of the ultra-cataclasite layer is similar along a strike distance of 2 km (Figure 7 from Chester, 1999).

Punchbowl fault zone, California, USA. *Pure and Applied Geophysics*, 124, 79-106, 1986.

Chester F.M. and J.M. Logan, Composite planar fabric of gouge from the Punchbowl fault, California. *Journal of Structural Geology*, 9, 621-634, 1987.

Cox, B.F., R.E. Powell, M.E. Hinkle, and D.A. Lipton, Mineral resource potential map of the Pleasant View Roadless Area, Los Angeles county, California. *U.S. Geological survey Miscellaneous Field Studies Map*, MF-1649-A, scale 1:62,500, 1983.

Dibblee, T.W. Jr., Displacements on the San Andreas fault system in the San Gabriel, San Bernardino, and san Jacinto Mountains, southern California, in Proc. Conf. on Geologic Problems of San Andreas Fault System. *Stanford University Publications of Geological Science*, 11, 260-276, 1968.

Dibblee, T.W. Jr., Geology of the Devil's Punchbowl, Los Angeles County Park, California. *Geological Society of America Centennial Field guide—Cordilleran Section*, Published by the Geological Society of America, Inc., California, vol. 1, 193-198, 1987.

Noble, L.F., Geology of the Valyermo Quadrangle and vicinity. *USGS*, Map GQ-50, 1954.

Solum, J.G., B.A. van der Pluijm, D.R. Pecor, and L.N. Warr, Influence of phyllosilicate mineral assemblages, fabrics, and fluids on the behavior of the Punchbowl fault, southern California. *Journal of Geophysical Research*, 108, B5, 2233, doi: 10.1029/2002JB001858, 2003.

Weldon, R.J. II, K.E. Meisling, and J. Alexander, A speculative history of the San Andreas fault in the central Transverse Ranges, California. In: R.E. Powell, R.J. Weldon, II and J.C. Matti (editors), The San Andreas Fault System: Displacement, Palinspastic Reconstruction, and Geologic Evolution. *Geological Society of America Memoir*, 178, 161-198, 1993.

Wilson, J., Microfracture fabric of the Punchbowl fault zone, San Andreas system, California, M.S. Thesis, T*exas A&M University*, in prep., 1998.

Wilson, J.E., J.S. Chester, and F.M. Chester, Microfracture analysis of fault growth and wear processes, Punchbowl Fault, San Andreas system, California. *Journal of Structural Geology*, 25, 1855-1873, 2003.

Chapter 2:

San Gabriel Fault

Introduction

The San Gabriel fault was the initial trace of the San Andreas system when it originated in the middle Miocene (Dibblee, 1968; Ehlig, 1971, 1973; Anderson et al., 1983). It is estimated that the San Gabriel fault system accumulated 42-45 km of right-lateral separation between ~12 Ma and 5 Ma (Powell and Weldon, 1992; Powell, 1993). It has since been abandoned and subsequently exhumed by tremendous uplift of the San Gabriel Mountains, beginning in the late Pliocene (Oakeshott, 1971; Ehlig, 1971; Morton and Baird, 1971; Dibblee, 1975; Anderson et al., 1983). This rapid uplift exposed crustal levels which were as deep as 2-5 km during the time that the San Gabriel fault was active (Oakeshott, 1971).

In the central San Gabriel Mountains, the San Gabriel fault diverges into the northern and southern branches. The North Branch San Gabriel fault continues eastward and terminates near the Vincent thrust and San Antonio faults, while the southern branch of the fault joins the frontal Cucamonga-Sierra Madre thrust (Figure 1). Two sites from the North Branch San Gabriel fault (i.e., east of the branch) are presented here: Big Tujunga and Bear Creek. One site, Little Tujunga, is from the main strand of the San Gabriel fault west of the branch (.

Like the Punchbowl fault, the North Branch San Gabriel fault localities have been important exposure for examining exhumed faults (Chester et al., 1993).

References

Anderson, J.L., R.H. Osborne, and D.F. Palmer, Cataclastic rocks of the San Gabriel fault—An expression of deformation at deeper crustal levels in the San Andreas fault. *Tectonophysics*, 98, 209-251, 1983.

Chester, F.M., J.P. Evans, and R.L. Biegel, Internal structure and weakening mechanisms of the San Andreas fault. *Journal of Geophysical Research*, 98, B1, 771-786, 1993.

Dibblee, T.W. Jr., Displacements on the San Andreas fault system in the San Gabriel, San Bernardino, and san Jacinto Mountains, southern California. In: *Proc. Conf. on Geologic Problems of San Andreas Fault System*. Stanford University Publications of Geological Science, 11, 260-276, 1968.

Dibblee, T.W., Jr., Late Quaternary uplift of the San Bernardino Mountains on the San Andreas and related faults, in San Andreas Fault in southern California; A guide to San Andreas fault from Mexico to Carrizo Plain, *California Division of Mines and Geology*, Spec. Rep., 118, edited by J.C. Crowell, 127-135, Sacramento, CA., 1975.

Ehlig, P.L., Pre-Cenozoic geology of the San Gabriel Mountains, southern California. *Geological Society of America*, 3, 116, 1971.

Ehlig, P.L., History, seismicity, and engineering geology of the San Gabriel fault, In: *Geology, Seismicity and Environmental Impact*, 247-251, Association of Engineering Geologists, Sudbury, Mass., 1973.

Morton, D.M. and A.K. Baird, The Paloma Valley ring-complex, southern California Batholith. *Geological Society of America*, 3, 167, 1971.

Oakeshott, G.B., Geology of the epicentral area. *California Division of Mines and Geology Bulletin*, 196, 19-30, 1971.

Powell, R.E., Balanced palinspastic reconstruction of pre-Late Cenozoic paleogeology, southern California: Geologic and kinematic constraints on evolution of the San Andreas fault system. In: R.E. Powell, R.J. Weldon, and J.C. Matti (editors), The San Andreas Fault System: Displacement, Palinspastic Reconstruction, and Geologic Evolution, *The Geological Society of America Memoirs*, 178, 1-107, 1993.

Powell, R.E. and R.J. Weldon, Evolution of the San Andreas Fault. *Annual Review of Earth Planetary Sciences*, 20, 431-468, 1992.

Schulz, S.E., Geochemical, petrologic, and structural characterization at multiple scales of deformation associated with the Punchbowl fault, southern California. M.S Thesis, *Utah State University*, 1997.

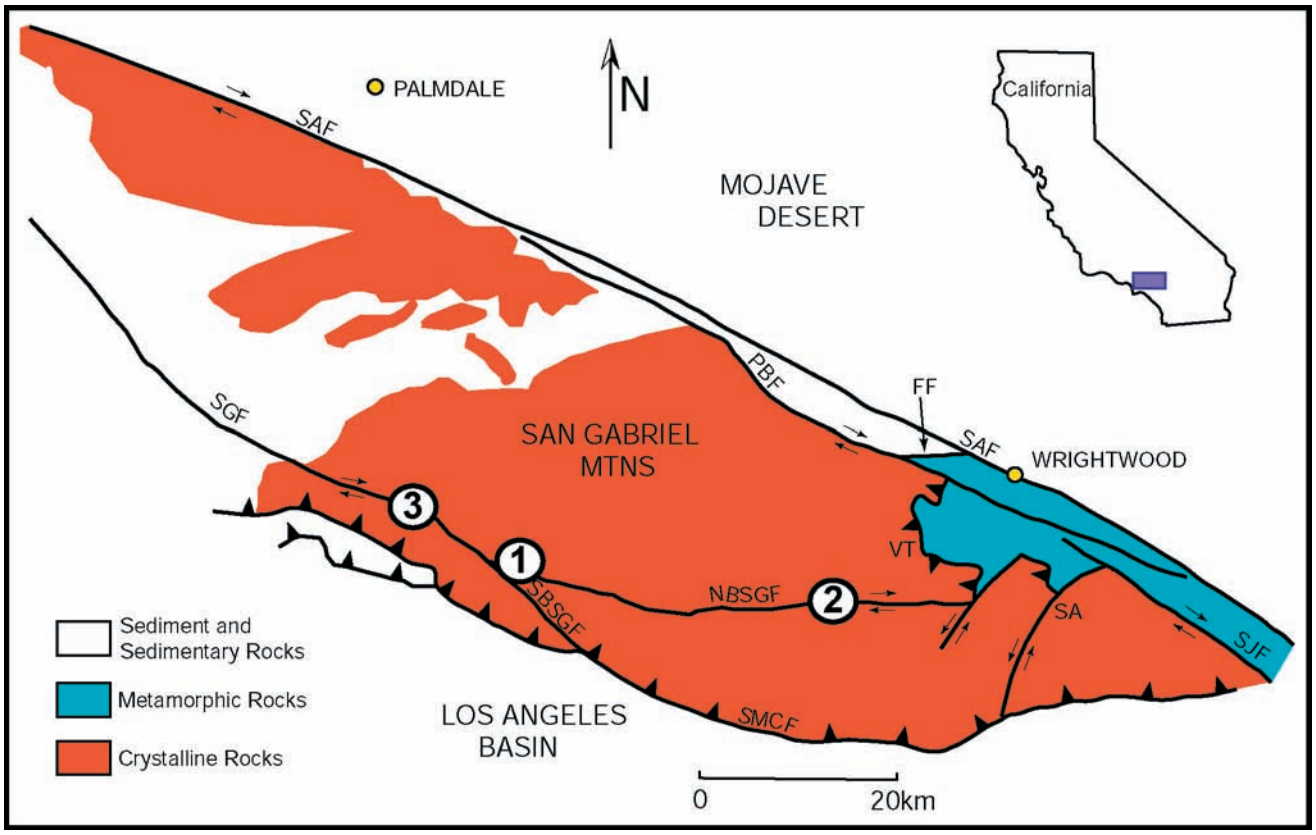

Figure 1. Simplified geologic map of the San Gabriel Mountains showing three sites along the San Gabriel fault: 1–Big Tujunga; 2–Bear Creek; 3–Little Tujunga. Other symbols include: FF–Fenner fault; PBF–Punchbowl fault; SAF–San Andreas fault; SA–San Antonio fault; SGF–San Gabriel fault (NBSGF–north branch; SBSGF–south branch); SJF–San Jacinto fault; SMCF–Sierra Madre-Cucamonga fault; VT–Vincent thrust. Adapted from Figure 3 of Schulz (1997).

Chapter 2: San Gabriel Fault

Site 1—Big Tujunga

Directions

All stops at this site are road cuts just off Big Tujunga Canyon Road (Figure 1).

From Sunland (north of Burbank)

1. Take the Sunland Blvd/Foothill Blvd exit off of I-210.
2. Go east on Foothill Blvd for ~ ¾ mile.
3. Turn left (north) onto Oro Vista Ave. This turns into Big Tujunga Canyon Road.

From La Canada (north of Pasadena)

1. Take Angeles Crest Highway (Highway 2) north until the intersection with Angeles Forest Highway.
2. At the intersection turn left onto Angeles Forest Highway, towards the junction with Big Tujunga Canyon Road.
3. At the junction, turn left onto Big Tujunga Canyon Road.

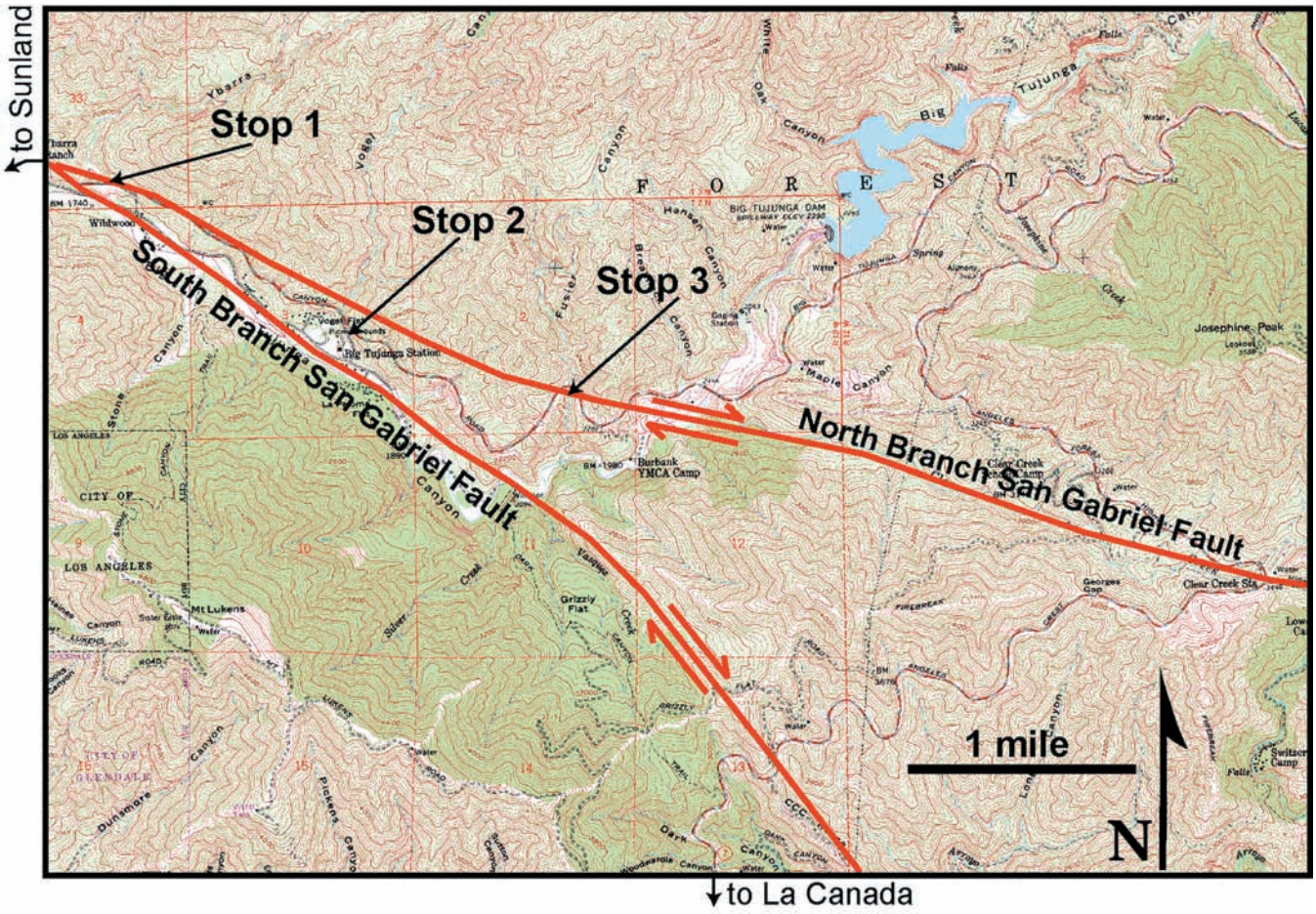

Figure 1. Topographic map from the Condor Peak Quadrangle of the Big Tujunga Canyon Road and accompanying stops. Approximate fault traces of the North and South Branch San Gabriel fault are shown, provided by Jennings and Strand (1969).

Geologic Setting

The San Gabriel fault was the initial trace of the San Andreas system when it originated in the middle Miocene (Dibblee, 1968; Ehlig, 1971, 1973; Anderson et al., 1983). It is estimated that the San Gabriel fault system accumulated 42-45 km of right-lateral separation between ~12 Ma and 5 Ma (Powell and Weldon, 1992; Powell, 1993). It has since been abandoned and subsequently exhumed through the tremendous uplift of the San Gabriel Mountains, beginning in the late Pliocene (Oakeshott, 1971; Ehlig, 1971; Morton and Baird, 1971; Dibblee, 1975; Anderson et al., 1983).

This rapid uplift exposed crustal levels which were as deep as 2-5 km during the time that the San Gabriel fault was active (Oakeshott, 1971). In the central San Gabriel Mountains, the San Gabriel fault diverges into the northern and southern branches. The North Branch San Gabriel fault (NBSGF) continues eastward and terminates near the Vincent thrust and San Antonio faults, while the southern branch of the fault joins the frontal Cucamonga-Sierra Madre thrust.

The Big Tujunga site consists of several road cuts that provide exposure of the North Branch San Gabriel fault just east of the branch (Figure 1). Rocks juxtaposed along the fault at these sites consist of granodiorite, gneiss, adamellite, and leucogranite (Anderson et al., 1983).

Figure 2. Photograph of the NBSGF at Stop 1 with view to the northwest. Note the variation in fault core thickness and the bulbous geometry in the upper portion of the photograph.

Locations and Descriptions of Stops 1, 2, and 3

Stop 1

This outcrop is located between Ybarra Ranch and the Wildwood picnic area on Big Tujunga Canyon Road. Parking is on the north side of the road.

UTM (WGS 84): 3795842 N, 0385464 E
Elevation: 1848 Feet

This stop has a good exposure of the fault core of the NBSGF (or possibly a parallel subsidiary fault) in granitic gneiss. The fault core has a strike of 315° and dips 65° to the north. The fault core is a mixture of maroon cataclasite and gray breccia, and it is typically 15-25 cm thick (Figure 2). Multiple slip surfaces can be seen within the fault core.

Stop 2 (Site 12, Anderson et al., 1983)

This outcrop is located at Vogel Flat on the east side of the road between Big Tujunga Canyon Road and Big Tujunga Station. Parking is available either on the west side of the road or next to a nearby picnic area.

UTM (WGS 84): 3794783 N, 0387167 E
Elevation: 1950 feet

The NBSGF at this stop is characterized by a 16.5 m wide fault zone. The fault rock is composed of granodiorite and consists primarily of gouge and breccia (Figure 3), which is different than the thin cataclasite fault core present at other locations along this fault. There are also more pronounced slip surfaces on the edges of the fault zone at this location.

Figure 3. Photomosaic of the NBSGF at Vogel Flats with view to the east. Note the broad zone of damage instead of a single centralized fault core.

Stop 3a

This stop is located on the west side of Fusier canyon, approximately ½ mile east of Big Tujunga Station. Parking is on both sides of the road and one can easily walk to Stop 3b from 3a.

UTM (WGS 84): 3794233 N, 0388682 E
Elevation: 2313 Feet

There are two strands of the NBSGF exposed on both sides of Fusier Canyon (Stops 3a and 3b). The north strand matches the description from Anderson et al. (1983) and is most likely the main strand. The north strand has a gray-maroon fault core composed predominantly of gouge and is typically less than 5 cm thick. The fault strikes 272° and dips 72° to the north.

Stop 3b (Site 14, Anderson et al. 1983)

This stop is located on the east side of Fusier Canyon, approximately ½ mile east of Big Tujunga Station.

UTM (WGS 84): 3794220 N, 0388862 E
Elevation: 2288 feet

There is excellent exposure of the NBSGF at this location (Figure 4). Anderson et al. (1983) describe the fault as being marked by a "… shear zone in adamellite and granitic gneiss. Strong foliation is locally developed. [The] fault has 5 cm wide zone of dense gouge, and granite on northwest side of the fault is shattered and friable." The thin, planar fault core has a strike of 280° and dips 86° to the north. There is also a 1-2 m thick shear zone (south strand) composed of highly foliated rock. There are green-coated slickensides present at the south strand that

Figure 4. Road cut exposing the NBSGF at Stop 3b with view to the southeast. Note the thin, planar fault core present at this location.

indicate predominantly strike-slip motion (i.e., very low rake angle), which is consistent with what we know about the NBSGF.

Seismological Implications

Grain-size analysis from the cataclastic rocks of the NBSGF reveals a finer grained gouge than what is present for the active trace of the San Andreas fault in southern California (Anderson et al., 1980). This zone is extremely narrow (several centimeters) at several localities along the NBSGF and the rock type is a dark, aphanitic, highly comminuted and indurated rock, or cataclasite (Anderson et al., 1983). The San Gabriel fault rocks show more mineralogic changes than the San Andreas fault rocks (Anderson et al., 1983). This may be attributed to the deeper crustal levels in which the San Gabriel fault exposures represent.

The dominant deformation mechanism for the San Gabriel fault is most likely cataclastic flow, where brittle deformation occurs via pervasive microfracturing, grain rotation, and sliding (Anderson et al., 1983). However, the overall fault core fabric is probably the result of subsequent flow, which combines the cataclastic process with diffusional and/or dislocation creep (Edington et al., 1976; Taplin et al., 1979; Anderson et al., 1983).

References

Anderson, J.L., R.H. Osborne, and D.F. Palmer, Petrogenesis of cataclastic rocks within the San Andreas fault zone of southern California, USA. *Tectonophysics*, 67, 221-249, 1980.

Anderson, J.L., R.H. Osborne, and D.F. Palmer, Cataclastic rocks of the San Gabriel fault—An expression of deformation at deeper crustal levels in the San Andreas fault. *Tectonophysics*, 98, 209-251, 1983.

Morton, D.M. and A.K. Baird, The Paloma Valley ring-complex, southern California Batholith. *Geological Society of America*, 3, 167, 1971.

Dibblee, T.W. Jr., Displacements on the San Andreas fault system in the San Gabriel, San Bernardino, and san Jacinto Mountains, southern California. In: Proc. Conf. on Geologic Problems of San Andreas Fault System. *Stanford University Publications of Geological Science*, 11, 260-276, 1968.

Dibblee, T.W., Jr., Late Quaternary uplift of the San Bernardino Mountains on the San Andreas and related faults, in San Andreas Fault in southern California; A guide to San Andreas fault from Mexico to Carrizo Plain, *California Division of Mines and Geology*, Spec. Rep. 118, edited by J.C. Crowell, 127-135, Sacramento, CA., 1975.

Edington, J.W., K.N. Melton, and C.P. Cutler, Superplasticity. *Progress in Materials Science*, 21, 63-170, 1976.

Ehlig, P.L., Pre-Cenozoic geology of the San Gabriel Mountains, southern California. *Geological Society of America*, 3, 116, 1971.

Ehlig, P.L., History, seismicity, and engineering geology of the San Gabriel fault, In: *Geology, Seismicity and Environmental Impact*, 247-251, Association of Engineering Geologists, Sudbury, Mass., 1973.

Jennings, C.W., and R.G. Strand, Los Angeles sheet, Geological map of California, scale 1:250,000. *California Division of Mines and Geology*, Sacramento, 1969.

Oakeshott, G.B., Geology of the epicentral area. *California Division of Mines and Geology Bulletin*, 196, 19-30, 1971.

Powell, R.E., Balanced palinspastic reconstruction of pre-Late Cenozoic paleogeology, southern California: Geologic and kinematic constraints on evolution of the San Andreas fault system. In: R.E. Powell, R.J. Weldon, and J.C. Matti (editors), The San Andreas Fault System: Displacement, Palinspastic Reconstruction, and Geologic Evolution, *The Geological Society of America Memoirs*, 178, 1-107, 1993.

Powell, R.E. and R.J. Weldon, Evolution of the San Andreas Fault. *Annual Review of Earth Planetary Sciences*, 20, 431-468, 1992.

Taplin, D.M.R., G.L. Dunlop, and T.G. Langdon, Flow and failure of superplastic materials. *Annual Review of Material Sciences*, 9, 151-189, 1979.

Chapter 2: San Gabriel Fault

Site 2—Little Tujunga

Directions

1. Take Osborne St. north from Foot Hill Blvd. just north of Hansen Dam Park in San Fernando. This becomes Little Tujunga Canyon Rd.
2. Continue on Little Tujunga Canyon Rd. towards Pacoima Resevoir.
3. Stop at "Earthquake Country" picnic site next to "945" red highway sign (Figure 1).
4. Fault exposure is ~30 feet up the trail.

   GPS (WGS 84): 3802234 N, 0372834 E
   Elevation: 2176 feet

Geologic Setting

The San Gabriel fault was the initial trace of the San Andreas system when it originated in the middle Miocene (Dibblee, 1968; Ehlig, 1971, 1973; Anderson et al., 1983). It is estimated that the San Gabriel fault system accumulated 42-45 km of right-lateral separation between ~12 Ma and 5 Ma (Powell and Weldon, 1992; Powell, 1993). It has since been abandoned and subsequently exhumed through the tremendous uplift of the San Gabriel Mountains, beginning in the late Pliocene (Oakeshott, 1971; Ehlig, 1971; Morton and Baird, 1971; Dibblee, 1975; Anderson et al., 1983).

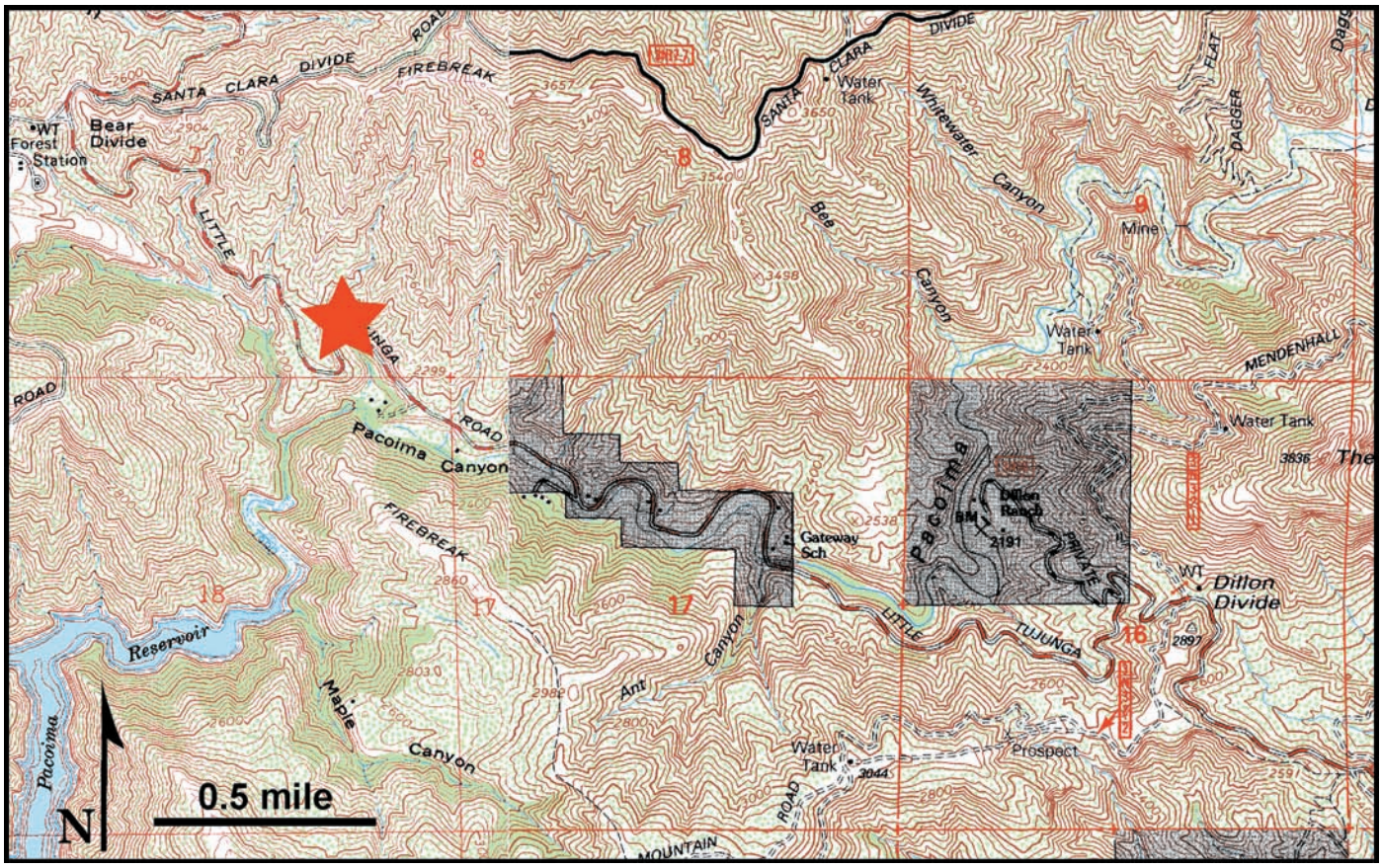

Figure 1. Stitched topographic map from the San Fernando and Sunland Quadrangles for the Little Tujunga site. The red star marks the location of the San Gabriel fault exposure.

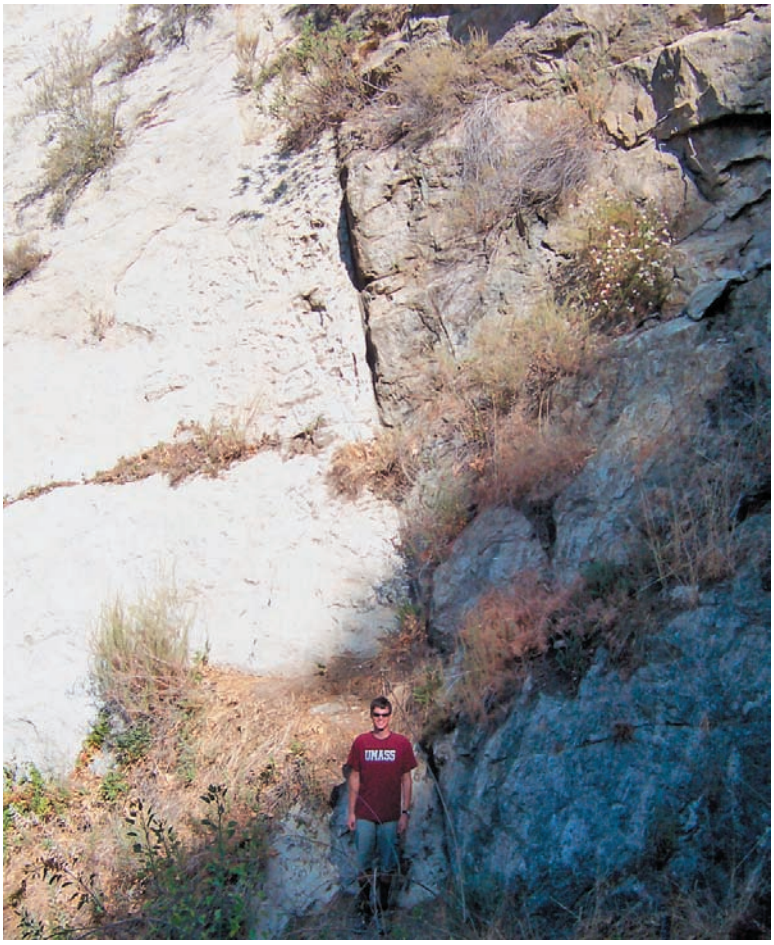

Figure 2. View to the west of the San Gabriel fault at Little Tujunga Canyon. Fault juxtaposes the Josephine Granodiorite on the left against the Mendenhall Gneiss on the right.

This rapid uplift exposed crustal levels which were as deep as 2-5 km during the time that the San Gabriel fault was active (Oakeshott, 1971). In the central San Gabriel Mountains, the San Gabriel fault diverges into the northern and southern branches. The North Branch San Gabriel fault (NBSGF) continues eastward and terminates near the Vincent thrust and San Antonio faults, while the southern branch of the fault joins the frontal Cucamonga-Sierra Madre thrust. The Little Tujunga site is west of the branch along the main portion of the San Gabriel fault.

Description (Site 8 of Anderson et al., 1983)

The San Gabriel fault at the Little Tujunga site has a strike of 270º and dips 81º to the north. The fault separates the late Cretaceous Josephine Granodiorite and the Precambrian Mendenhall Gneiss (Anderson et al., 1983). These distinct igneous and metamorphic protoliths on either side of the fault are cataclastically deformed, but show relatively little mineralogic alteration to within several meters of the fault core. The fault core has very defined, sharp boundaries and is approximately 4 cm thick. The cataclasite composing the fault core consists of 10-15% subangular porphyroclasts of feldspar, quartz, and lesser amounts of epidote, biotite, magnetite, and actinolite dispersed in a dense, aphanitic, and dark-colored matrix (Anderson et al., 1983).

Scanning electron microscope (SEM) photographs from the fault core at this site show that the very fine grained dark matrix is composed of interlocking, equidimensional grains (Anderson et al. 1983). Whole-rock geochemical analysis indicates

that the cataclasite was derived more from the Mendenhall Gneiss in the hanging wall than from the Josephine Granodiorite in the footwall (Anderson et al., 1983). This dense cataclasite of the fault core is thought to be associated with more deeply-eroded fault zones unlike the present trace of the San Andreas fault (Anderson et al., 1983).

Seismological Implications

Fault gouge and breccia are common along the San Gabriel fault where the cataclasized zone is several tens of meters wide (Anderson et al., 1983). Where this zone is extremely narrow (several centimeters), such as at Little Tujunga, the rock type is cataclasite; a dark, aphanitic, and highly-comminuted and indurated rock. Narrowing og the cataclasized zone is what would be expected at deeper, upper-crestal levels that are in the brittle deformation regine, and is consisitent with the estimated formation depth of the San Gabriel fault (Anderson et al., 1983)

The dominant deformation mechanism for the San Gabriel fault is most likely cataclastic flow, where brittle deformation occurs via pervasive microfracturing, grain rotation, and sliding (Anderson et al., 1983). However, the overall fault core fabric is probably the result of subsequent flow, which combines the cataclastic process with diffusional and/or dislocation creep (Edington et al., 1976; Taplin et al., 1979; Anderson et al., 1983).

References

Anderson, J.L., R.H. Osborne, and D.F. Palmer, Cataclastic rocks of the San Gabriel fault—An expression of deformation at deeper crustal levels in the San Andreas fault. *Tectonophysics*, 98, 209-251, 1983.

Baird, A.K., K.W. Baird, and D.M. Morton, On deciding whether trend surfaces of progressively higher order are meaningful; discussion. *Geological Society America Bulletin*, 82, 1219-1233, 1971.

Dibblee, T.W. Jr., Displacements on the San Andreas fault system in the San Gabriel, San Bernardino, and san Jacinto Mountains, southern California. In: Proc. Conf. on Geologic Problems of San Andreas Fault System. *Stanford University Publications of Geological Science*, 11, 260-276, 1968.

Dibblee, T.W., Jr., Late Quaternary uplift of the San Bernardino Mountains on the San Andreas and related faults, in San Andreas Fault in southern California; A guide to San Andreas fault from Mexico to Carrizo Plain, *California Division of Mines and Geology*, Spec. Rep. 118, edited by J.C. Crowell, 127-135, Sacramento, CA., 1975.

Ehlig, P.L., History, seismicity, and engineering geology of the San Gabriel fault, In: Geology, Seismicity and Environmental Impact, 247-251, *Association of Engineering Geologists*, Sudbury, Mass., 1973.

Ehlig, P.L., Origin and tectonic history of the basement terrain of the San Gabriel Mountains, central Transverse Ranges. In: W.G. Ernst (editor), *The Geotectonic Development of California*, Rubey vol. 1, pp. 584-600, Prentice-Hall, Englewood Cliffs, N.J., 1981.

Oakeshott, G.B., Geology of the epicentral area. *California Division of Mines and Geology Bulletin*, 196, 19-30, 1971.

Powell, R.E., Balanced palinspastic reconstruction of pre-Late Cenozoic paleogeology, southern California: Geologic and kinematic constraints on evolution of the San Andreas fault system. In: R.E. Powell, R.J. Weldon, and J.C. Matti (editors), The San Andreas Fault System: Displacement, Palinspastic Reconstruction, and Geologic Evolution, *The Geological Society of America Memoirs*, 178, 1-107, 1993.

Powell, R.E. and R.J. Weldon, Evolution of the San Andreas Fault. *Annual Review of Earth Planetary Sciences*, 20, 431-468, 1992.

Chapter 2: San Gabriel Fault

Site 3—Bear Creek

Directions

1. Drive north on Highway 39 from Azusa, passing both Morris and San Gabriel Reservoirs.
2. After approximately 10 miles, you will reach the West Fork of the San Gabriel River. Park either at the larger parking lot just past the gated trail head and walk across the bridge, or park at much smaller lot just before gate.
3. Hike west on the paved trail beside the West Fork San Gabriel River, which goes towards Bear Creek.
4. At the 1 mile marker, turn north on the hiking trail along Bear Creek (it is easiest to turn left and go underneath the bridge).
5. Just past the 6th stream crossing (usually marked with yellow spray paint), go through a campground towards a boulder-filled drainage. There is a wilderness sign between the 5th and 6th stream crossings.
6. The fault is exposed on the left (west) side of the stream at the mouth of the drainage (Figure 1).

   UTM (WGS 84): 3790138 N, 0418479 E
   Elevation: 1726 feet

The area discussed in Chester et al (1993) lies along the vertical exposure near the creek bed. This out crop can be difficult to access, due to the creek, and the vertical rock face is unstable.

Geologic Setting

The San Gabriel fault was the initial trace of the San Andreas system when it originated in the middle Miocene (Dibblee, 1968; Ehlig, 1971, 1973; Anderson et al., 1983). It is estimated that the San Gabriel fault system accumulated 42-45 km of right-lateral

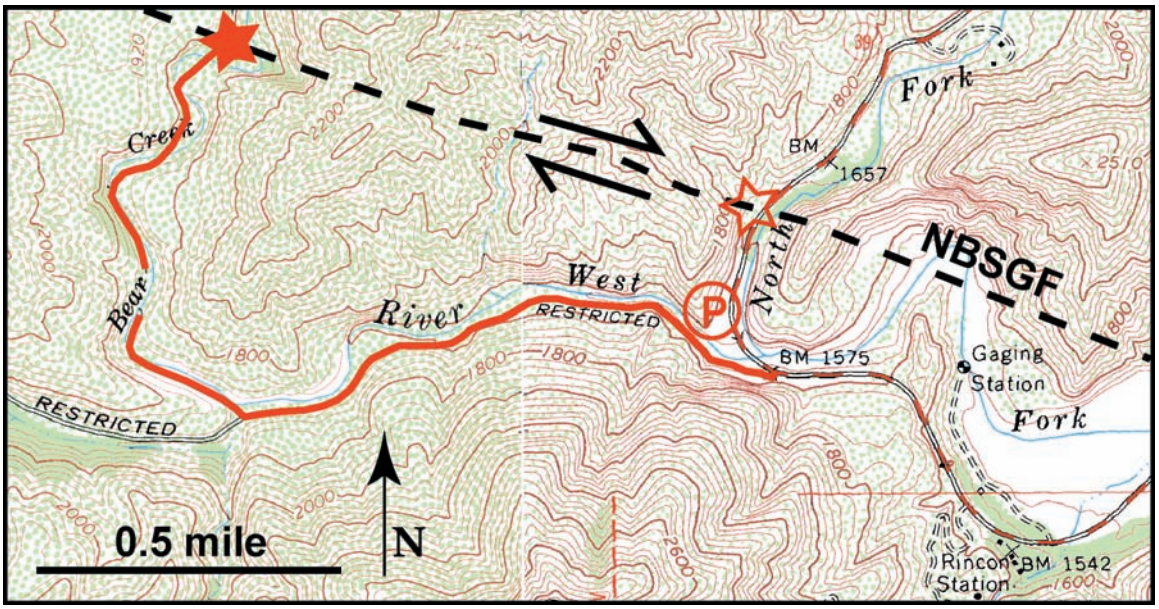

Figure 1. Stitched topographic map from the Glendora and Azusa Quadrangles for the Bear Creek site of the North Branch San Gabriel Fault (NBSGF). The circled "P" shows the parking lot, the solid star is the Bear Creek site, and the open star marks an additional fault exposure visible from the highway road cut.

separation between ~12 Ma and 5 Ma (Powell and Weldon, 1992; Powell, 1993). It has since been abandoned and subsequently exhumed by tremendous uplift of the San Gabriel Mountains, beginning in the late Pliocene (Oakeshott, 1971; Ehlig, 1971; Morton and Baird, 1971; Dibblee, 1975; Anderson et al., 1983).

This rapid uplift exposed crustal levels that were as deep as 2-5 km during the time that the San Gabriel fault was active (Oakeshott, 1971). In the central San Gabriel Mountains, the San Gabriel fault diverges into the northern and southern branches. The North Branch San Gabriel fault (NBSGF) continues eastward and terminates near the Vincent thrust and San Antonio faults, while the southern branch of the fault joins the frontal Cucamonga-Sierra Madre thrust. The northern branch cuts the San Gabriel crystalline basement complex and offsets distinct rock contacts by 16 km (Ehlig, 1981). The Bear Creek site is on the NBSGF on the West Fork of the San Gabriel River (Figure 1).

Description

The NBSGF at the Bear Creek site has a strike of 310° and dips steeply to the north. The fault zone contains a distinct igneous and metamorphic protolith on either side of the fault that is cataclastically deformed, but shows relatively little mineralogic alteration within several meters of the fault core (Evans and Chester, 1995). The protolith to the north consists of granite and granodiorite and the protolith to the south consists of diorite and granite (Evans and Chester, 1995). The fault zone is compartmentalized into a centralized layer of ultracataclasite within a narrow zone of foliated cataclasites that are in turn bounded by a much thicker damage zone (Chester et al., 1993) (Figure 2).

The total fault core thickness (i.e., ultracataclasite and cataclasite) at this site is approximately 35 cm, whereas the central ultracataclasite is only centimeters in thickness (Figure 3). The measured fracture density and mineralogic alteration increases dramatically in the foliated cataclasite as the fault core is approached (Chester et al., 1993). This increase in damage towards the fault core is seen well in thin section (Figure 4).

The foliated cataclasite consists of fault-parallel, planar to irregular layers of laumontite veins and clays that may account for as much as 50% of the total cataclasite volume (Evans and Chester, 1995). The mineralogy of the ultracataclasite in the fault core is composed of very fine-grained illite/smectite, montmorillonite, and laumontite (Chester et al., 1993). Overall, the rock in the fault core displays composite planar fabrics defined by mesoscopic shear surfaces and cataclastic S foliations (Chester et al., 1993). This fabric suggests that strain was partitioned into simple shear in the fault core and

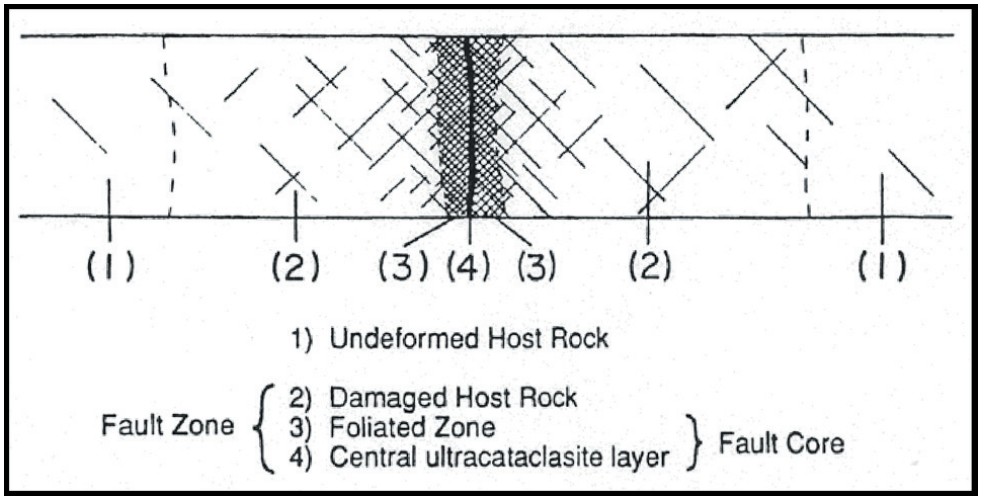

Figure 2. Schematic section across the NBSGF illustrating position of the structural zones of the fault. The diagram is not to scale (Figure 2 from chester et al. ,1993).

Figure 3. Close-up view of the fault zone looking to the northwest. The red arrow shows the extent of the 35 cm thick fault core. The outcrop is weathered and partially covered with vegetation and may require some cleaning in order to properly observe the fault character.

nearly fault-normal contraction in the damage zone (Chester et al., 1993).

The Bear Creek site shows extensive evidence of fluid-rock interactions, based on geochemical and petrographic analysis (Evans and Chester, 1995). Chester et al. (1993) show that fluids must have been present during deformation in order to create the hydrous syntectonic reaction products evidenced in the matrix and veins, high loss on ignition values, and overall textures of the fault rocks.

*Note: There is another exposure of the NBSGF beside the road approximately ¼ mile north of the parking lot (west of the North Fork of the San Gabriel River). There is not an observable fault core here like the Bear Creek site (it may be covered by vegetation). The rocks to the south are more altered with some foliation and subsidiary slip surfaces, whereas the rocks to the north are much harder and the deformation appears more ductile, as opposed to purely brittle cataclasis.

UTM (WGS 84): 3789687 N, 0419956 E
Elevation: 1626 feet

Seismological Implications

Numerous observations gathered from the San Andreas fault indicate that the fault zone is weak relative to the surrounding crust [see Hickman (1991) for a complete review]. Study of the internal structure of the NBSGF at the Bear Creek site may represent the structure of active mature faults near the top of the seismogenic regime (i.e., several kilometers depth) and thus can serve as a good mechanical analog to the modern San Andreas fault (Chester et al., 1993).

The weak nature of mature large-displacement fault zones can be explained if there is a dynamic weakening mechanism for propagating and sustaining unstable slip (Chester et al., 1993). Several dynamic weakening mechanisms have been proposed: (1) dynamic lubrication processes (Brodsky and Kanamori, 2001), (2) transient normal stress reductions (e.g., Melosh, 1979; Heaton, 1990), and (3) thermal pressurization (Sibson, 1973). The lack of pseudotachylyte in the San Gabriel fault (as well as the Punchbowl fault) suggests that the lubrication of fault surfaces by frictional melt is not appropriate here. A dynamic weakening by transient normal stress reduction is compatible with the interpretation that the ultracataclasite microstructures are diagnostic of slip at low effective stress, but the significance of this process to seismic faulting is uncertain (Brune, 1991) and it is unclear why this mechanism would operate on the San Andreas fault, but not all other seismogenic faults (Chester et al., 1993).

The favored mechanism of dynamic weakening is thermal pressurization due to the thermal expansion of fluids caused by frictional heating in the fault core during coseismic slip (Chester et al., 1993). This increase in pore-fluid pressure reduces the effective normal stress and the dynamic shear strength of the fault (Sibson, 1973) and could be generated during the life of the fault by a combination of processes including coseismic dilatancy and creation of permeability in the fault core, fault-valve behavior to recharge the fault core with fluid, post-seismic self-healing of fracture networks to reduce permeability and therefore trap fluids in the fault core, and time-dependent compaction of the core during interseismic periods to generate high pore pressure (Chester et al., 1993). Observations from the NBSGF indicate that the characteristics neces-

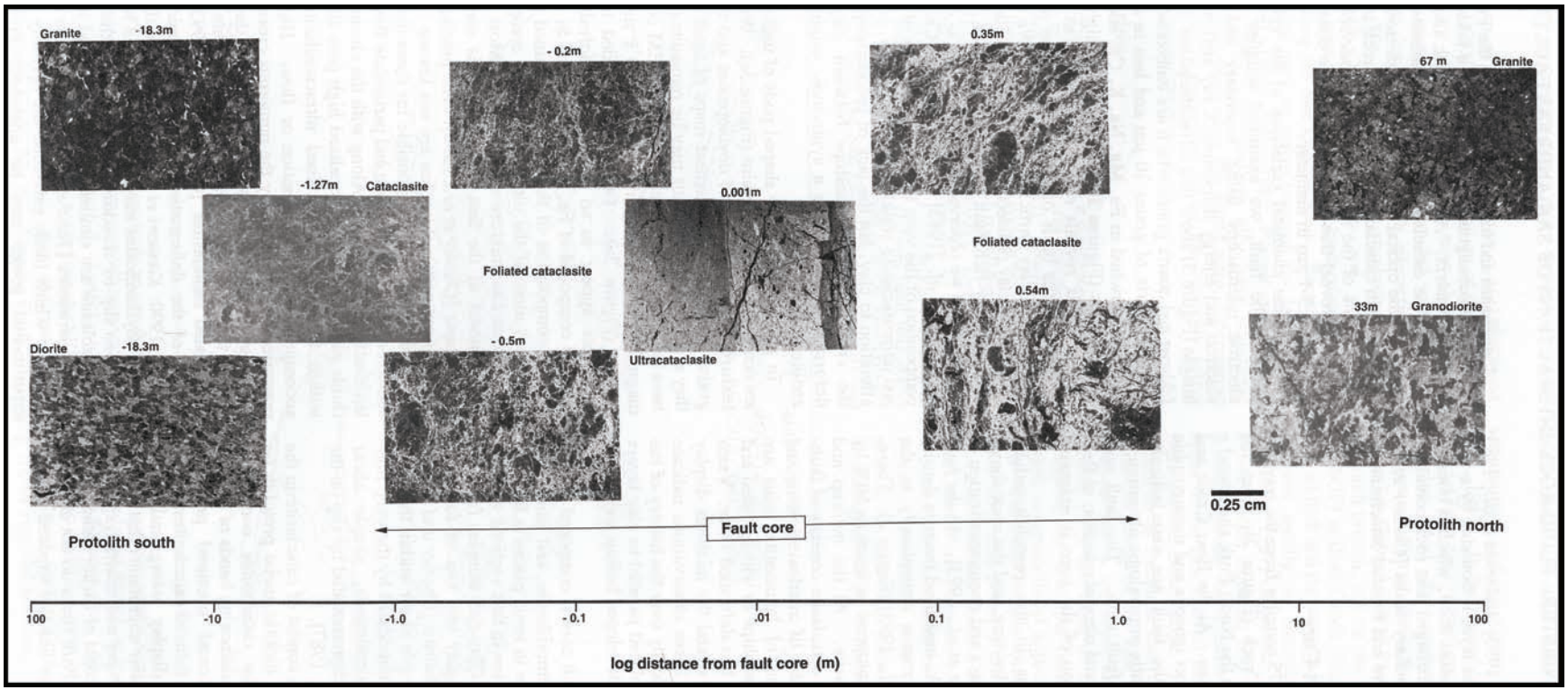

Figure 4. Petrographic traverse across the San Gabriel fault at Bear Creek. Photos are direct exposures of thin sections and thus provide a negative image of the thin sections. Rocks from the traverse reveal groupings into relatively unaltered and undeformed granitic and granodiorite protoliths to the north and diorite and granite to the south, which bound the fault core composed of foliated cataclasite and ultracataclasite. Fault core thickness is approximately 3 m. Scale bar applies to all photos. (Figure 2 from Evans and Chester, 1995.)

sary for frictional heating and thermal pressurization are present and that localization of slip to the thin (i.e., centimeters) ultracataclasite layer would cause frictional heating to be concentrated during seismic slip (Chester et al., 1993).

References

Anderson, J.L., R.H. Osborne, and D.F. Palmer, Cataclastic rocks of the San Gabriel fault—An expression of deformation at deeper crustal levels in the San Andreas fault. *Tectonophysics*, 98, 209-251, 1983.

Brodsky, E.E. and H. Kanamori, Elastohydrodynamic lubrication of faults. *Journal of Geophysical Research*, 106, B8, 16,357-16,374, 2001.

Brune, J.N., Seismic source dynamics, radiation and stress. *Reviews of Geophysics*, 29, 688-699, 1991.

Chester, F.M., J.P. Evans, and R.L. Biegel, Internal structure and weakening mechanisms of the San Andreas fault. *Journal of Geophysical Research*, 98, B1, 771-786, 1993.

Dibblee, T.W. Jr., Displacements on the San Andreas fault system in the San Gabriel, San Bernardino, and san Jacinto Mountains, southern California. In: Proc. Conf. on Geologic Problems of San Andreas Fault System. *Stanford University Publications of Geological Science*, 11, 260-276, 1968.

Dibblee, T.W., Jr., Late Quaternary uplift of the San Bernardino Mountains on the San Andreas and related faults, in San Andreas Fault in southern California; A guide to San Andreas fault from Mexico to Carrizo Plain, California *Division of Mines and Geology*, Spec. Rep. 118, edited by J.C. Crowell, 127-135, Sacramento, CA., 1975.

Ehlig, P.L., History, seismicity, and engineering geology of the San Gabriel fault, In: *Geology, Seismicity and Environmental Impact*, 247-251, Association of Engineering Geologists, Sudbury, Mass., 1973.

Ehlig, P.L., Origin and tectonic history of the basement terrain of the San Gabriel Mountains, central Transverse Ranges. In: W.G. Ernst (editor), *The Geotectonic Development of California*, Rubey vol. 1, pp. 584-600, Prentice-Hall, Englewood Cliffs, N.J., 1981.

Evans, J.P. and F.M. Chester. Fluid-rock interaction in faults of the San Andreas system: Inferences form San Gabriel fault rock geochemistry and microstructures. *Journal of Geophysical Research*, 100, B7, 13,007-13,020, 1995.

Heaton, T.H., Evidence for and implication of self-healing pulses of slip in earthquake rupture. *Physics of The Earth and Planetary Interiors*, 64, 1-20, 1990.

Hickman, S.H., Stress in the lithosphere and the strength of active faults. U.S. Natl. Rep. Int. Union Geod. Geophys., 1987-1990, *Reviews of Geophysics*, 29, 759-775, 1991.

Melosh, H.J., Acoustic fluidization: A new geologic process? *Journal of Geophysical Research*, 84, 7513-7520, 1979.

Oakeshott, G.B., Geology of the epicentral area. *California Division of Mines and Geology Bulletin*, 196, 19-30, 1971.

Powell, R.E., Balanced palinspastic reconstruction of pre-Late Cenozoic paleogeology, southern California: Geologic and kinematic constraints on evolution of the San Andreas fault system. In: R.E. Powell, R.J. Weldon, and J.C. Matti (editors), The San Andreas Fault System: Displacement, Palinspastic Reconstruction, and Geologic Evolution, *The Geological Society of America Memoirs*, 178, 1-107, 1993.

Powell, R.E. and R.J. Weldon, Evolution of the San Andreas Fault. *Annual Review of Earth Planetary Sciences*, 20, 431-468, 1992.

Sibson, R.H., Interactions between temperature and fluid pressure during earthquake faulting, a mechanism for partial or total stress relief. *Nature*, 243, 66-68, 1973.

Chapter 3: San Andreas Fault

Introduction

The San Andreas fault is the most prominent member of the active transform plate boundary between the North American and Pacific plates and forms a continuous 1,100-km-long link between the Mendocino fracture zone to the north and the spreading system in the Gulf of California to the south (Powell, 1993). The San Andreas fault may very well be the most intensely studied transform fault in the world. Total displacement on the San Andreas fault system since its inception in the Miocene is generally thought to be 315 ± 10 km (Matti and Morton, 1993).

However, in southern California this total displacement is partitioned into several distinct fault strands such as the San Andreas, San Jacinto, Punchbowl, San Gabriel, and Banning faults, as well as other less-known structures (Matti and Morton, 1993). There is significant disagreement with respect to the total displacement of the San Andreas fault proper in southern California. Matti and Morton (1993) propose that the San Andreas fault proper in southern California has had no more than 160 km of displacement.

Numerous observations suggest that the San Andreas fault zone is weak relative to the surrounding crust (Hickman, 1991; Chester et al., 1993; Evans and Chester, 1995). Heat flow measurements (Brune et al., 1969; Lachenbruch and Sass, 1980), in situ stress measurements (Hickman, 1991; Zoback and Healy, 1992), and focal mechanism data (Jones, 1988) indicate that fault slip occurs under low shear stress, with the maximum principal stress at a high angle to the fault plane. Several mechanisms have been proposed to explain this "weak fault" phenomenon and include high pore fluid pressures in the fault (Byerlee, 1990; Rice, 1992), low coefficient of friction of fault zone materials (Chester et al., 1993), and weakening processes induced by dynamic slip (Heaton, 1990).

This field guide presents three sites to look at the San Andreas fault (Figure 1). It also summarizes the paleoseismic work from the Wrightwood area. We would like to remind the reader that these localities are the surface representation of this large transform fault and do not necessarily represent the fault geometry at seismic depth. It is thought that wrench faults, like the San Andreas, may become wider towards the surface of the earth, possibly branching into multiple strands called flower structures (Weldon et al., 2002). Therefore, the San Andreas fault does not provide good exposure to examine fault structure and composition in order to asses earthquake processes at depth.

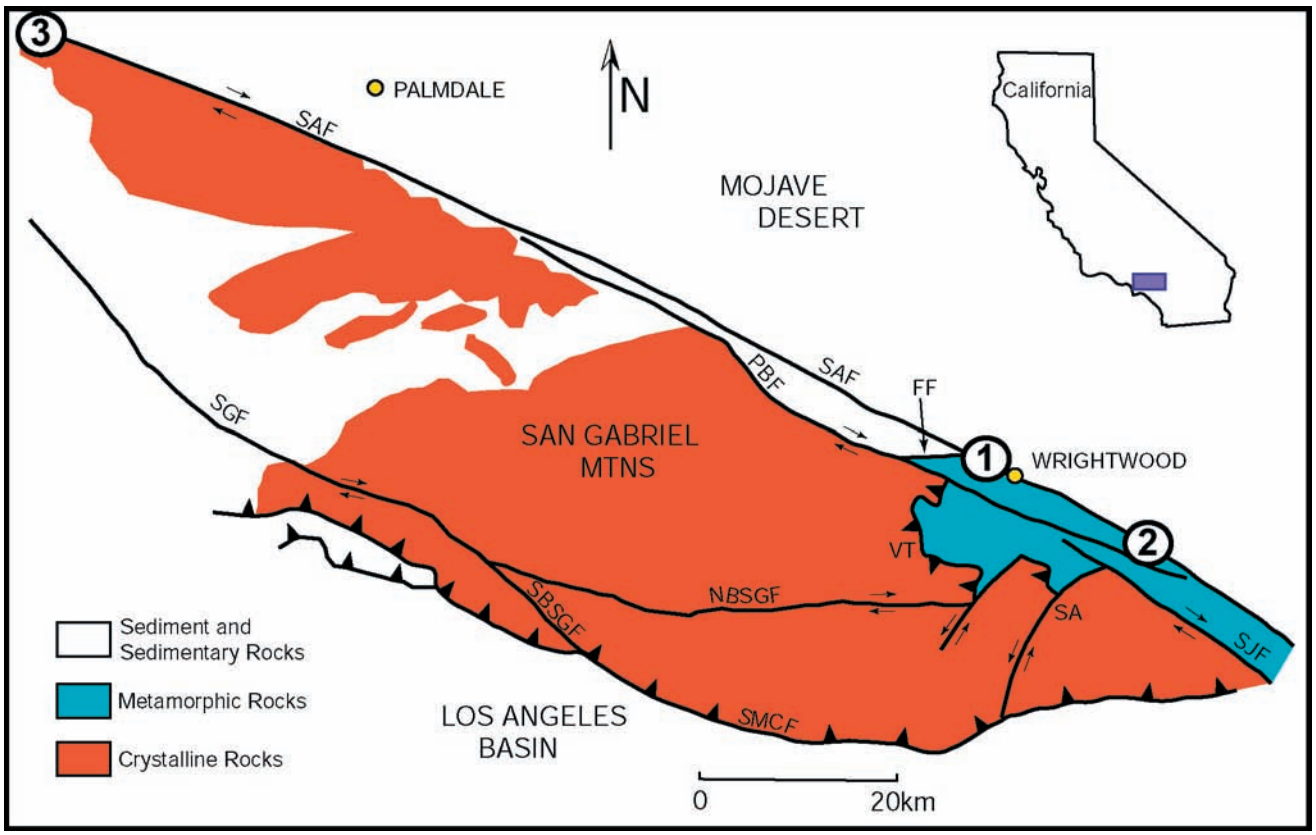

Figure 1. Simplified geologic map of the San Gabriel Mountains showing three sites along the San Andreas fault: 1–Apple Valley; 2–Cajon Pass; 3–Lake Hughes. Other symbols include: FF–Fenner fault; PBF–Punchbowl fault; SAF–San Andreas fault; SA–San Antonio fault; SGF–San Gabriel fault (NBSGF–north branch; SBSGF–south branch); SJF–San Jacinto fault; SMCF–Sierra Madre-Cucamonga fault; VT–Vincent thrust. Adapted from Figure 3 of Schulz (1997).

References

Brune, J.N., T.L. Henyey, and R.F. Roy, Heat flow, stress and rate of slip along the San Andreas fault, California. *Journal of Geophysical Research*, 74, 3821-3827, 1969.

Byerlee, J., Friction, overpressure, and fault normal compression. *Geophysical Research Letters*, 17, 2109-2112, 1990.

Chester, F.M., J.P. Evans, and R.L. Biegel, Internal structure and weakening mechanisms of the San Andreas fault. *Journal of Geophysical Research*, 98, B1, 771-786, 1993.

Evans, J.P. and F.M. Chester. Fluid-rock interaction in faults of the San Andreas system: Inferences form San Gabriel fault rock geochemistry and microstructures. *Journal of Geophysical Research*, 100, B7, 13,007-13,020, 1995.

Heaton, T.H., Evidence for and implication of self-healing pulses of slip in earthquake rupture. *Physics of The Earth and Planetary Interiors*, 64, 1-20, 1990.

Hickman, S.H., Stress in the lithosphere and the strength of active faults. U.S. Natl. Rep. Int. Union Geod. Geophys., 1987-1990, *Reviews of Geophysics*, 29, 759-775, 1991.

Jones, L.M., Focal mechanisms and the state of stress on the San Andreas fault in southern California. *Journal Geophysical Research*, 93, 11,883-11844, 1988.

Lachenbruch, A.H. and J.H. Sass, Heat flow and energetics of the San Andreas fault zone. *Journal of Geophysical Research*, 85, 6185-6222, 1980.

Matti, J.C. and D.M. Morton, Paleogeographic evolution of the San Andreas fault in southern California: A reconstruction based on a new cross-fault correlation. In: Powell, R.E., Weldon II, R.J., Matti, J.C. (editors), The San Andreas Fault System: Displacement, Palinspastic Reconstruction, and Geologic Evolution. *The Geological Society of America Memoirs*, 178, 107-160, 1993.

Powell, R.E., Balanced palinspastic reconstruction of pre-Late Cenozoic paleogeology, southern California: Geologic and kinematic constraints on evolution of the San Andreas fault system. In: R.E. Powell, R.J. Weldon, and J.C. Matti (editors), The San Andreas Fault System: Displacement, Palinspastic Reconstruction, and Geologic Evolution, *The Geological Society of America Memoirs*, 178, 1-107, 1993.

Rice, J.R., Fault stress states, pore pressure distributions, and the weakness of the San Andreas fault. In: Evans, B. and T. F. Wong (editors), *Fault Mechanics and Transport Properties in Rocks*, 475-503, Academic, San Diego, Calif., 1992.

Schulz, S.E., Geochemical, petrologic, and structural characterization at multiple scales of deformation associated with the Punchbowl fault, southern California. M.S Thesis, *Utah State University*, Utah, 1997.

Weldon, R.J. II, T.E. Fumal, T.J. Powers, S.K. Pezzopane, K.M. Scharer, and J.C. Hamilton. Structure and earthquake offsets on the San Andreas fault at the Wrightwood, California, Paleoseismic site. *Bulletin of the Seismological Society of America*, 92, no. 7, 2704-2725, 2002.

Zoback, M.D. and J.H. Healy, In situ stress measurements to 3.5 km depth in the Cajon Pass scientific borehole: Implications for the mechanics of crustal faulting. *Journal of Geophysical Research*, 97, 5039-5057, 1992.

Chapter 3: San Andreas Fault

Site 1—Apple Valley

Directions

1. Drive west on Highway 2 from Wrightwood.
2. Take the right hand fork at Big Pines Station towards Pear Blossom on Big Pines Hwy.
3. Continue 1.7 miles to Appletree Flat, just past a sharp left curve in the road.
4. Parking is on the right (northwest) side of the road and the outcrop is on the southeast side (Figure 1).

   UTM (WGS 84): 3805576 N, 0434734 E
   Elevation: 6234 feet

Geological Setting

The San Andreas fault is the most prominent member of the active transform plate boundary between the North American and Pacific plates and forms a continuous 1,100-km-long link between the Mendocino fracture zone to the north and the spreading system in the Gulf of California to the south (Powell, 1993). Total displacement on the San Andreas fault system since its inception in the Miocene is generally thought to be 315 ± 10 km (Matti and Morton, 1993). However, in southern California this total displacement is partitioned into several distinct fault strands such as the San Andreas, San Jacinto, Punchbowl, San Gabriel, and Banning faults, as well as other less-known structures (Matti and Morton, 1993). Matti and Morton (1993) propose that the San Andreas fault proper in southern California has had no more than 160 km of displacement.

Numerous observations suggest that the San Andreas fault zone is weak relative to the surround-

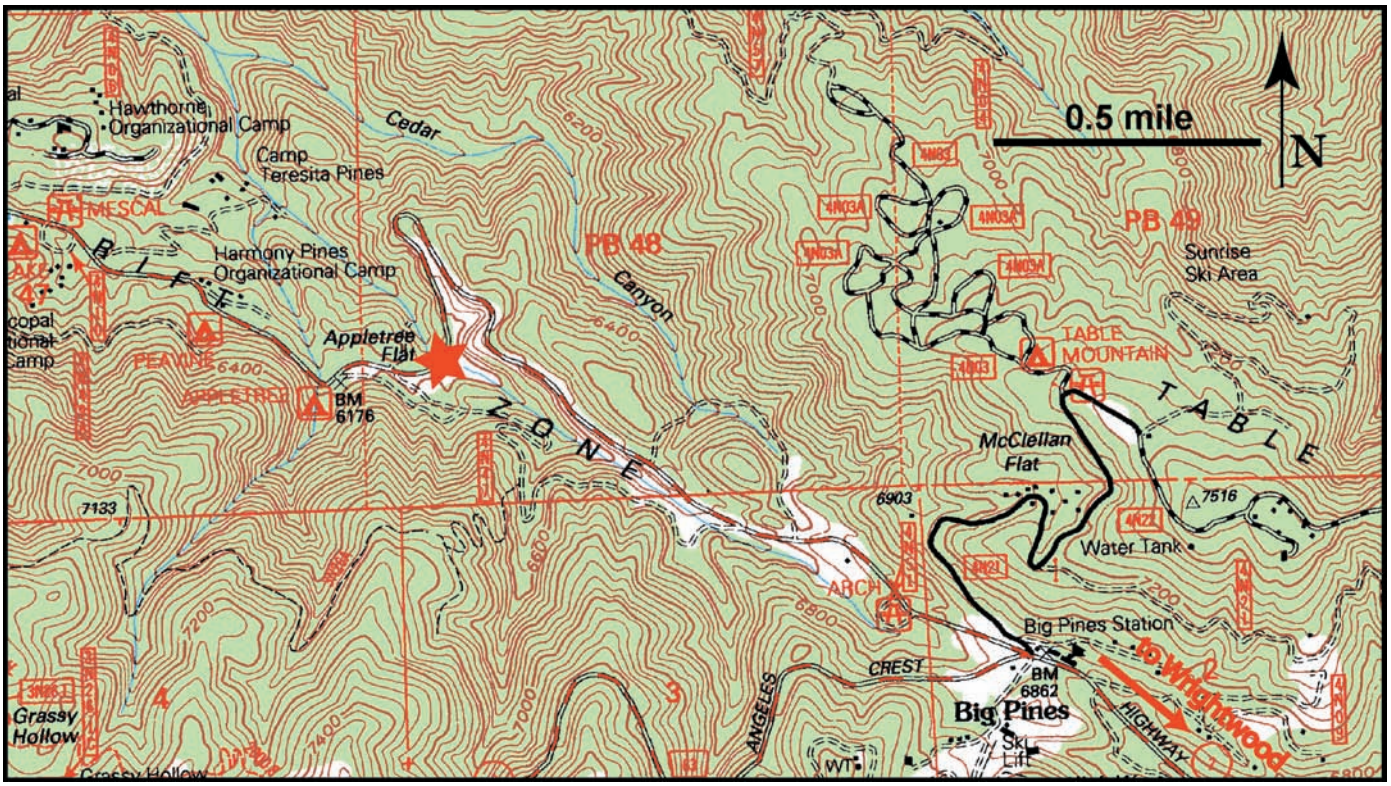

Figure 1. Topographic map from the Mescal Creek Quadrangle of the Appletree Flat exposure of the San Andreas fault. The red star marks the site location.

ing crust (Hickman, 1991; Chester et al., 1993; Evans and Chester, 1995). Heat flow measurements (Brune et al., 1969; Lachenbruch and Sass, 1980), in situ stress measurements (Hickman, 1991; Zoback and Healy, 1992), and focal mechanism data (Jones, 1988) indicate that fault slip occurs under low shear stress, with the maximum principal stress at a high angle to the fault plane. Several mechanisms have been proposed to explain this "weak fault" phenomenon and include high pore fluid pressures in the fault (Byerlee, 1990; Rice, 1992), low coefficient of friction of fault zone materials (Chester et al., 1993), and weakening processes induced by dynamic slip (Heaton, 1990).

Description (Site 2 from Anderson et al., 1980)

The San Andreas fault is expressed here as a wide zone of damage, with no primary fault core (Figure 2). The fault zone is < 0.5 km wide and separates granite gneiss from the Pelona schist (Anderson et al., 1980). There are some vertical slip features as well as chemical alteration of the host rock. Veins and fractures are also prevalent. It is thought that the fault zone may narrow at depth, more like the exhumed exposures of the Punchbowl and San Gabriel faults.

Samples from gouge zones near this site were texturally analyzed by Anderson et al. (1980). The results show that most of the particles fall in the sand and silt range (Figure 3). Fault gouge from the San Andreas fault at this site is essentially a rock flour with a mineralogy representing the comminuted equivalent of the host rock (Anderson et al., 1980). Clay development in the gouge is minimal and geochemical alterations involve oxidation, some hydration of ferromagnesian silicates, and the introduction of calcite (Anderson et al., 1980).

Figure 2. Typical surface expression of the San Andreas fault at the Appletree Flat Site showing a wide zone of damage.

Seismological Implications

Anderson et al. (1980) describe several points of interest at this site:

> "The original fabric of these rocks is commonly not disrupted during the cataclasis. It is evident that the gouge development in these primarily igneous crystalline terranes is largely an in situ process with minimal mixing of rock types. Fabric analyses reveal that brecciation (shattering), not shearing, is the major deformational mechanism at these upper crustal levels....
>
> Scholz et al. (1972) noted that the development of gouge [in experimental studies] allowed the samples to reach a steady-state frictional behavior and that the gouge seems to have the effect of reducing the stress drops to a small fraction of their value for clean ground surfaces. The latter feature concurs with the suggestion by Stesky and Brace (1973) that the presence of low strength alteration materials in the San Andreas fault zone may account for the low frictional shear stress estimates provided from heat flow data relative to the much higher estimates from high-temperature frictional studies….
>
> Logan (1977;1978 a, b) has shown that stable sliding is a consequence of low pressure and, even with the presence of fault gouge, the failure characteristics become increasingly unstable and change to a catastrophic stick-slip mode of displacement as the confining pressure is increased. The transition from stable to stick-slip motion is very dependent upon mineralogy. For quartz and feldspar gouge the mechanical transition is at about 2.5kb. For soft minerals with a high degree of compaction characteristics, such as carbonates, the transition occurs at about 1.0 kb." (Anderson, et al., 1980, pg. 221-223).

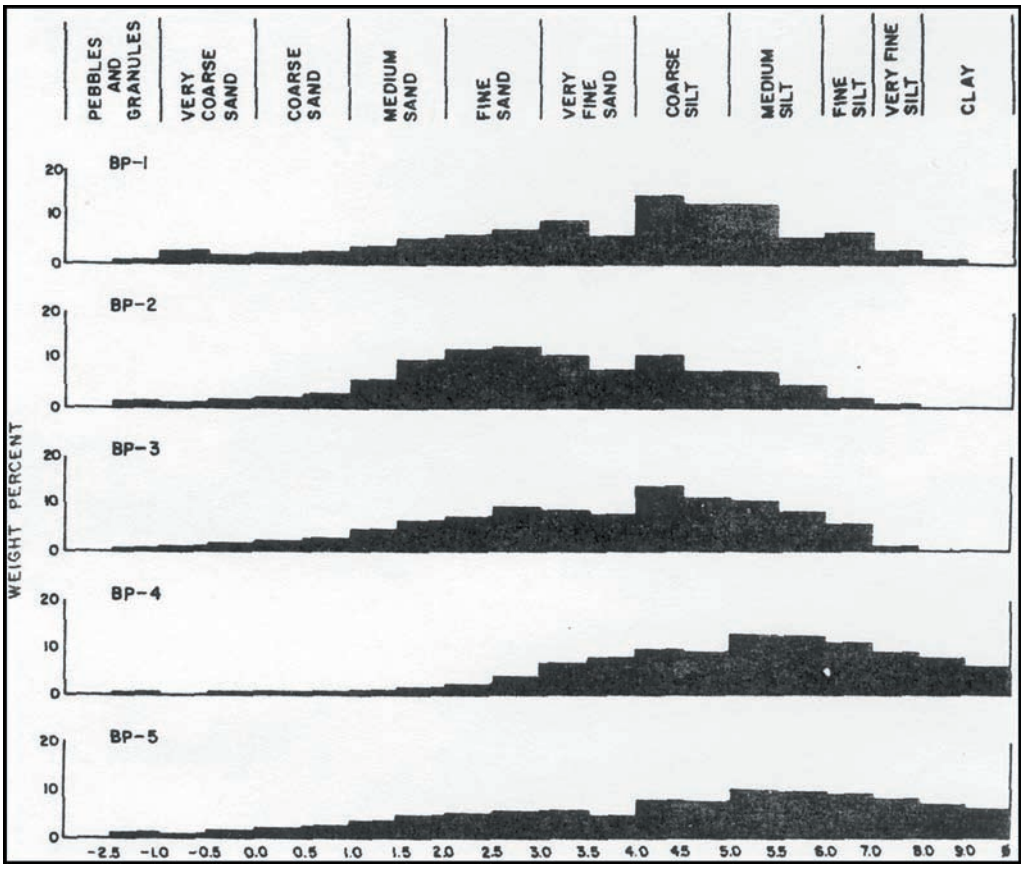

Figure 3. Histograms showing grain-size distribution of five gouge samples at this site. [Figure 7 from Anderson et al. (1980).]

References

Anderson, J.L., R.H. Osborne, and D.F. Palmer, Petrogenesis of cataclastic rocks within the San Andreas fault zone of southern California, USA. *Tectonophysics*, 67, 221-249, 1980.

Brune, J.N., T.L. Henyey, and R.F. Roy, Heat flow, stress and rate of slip along the San Andreas fault, California. *Journal of Geophysical Research*, 74, 3821-3827, 1969.

Byerlee, J., Friction, overpressure, and fault normal compression. *Geophysical Research Letters*, 17, 2109-2112, 1990.

Chester, F.M., J.P. Evans, and R.L. Biegel, Internal structure and weakening mechanisms of the San Andreas fault. *Journal of Geophysical Research*, 98, B1, 771-786, 1993.

Evans, J.P. and F.M. Chester. Fluid-rock interaction in faults of the San Andreas system: Inferences form San Gabriel fault rock geochemistry and microstructures. *Journal of Geophysical Research*, 100, B7, 13,007-13,020, 1995.

Heaton, T.H., Evidence for and implication of self-healing pulses of slip in earthquake rupture. *Physics of The Earth and Planetary Interiors*, 64, 1-20, 1990.

Hickman, S.H., Stress in the lithosphere and the strength of active faults. U.S. Natl. Rep. Int. Union Geod. Geophys., 1987-1990, *Reviews of Geophysics*, 29, 759-775, 1991.

Jones, L.M., Focal mechanisms and the state of stress on the San Andreas fault in southern California. *Journal Geophysical Research*, 93, 11,883-11844, 1988.

Lachenbruch, A.H. and J.H. Sass, Heat flow and energetics of the San Andreas fault zone. *Journal of Geophysical Research*, 85, 6185-6222, 1980.

Logan, J.M., Creep, stable sliding and premonitory slip. In: *Proceedings of Conference II; experimental studies of rock friction with application to earthquake prediction*, U.S. Geological Survey, Menlo Park, California, 1977.

Logan, J.M., Creep, stable sliding and premonitory slip. In: Rock friction and earthquake prediction, *Pure and Applied Geophysics*, 116, 773-789, 1978a.

Logan, J.M., Experimental studies of fold and thrust faults. *Abstracts with Programs–Geological Society of America*, 10, 21, 1978b.Matti, J.C. and D.M. Morton, Paleogeographic evolution of the San Andreas fault in southern California:

A reconstruction based on a new cross-fault correlation. In: Powell, R.E., Weldon II, R.J., Matti, J.C. (editors), The San Andreas Fault System: Displacement, Palinspastic Reconstruction, and Geologic Evolution. *The Geological Society of America Memoirs*, 178, 107-160, 1993.

Powell, R.E., Balanced palinspastic reconstruction of pre-Late Cenozoic paleogeology, southern California: Geologic and kinematic constraints on evolution of the San Andreas fault system. In: R.E. Powell, R.J. Weldon, and J.C. Matti (editors), The San Andreas Fault System: Displacement, Palinspastic Reconstruction, and Geologic Evolution, *The Geological Society of America Memoirs*, 178, 1-107, 1993.

Rice, J.R., Fault stress states, pore pressure distributions, and the weakness of the San Andreas fault. In: Evans, B. and T. F. Wong (editors), *Fault Mechanics and Transport Properties in Rocks*, 475-503, Academic, San Diego, Calif., 1992.

Scholz, C., P. Molnar, and T. Johnson, Detaile studies of frictional sliding of granite and implications for the earthquake mechanism. *Journal of Geophysical Research*, 77, 6392-6406, 1972.

Stesky, R.M. and W.F. Brace, Estimation of frictional stress on the San Andreas Fault from laboratory measurements. Stanford University Publications, *Geological Sciences*, 13, 206-214, 1973.

Zoback, M.D. and J.H. Healy, In situ stress measurements to 3.5 km depth in the Cajon Pass scientific borehole: Implications for the mechanics of crustal faulting. *Journal of Geophysical Research*, 97, 5039-5057, 1992.

Chapter 3: San Andreas Fault

Site 2—Cajon Pass

Directions

1. Head northbound on I-15 from Rancho Cucamonga. Approximately 4 miles past the I-215 merger, pull off interstate at a wide parking lot on the right (Figure 1). It is marked with an emergency parking only sign.

   UTM (WGS 84) [of parking area]**:** 3791126 N, 0458648 E
   Elevation: 2875 feet
2. From the parking lot hike east down the gravel road.
3. At the bottom of the road, turn left (north) and proceed uphill for approximately half a mile to the paved road coming in from the west.

   UTM (WGS 84): 3791359 N, 0458909 E
   Elevation: 3060 feet

Geologic Setting

The San Andreas fault is the most prominent member of the active transform plate boundary between the North American and Pacific plates and forms a continuous 1,100-km-long link between

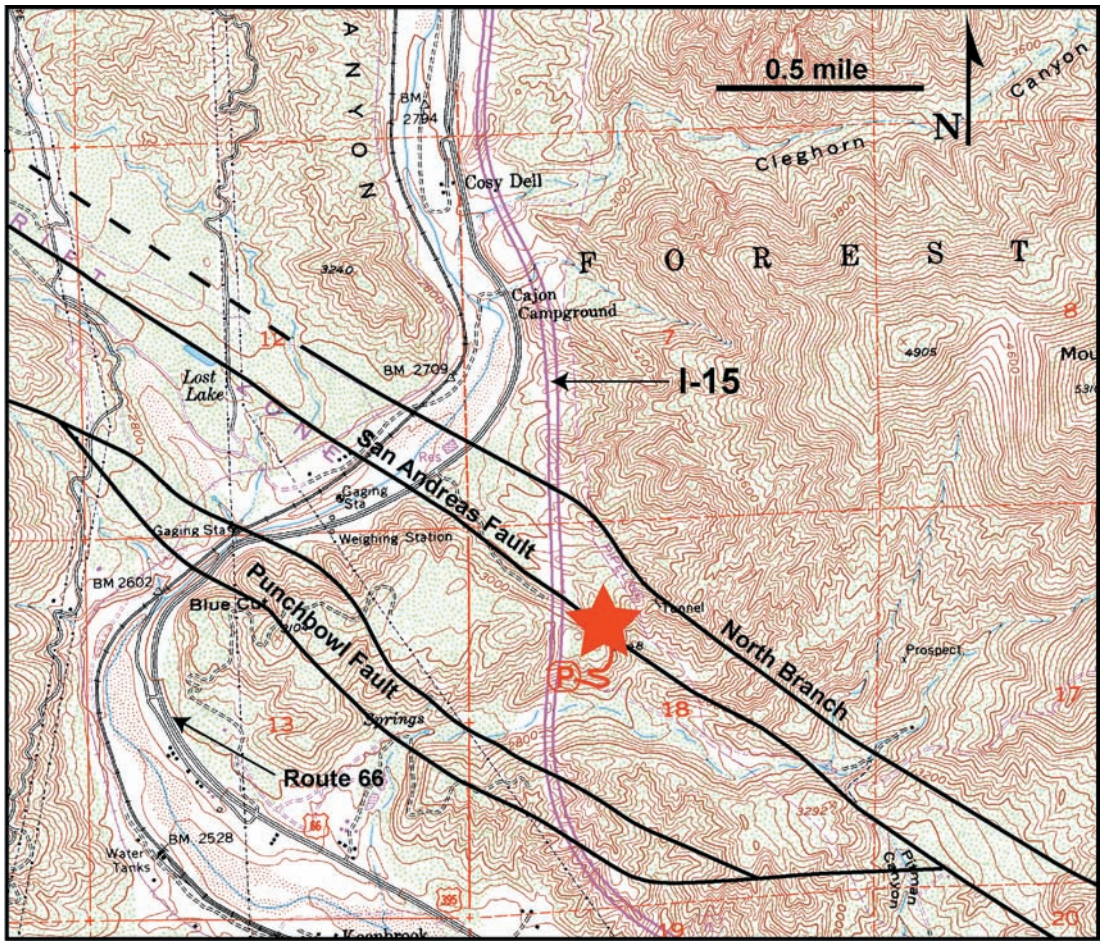

Figure 1. Topographic map from the Cajon Pass Quadrangle. Fault traces are from Weldon (1987). P: parking area; Red Star: location of site.

the Mendocino fracture zone to the north and the spreading system in the Gulf of California to the south (Powell, 1993). Matti and Morton (1993) propose that the San Andreas fault proper in southern California has had no more than 160 km of displacement. Total displacement on the San Andreas fault system since its inception in the Miocene is generally thought to be 315 ± 10 km (Matti and Morton, 1993).

The Transverse ranges of Cajon Pass were uplifted in the Quaternary up until recent. Major rock types in the area include gneiss, Pelona Schist, San Francisquito Sandstone, and an unnamed Tertiary sandstone (Weldon, 1987).

Figure 2. View to the northwest of the San Andreas fault trace.

Description of Station A (Site o of Weldon, 1987)

This station provides a nice view of the trace of the San Andreas fault through Lone Pine Canyon to the northwest towards Wrightwood (Figure 2). Exposure of the San Andreas fault can be seen 100-200 m down this paved road (towards the interstate) on the left in an erosion gully (Figure 3).

The zone is foliated and sheared with relict clasts of host rock. The fault juxtaposes Pelona Schist on the southwest with an unnamed Tertiary sandstone (Weldon, 1987). The foliation in the shear zone has an orientation of 145/70 SW, which is consistent with the strike of the San Andreas fault though this area.

Description of Station B (Site p of Weldon, 1987)

Of additional interest is a thrust fault that places older gneiss on top of the late Cretaceous San

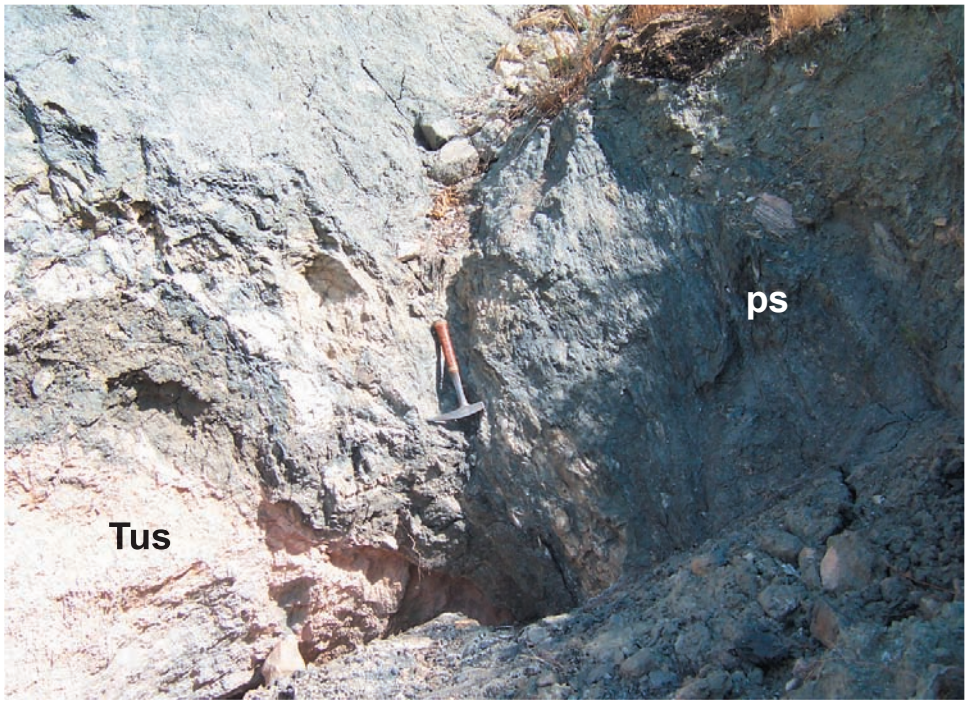

Figure 3. View to the southeast of the San Andreas fault. Tus: unnamed Tertiary sandstone; ps: Pelona Schist.

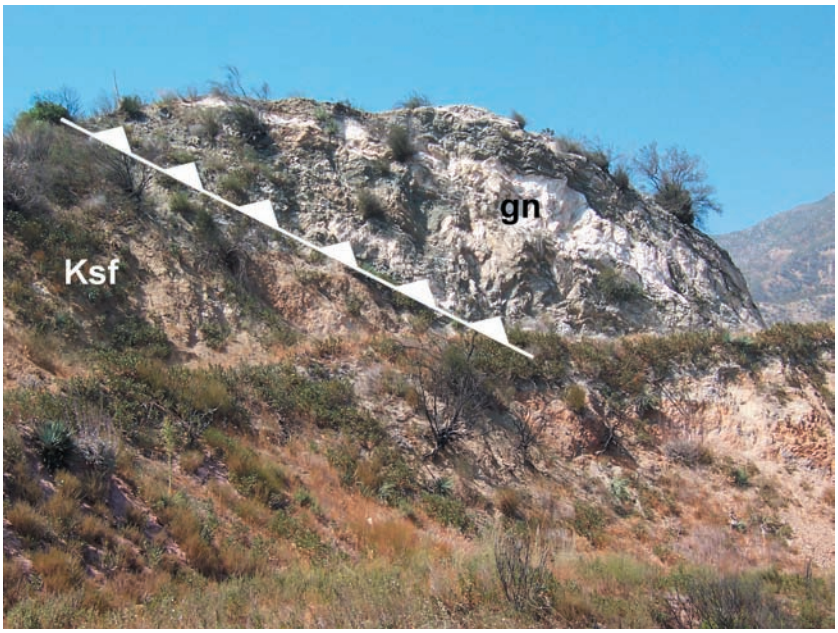

Figure 4. View to the north of an unnamed thrust fault. gn: gneiss; Ksf: Cretaceous San Francisquito Formation.

Francisquito sandstone. The outcrop is just past the paved road (Figure 4). The fault core is weathered and covered with vegetation. However, the fault appears very thin and sharp. The fault strikes NW-SE and has a dip of approximately 35° to the NE. This thrust fault is exposed due to reactivation of the North Branch as a dip-slip fault, thus uplifting the overlying thrust (Weldon, 1987).

Seismological Implications

Weldon (1987) explains the importance of the study of the San Andreas fault in Cajon Pass:

> "A 3 mi (5 km) stretch of the San Andreas fault, centered at Cajon Creek, contains excellent examples of the style of faulting and the geomorphology associated with the San Andreas fault. Abandoned traces of the San Andreas fault, evidence for lateral and vertical deformation across the fault zone, and late Quaternary offset river terraces, landslides, and sag ponds can all be found in this small area. The relationships seen here have been used to characterize the uplift of the Transverse Ranges and the Quaternary slip rate and recurrence interval of earthquakes on the San Andreas fault." (Weldon, 1987, pg. 194)

> "A Holocene history of sedimentation and terrace formation has been combined with the numerous offsets of geomorphic features to calculate an average slip rate of 24.5 ± 3.5 mm/yr on the San Andreas fault (Weldon and Sieh, 1985)…. The data from this site, coupled with the distribution of shaking intensities associated with the 1857 earthquake (Agnew and Sieh, 1978), suggest that rupture during that earthquake terminated northwest of Cajon Pass. The observations that the fault is locked here and probably has been for more than the 215 years of historical record, and that rupture occurs in discrete displacements of about 13 ft (4 m) every few hundred years require a large earthquake in the near future to relieve the more than 16 ft (5 m) of strain that has accumulated since the last earthquake." (Weldon, 1987, pg. 197).

The complex geology of the Cajon Pass area may be the result of fault segment interactions and other interations with the Punchbowl fault (Weldon, 1987).

References

Agnew, D.C. and K.E. Sieh, A documentary study of the felt effects of the great California earthquake of 1857. *Bulletin of the Seismological Society of America*, 68, 1717-1729, 1978.

Matti, J.C. and D.M. Morton, Paleogeographic evolution of the San Andreas fault in southern California: A reconstruction

based on a new cross-fault correlation. In: Powell, R.E., Weldon II, R.J., Matti, J.C. (editors), The San Andreas Fault System: Displacement, Palinspastic Reconstruction, and Geologic Evolution. *The Geological Society of America Memoirs*, 178, 107-160, 1993.

Powell, R.E., Balanced palinspastic reconstruction of pre-Late Cenozoic paleogeology, southern California: Geologic and kinematic constraints on evolution of the San Andreas fault system. In: R.E. Powell, R.J. Weldon, and J.C. Matti (editors), The San Andreas Fault System: Displacement, Palinspastic Reconstruction, and Geologic Evolution, *The Geological Society of America Memoirs*, 178, 1-107, 1993.

Weldon, R.J., San Andreas fault, Cajon Pass, southern California. *Geological Society of America Centennial Field Guide—Cordilleran Section*. Published by the Geological Society of America, Inc., California, vol. 1, 193-198, 1987.

Weldon, R.J. and K.E. Sieh, Holocene rate of slip and tentative recurrence interval for large earthquakes on the San Andreas Fault, Cajon Pass, Southern California. *Geological Society of America Bulletin*, 96, 793-812, 1985.

Chapter 3: San Andreas Fault

Site 3—Lake Hughes

Directions

1. In Palmdale, exit I-14 heading west on W. Palmdale Blvd., which becomes Elizabeth Lake Rd.
2. In the Town of Elizabeth Lake turn left at the T shaped junction.
3. The described zone starts about 6 km west of Lake Hughes in an old (not maintained) rest area north of the road.
4. The site can be accessed from the west through Hwy 138 (exit I-5 near Gorman) and Pine Canyon Rd. From both routes, most of the drive follows the San Andreas Fault.

UTM (WGS 84): 3840700 N, 361746 E (point B in Figure 3)
Elevation: 3790 feet

Geologic setting

This site is a 1.5 km long section of the San Andreas Fault (SAF) where it has a single major strand and a relatively straight and simple geomorphic expression, except in the eastern part where the fault line is diorite and gneiss complex on the south. Crystalline rocks within the fault zone show different degrees of pulverization. The map in Figure 2 (which refers to the red elongated box in Figure 1) delineates outcrops of crystalline rocks and their degree of damage in a strip along the fault in this area (part of a strip map of the entire SAF in the Mojave by Dor et al. 2005b).

Remarkably, almost all the mapped outcrops within ~100 m from the fault are pulverized to some degree (red and orange spots in Figure 2). Most of the pulverized crystalline rocks were found north of the geomorphically expressed active trace of the fault. The active fault trace is used here as a frame of reference when comparing the two sides of the fault. Texture and field appearance of pulverized rocks are defined after similar rocks that were studied by Wilson et al. (2005) in Tejon Pass.

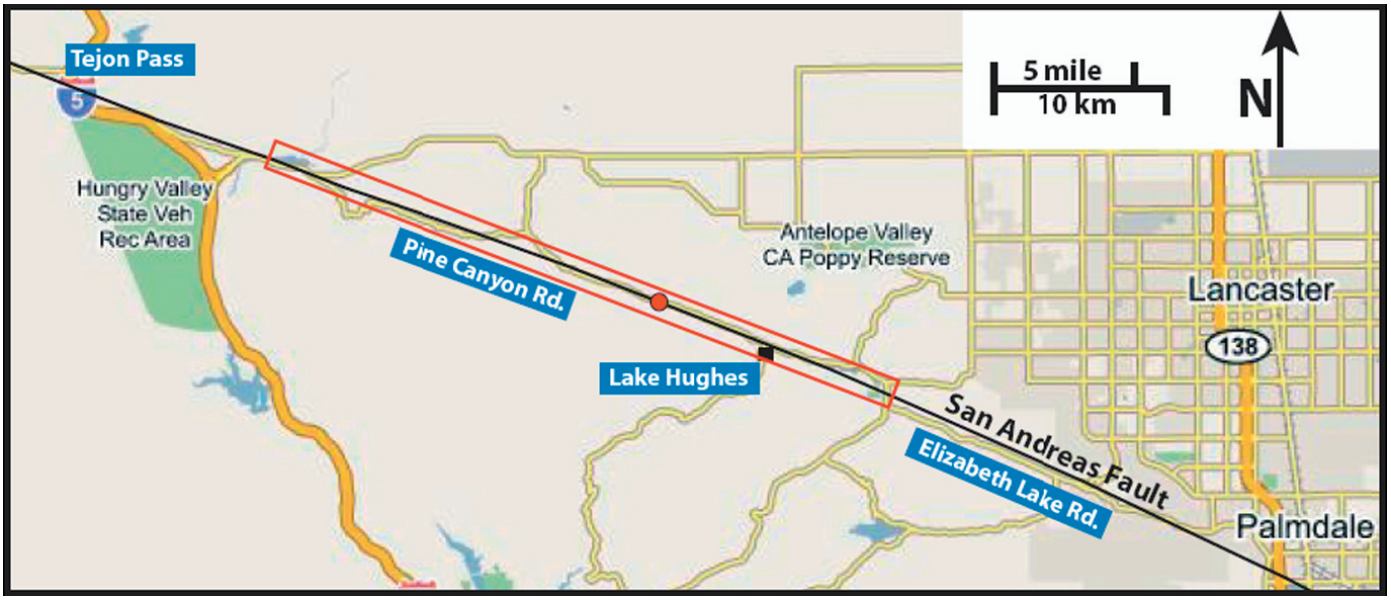

Figure 1. Location map of the Lake Hughes site (red circle). Elongated red box refers to Figure 2. (Base map is from http://maps.google.com.)

Description

Different aspects of the structure and composition of the fault zone can be seen in the different locations marked by letters in figures 3a and 3b:

A) A creek provides fault-normal, almost continuous exposure of intensely pulverized fault zone rocks, mainly granodiorites. The geomorphic expression of the fault itself can not be easily traced and there is no exposure

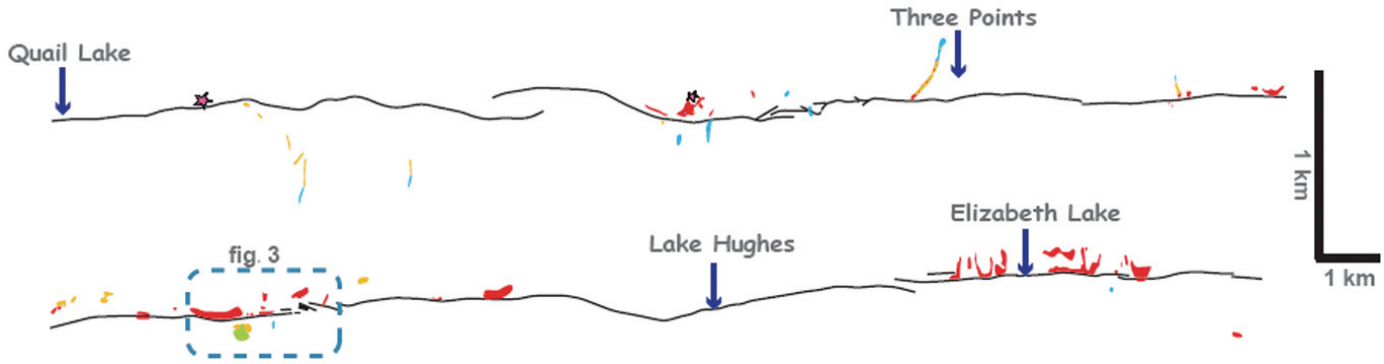

Figure 2. Geologic strip map of crystalline rocks and their degree of damage within the SAF zone (lower section continues the upper one); refers to the red box in Figure 1. Red—pervasive homogeneous pulverization; orange—selective pulverization; blue—macrofracturing. [Part of a map of the entire Mojave section of the SAF in Dor et al. (2005b).]

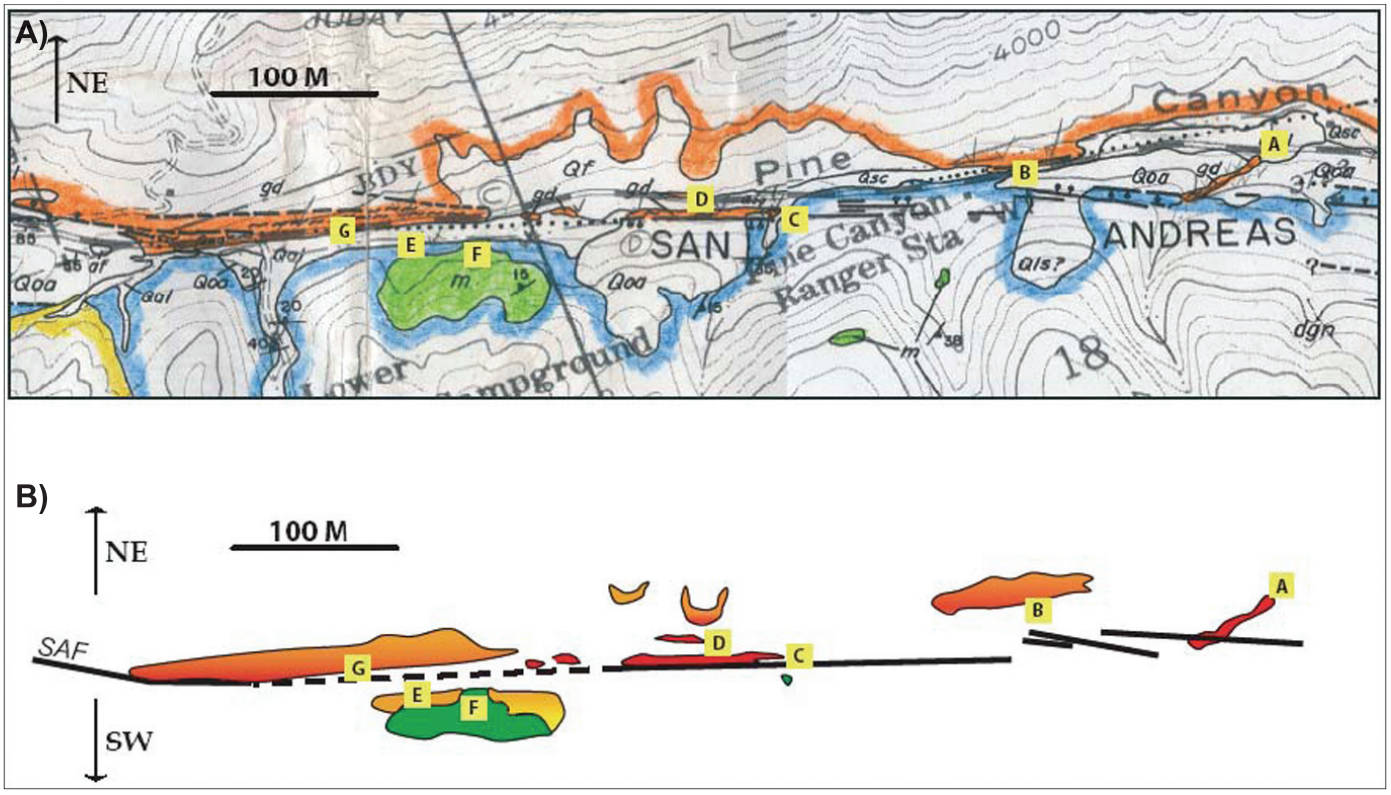

Figure 3. a) Map of active fault trace of the SAF northwest of Lake Hughes marked on a :12,000 scale topographic map (from Barrows, Kahle and Beeby, 1985). Colors mark boundaries of crystalline rock bodies in the fault vicinity: orange – granodiorites north of the fault; light blue – diorite and gneiss complex south of the fault; green – marble. Letters in yellow boxes refer to locations that are described here in the text. b) A detailed distribution of damaged fault zone rocks. The colors correspond to the scale in Figure 4.

of gouge. “Intensely pulverized” is a field definition that applies when all the grains within a rock sample can be smashed by hand to yield a fine-grained “rock flour”, and when locally the outcrop homogeneously behaves the same way.

B) The channel of Pine Canyon bounds the parking lot from the north. Its far wall exposes intensely pulverized and weathered granodiorite with some layers of gouge.

C) A deflection in a creek about 15 m south of the road marks the location of the active strand of the fault. Access to the active fault trace requires some bush-walking and cleaning, but it provides some classic fault features like linear gully, shutter ridge, “fault-grass”, and partial exposure of the active fault gouge. The eastern face of the shutter ridge is exposed along the creek north of the active fault trace and shows another, presumably inactive wide gouge zone with coherent slip surfaces. The wall-rocks are pulverized.

D) Some layers of inactive gouge exposed on the northern slope of this elongated shutter ridge, embedded in pulverized wall-rocks.

E) Metamorphic rocks that are selectively pulverized can be seen on the creek wall, south of the fault. Certain rock domains are macroscopically fractured while others are intensely pulverized. In places, pulverization is selective with respect to the different minerals: feldspar grains are pulverized where quartz grains are intact or only macroscopically broken.

F) Large body of marble with considerably larger fractures with respect to the country fault zone rocks: fractures are in the mm-cm scale with diverse orientation. The rock lacks fine grain material or any other evidence for pulverization. The marble fragments are angular and rigid. Preliminary microstructural analysis indicates that the marble here accommodates large amount of plastic strain.

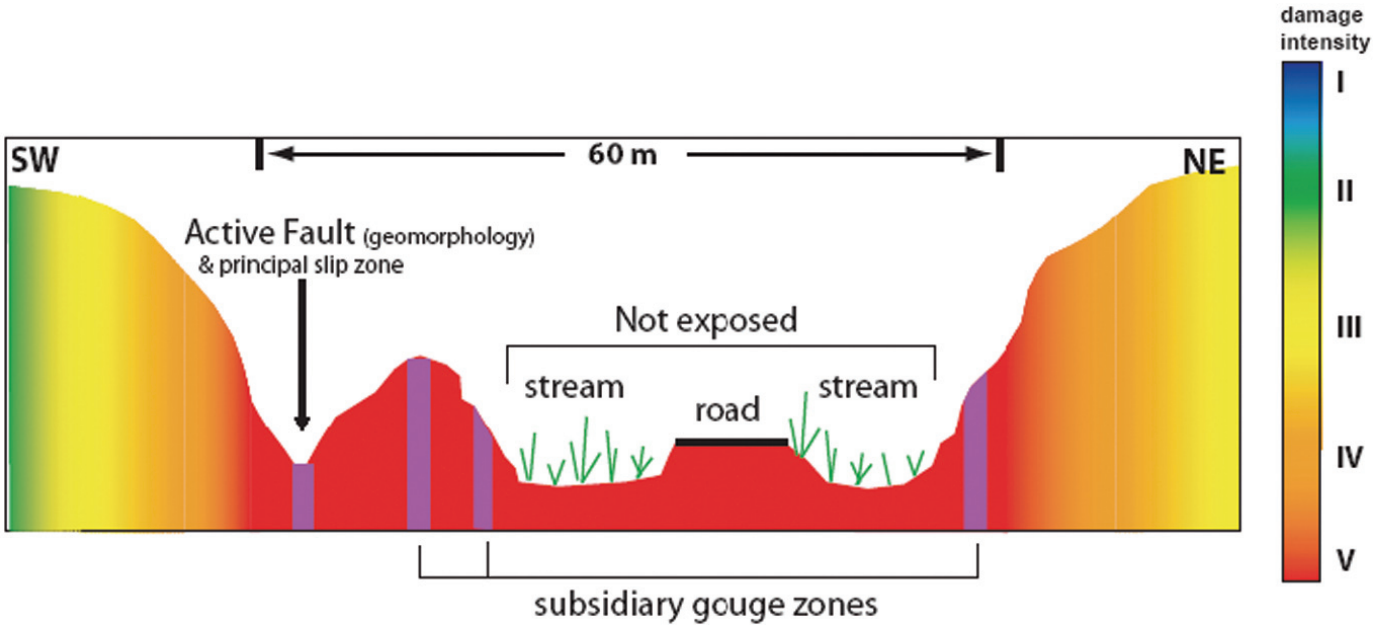

Figure 4. Composite cross-section of the fault zone obtained by stacking features from (3b) into a vertical plane perpendicular to the fault. The principal slip zone is on the southwest side of a ~60 m wide layer of intensely pulverized rocks. Additional strike slip activity is apparent by subsidiary gouge zones northeast of the principal slip zone. A ‘fault zone valley’ correlates with the zone of intense damage. The degrees of damage shown by the scale range from weak fracturing (blue) to intense pulverization (red).

G) Intensely and pervasively pulverized granodiorite in a road cut exposure north of the fault. Note the typical bed-land topography with high drainage density that is typical to impermeable fine-grained rocks.

Figure 4 is a generalized cross-fault view that compiles and stacks all the features that are described above and that were found along this fault section into one vertical plain. The apparent fault zone structure here is asymmetric: the zone of localized slip is located on the southwest side of the fault zone with more subsidiary gouge zones and larger width of the pulverized rocks layer found on its northeast side. This structure indicates that more shear and damage accumulated northeast of the principal slip zone so far.

Seismological Implications

The existence of a consistent asymmetric damage distribution pattern with respect to the principal slip zone can possibly indicate that a fault section has a preferred rupture propagation direction. Since more damage is expected in the tensional quadrant of the radiated seismic field of a propagating rupture, a random propagation direction of ruptures over time would result in an approximately symmetric damage pattern across the fault in the absence of other factors. Instead, if ruptures on a given fault section tend to propagate preferentially to one direction, the tensional quadrant will be in most cases on one side of the fault and so as the long term damage.

A faulting mechanism that results in a preferred rupture direction is rupture along a material interface (Ben-Zion, 2001 and references therein). The theory shows that mode II ruptures on a material interface tend to evolve wrinkle-like pulses that propagate preferentially in the direction of motion of the slower velocity block. The theory also (Shi and Ben-Zion, 2005) shows that more damage is expected on the side of the fault with higher seismic velocity, which for the preferred propagation direction is the side that is consistently in the tensional quadrant of the radiated seismic field.

The sense of asymmetry of the fault structure in this site is consistent with the overall distribution pattern of pulverized rocks along the SAF in the Mojave and with other smaller scale observations of damage distribution across the SAF in this area (Dor et al. 2005a,b). Seismic imaging (Fuis et al. 2003; Shapiro et al. 2005) suggest that the northeast more damaged side of the SAF in the Mojave has faster seismic velocities. This correlation is compatible with northwestward preferred direction of large ruptures along the SAF in the Mojave.

References

Barrows, A.G., J.E. Kahle, and D.J. Beeby, Earthquake hazard and tectonic history of the San Andreas Fault Zone, Los Angeles County, California. *Open file report 85-10 LA*, California Department of Conservation, Division of Mines and Geology, 1985.

Ben-Zion, Y., Dynamic rupture in recent models of earthquake faults. *Journal of the Mechanics and Physics of Solids*, 49, 2209-2244, 2001.

Ben-Zion, Y. and Z. Shi, Dynamic rupture on a material interface with spontaneous generation of plastic strain in the bulk. *Earth and Planetary Science Letters*, in press, 2005.

Dor, O., T.K. Rockwell, and Y. Ben-Zion, Geologic observations of damage asymmetry in the structure of the San Jacinto, San Andreas and Punchbowl faults in southern California: A possible indicator for preferred rupture propagation direction. Submitted to *Pure application of Geophysics*, 2005a.

Dor, O., Y. Ben-Zion, T.K. Rockwell, and J.N. Brune, Pulverized fault zone rocks along the Mojave section of the San Andreas fault. Submitted to *EPSL*, 2005b.

Fuis, G.S., R.W. Clayton, P.M. Davis, T. Ryberg, W.J. Lutter, D.A. Okaya, E. Hauksson, C. Prodehl., J.M., Murphy, M.L. Benthien, S.A. Baher, M.D. Kohler, K. Thygesen, G. Simila, and G.R. Keller, Fault systems of the 1971 San Fernando and 1994 Northridge earthquakes, southern California: Relocated aftershocks and seismic images from LARSE II. *Geology*, 31, 171-174, 2003.

Shapiro, N.M., M. Campillo, L. Stehly, and M.H. Ritzwoller, High resolution surface wave tomography from ambient seismic noise. *Science*, 307, 1615-1618, 2005.

Summary of The Wrightwood Trilogy: Three Landmark Articles on the Paleoseismology of the San Andreas Fault System. [Weldon et al. (2002), Fumal et al. (2002), Biasi, et al. (2002).]

Introduction

These three key articles discuss various aspects of the paleoseismology at the Wrightwood site as well as other sites along the San Andreas fault (Figure 1). The Wrightwood site is located about 3 km northwest of Wrightwood, California in Swarthout Valley, where the San Andreas fault crosses Swarthout Creek and the Government Canyon alluvial fan (Figure 2).

Although this site is not the topic of this field guide, these articles contain critically important information on describing the paleoseismicity of the San Andreas fault. Weldon et al. (2002) present the structural setting of the Wrightwood site, along with numerous structural models and an analysis of lateral offsets resulting from each earthquake.

Fumal et al. (2002) present the structural and stratigraphic evidence of 14 large earthquakes that have occurred on the southern San Andreas Fault since about A.D. 500. Biasi et al. (2002) employ a statistical method for analyzing radiocarbon ages for individual stratigraphic layers in order to estimate the ages of paleoearthquakes at the Wrightwood and Pallett Creek sites. The third article also calculates recurrence intervals and conditional probabilities of future large earthquakes at each site.

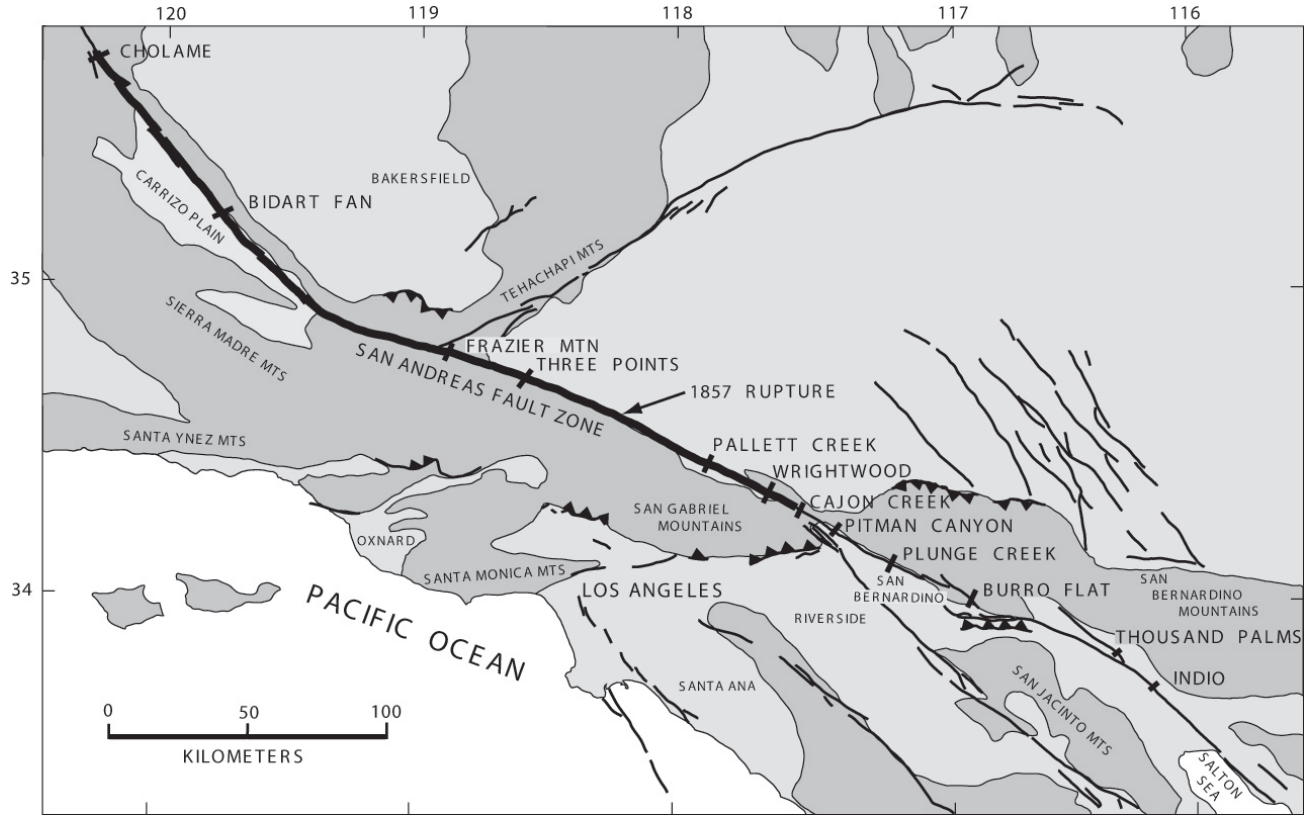

Figure 1. Map of southern California showing major faults, major cities, missions, and mountainous areas (dark shading). Locations of paleoseismic sites on the San Andreas fault with multiple event records are labeled and shown with bars. The 1857 Fort Tejon earthquake rupture is shown with the very heavy line. [Figure 1 from Fumal et al. (2002).]

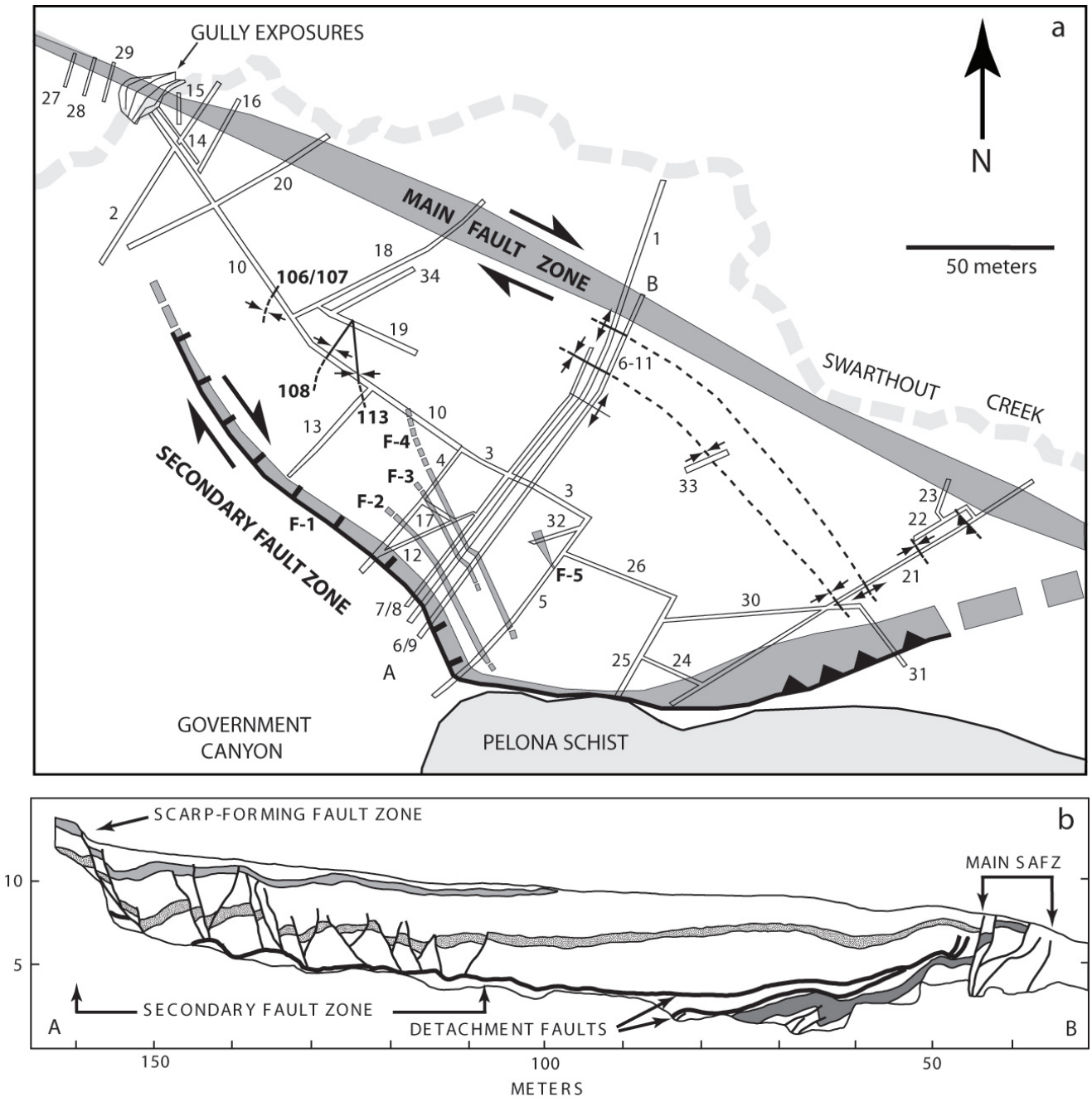

Figure 2. (A) Map of Wrightwood paleoseismic site showing location of trenches (numbered double lines), major fault zones (shaded), and selected folds. For clarity, the lower level trenches (8,9) are not shown, Note location of gully exposures shown in Figures 3, 5, 6, and 7. (B) Schematic cross-section across the site (line marked AB in A) using data from trenches 1, 6, 9, and 11. Faults are shown with heavy lines; three thick debris flows (shaded) are shown to illustrate the style of deformation across each fault zone. [Figure 2 from Fumal et al. (2002).]

1. Structure and Earthquake Offsets on the San Andreas Fault at the Wrightwood, California, Paleoseismic Site. (Weldon, et al., 2002)

Key Points

The Wrightwood paleoseismic site is characterized by 38 trenches and natural exposures across the San Andreas fault zone (Figure 2). Trenching has been performed across the main trace of the San Andreas fault as well as a secondary fault zone (Figure 2). The main fault zone dips steeply to the southwest and is characterized by a transtensive style (i.e., a combination of right-lateral and normal slip) of deformation (Figure 3).

The secondary fault zone is composed of a transtensive portion to the northwest and a transpressive portion to the southeast (Figure 2). The Wrightwood site has a 25-m thick stratigraphic section that shows widely distributed evidence for individual earthquakes.

The upper 12 m show evidence of 14 prehistoric earthquakes, which suggests a mean displacement of 2-4 m per event (based on a cumulative slip of 30-60 m), or a slip rate of 2-4 cm per year (based on a recurrence interval of ~100 yr) for the San Andreas fault north of its junction with the San Jacinto fault. This range of mean displacement and slip rate is consistent with events at the Pallett Creek site and what is known about rupture size on this part of the San Andreas fault.

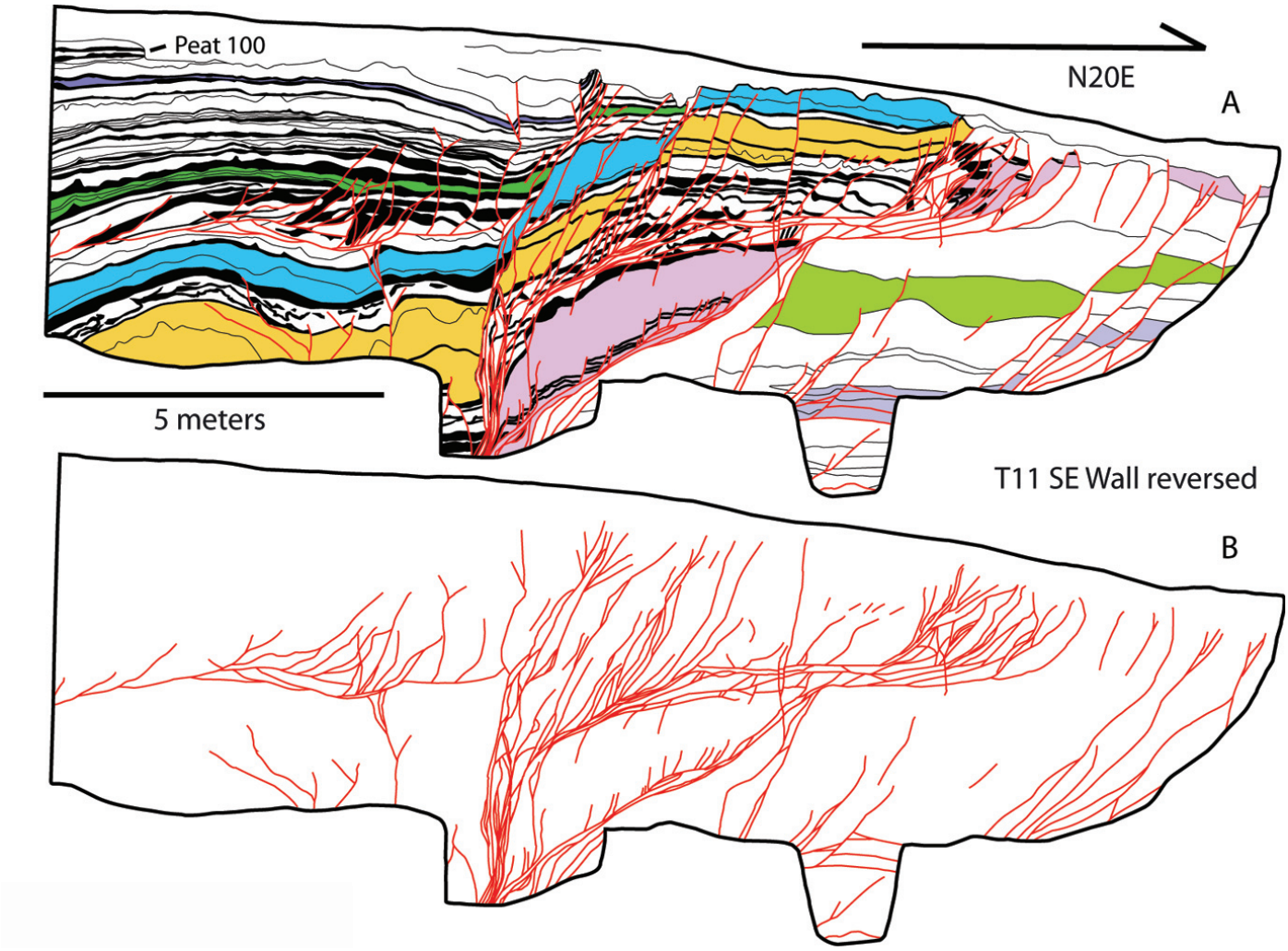

Figure 3. (A) Map of the main fault trace of the San Andreas fault and (B) faults only. Red lines are faults, black lines are contacts, black polygons are peat layers, and colored polygons highlight selected clastic units. In (A) the separation of all units suggest southwest down normal slip; thickness and facies mismatches demonstrate lateral slip. The fault pattern in (B) illustrates how rupture follows bedding. [Figure 5 from Weldon et al. (2002).]

Discussion

The preferred structural model at the Wrightwood site that relates the secondary fault zone to the main fault zone is that of a "flake", or flower structure, which is commonly associated with strike-slip faults. A simplified sketch (Figure 4) illustrates the structures and geomorphology of the "flake" model. Rupture along the main trace of the fault produces right-lateral traction that causes slip across subhorizontal planes (i.e., detachment) in the fan.

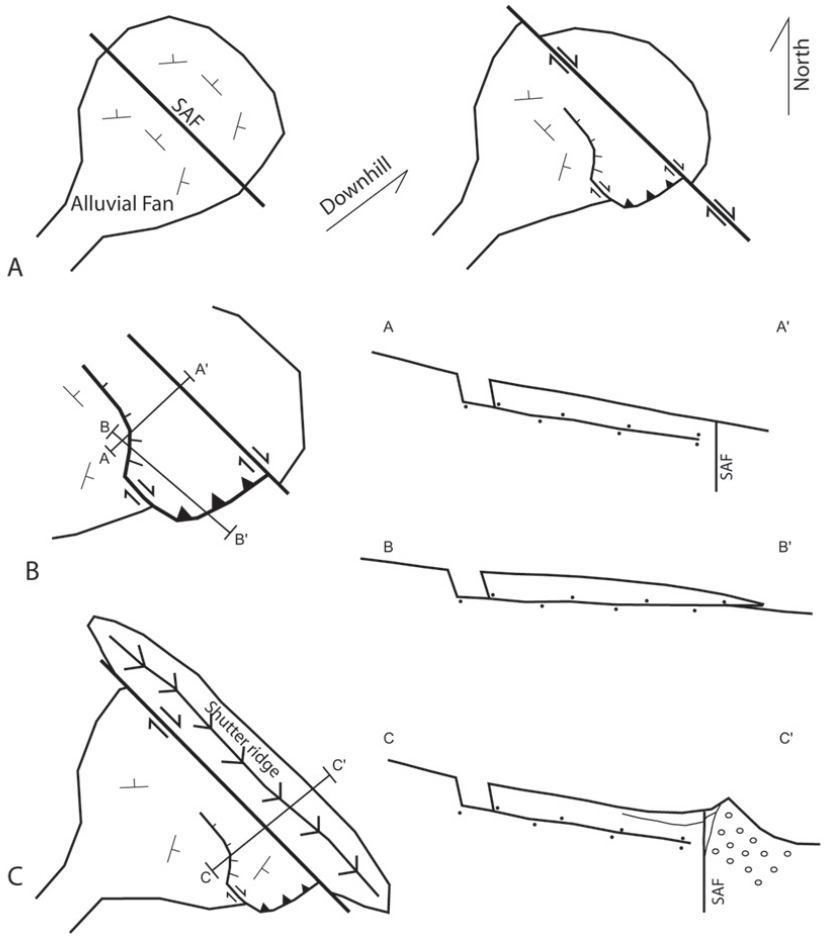

Figure 4. Cartoon of the flake model explaining structures and geomorphology at the Wrightwood site. (A) Slip on the San Andreas fault grabs or entrains a flake of the alluvial fan. (B, C) Cross sections AA' and CC' show that profiles perpendicular to the fault will show a progressively diminishing, bedding-parallel slip (represented schematically by offset dots across the detachment). Cross sections parallel to the San Andreas (BB') will show extension across the uphill scarp and compression across the east edge of the fan, where the flake runs over the material below the fan. (C) A shutter ridge along the northeast side of the fault helps to pond sediment, extends sedimentation to the southeast, and may provide additional traction to the flake. Strike and dip symbols represent dip of layers in fan. [Figure 16 from Weldon et al. (2002).]

2. Evidence for Large Earthquakes on the San Andreas Fault at the Wrightwood, California, Paleoseismic Site: A.D. 500 to Present. (Fumal, et al., 2002)

Key Points

"The combination of widespread deformation, frequent sedimentation events, and the presence of thin, dateable peat layers bounding virtually every clastic deposit makes Wrightwood an unusually good site for recognizing and dating paleoearthquakes. Also, because the locus of sedimentation has generally shifted westward with time, deposits spanning about the past 5000 years are readily accessible with shallow excavations." (Fumal, et al., 2002, pg. 2729)

There is structural and stratigraphic evidence (using fissure fill, scarps, rupture terminations, folding, and tilting) of 14 large magnitude earthquakes on the southern portion of the San Andreas fault during the past 1500 years. Evidence for most of the 14 earthquakes occurs in both the main and secondary fault zones (Figure 2).

Discussion

Comparing the Wrightwood site with other paleoseismic sites, such as Pallett Creek, provides a means of event confirmation, as well as a means to determining which sections of the fault ruptured during a particular paleoearthquake. Out of the 14 major events at Wrightwood, 9 can be correlated with Pallet Creek (Figure 5). The correlation between this and other sites on the San Andreas fault suggest that individual surface ruptures were commonly several hundred km long, which are consistent with displacements of 2-4 m per single event from Weldon et al. (2002).

The 14 major earthquakes represented at the Wrightwood paleoseismic site have a mean recurrence interval (and 95% range) of 105 (62-192) years. Including an additional two events at Pallet Creek reduces the mean recurrence interval to approximately 95 years.

The time since the 1857 Fort Tejon earthquake is about 40% greater than the mean recurrence interval for both cases.

> "Assuming non-stationary recurrence behavior, these observations indicate to us that at least the southernmost 200 km of the San Andreas fault is near failure and could rupture in a single large magnitude earthquake in the near future." (Fumal, et al., 2002, pg. 2758)

3. Paleoseismic Event Dating and the Conditional Probability of Large Earthquakes on the Southern San Andreas Fault, California. (Biasi, et al., 2002)

Key Points

The ages of paleoearthquakes can be quantitatively estimated by using stratigraphic ordering along with sedimentological and historical data. Dates were determined using radiocarbon, thermoluminescence, soil development, and sediment accumulation. The results serve to confirm previously determined earthquake dates and intervals from the two companion articles previously discussed. The paleoseismic evidence suggests mean recurrence intervals for the Wrightwood and Pallett Creek sites of 105 and 135 years, respectively. The mean age estimates (and 95% range) for major events from A.D. 500 to present from the Wrightwood site are as follows:

Wrightwood Event (W) Chronologies

W1	*1857*
W2	*1812*
W3	*1685 (1647-1717)*
W4	*1536 (1508-1569)*
W5	*1487 (1448-1518)*
W6	*1263 (1191-1305)*
W7	*1116 (1047-1181)*
W8	*1016 (957-1056)*
W9	*850 (800-881)*
W10	*781 (736-811)*
W11	*722 (695-740)*
W12	*697 (657-722)*
W13	*634 (551-681)*
W14	*534 (407-628)*

Discussion

> "Mean estimates of conditional probabilities of earthquake recurrence in the next 30 years are somewhat higher at Wrightwood than at Pallett Creek, reflecting the greater number of events in a similar overall amount of time. Uncertainties in conditional probabilities are somewhat reduced by the longer event series at Wrightwood for the same reason. The Poisson model suggests approximately 20% and 25% probabilities of a ground-rupturing event in 30 years for Pallett Creek and Wrightwood, respectively." (Biasi et al., 2002, pg. 2780)

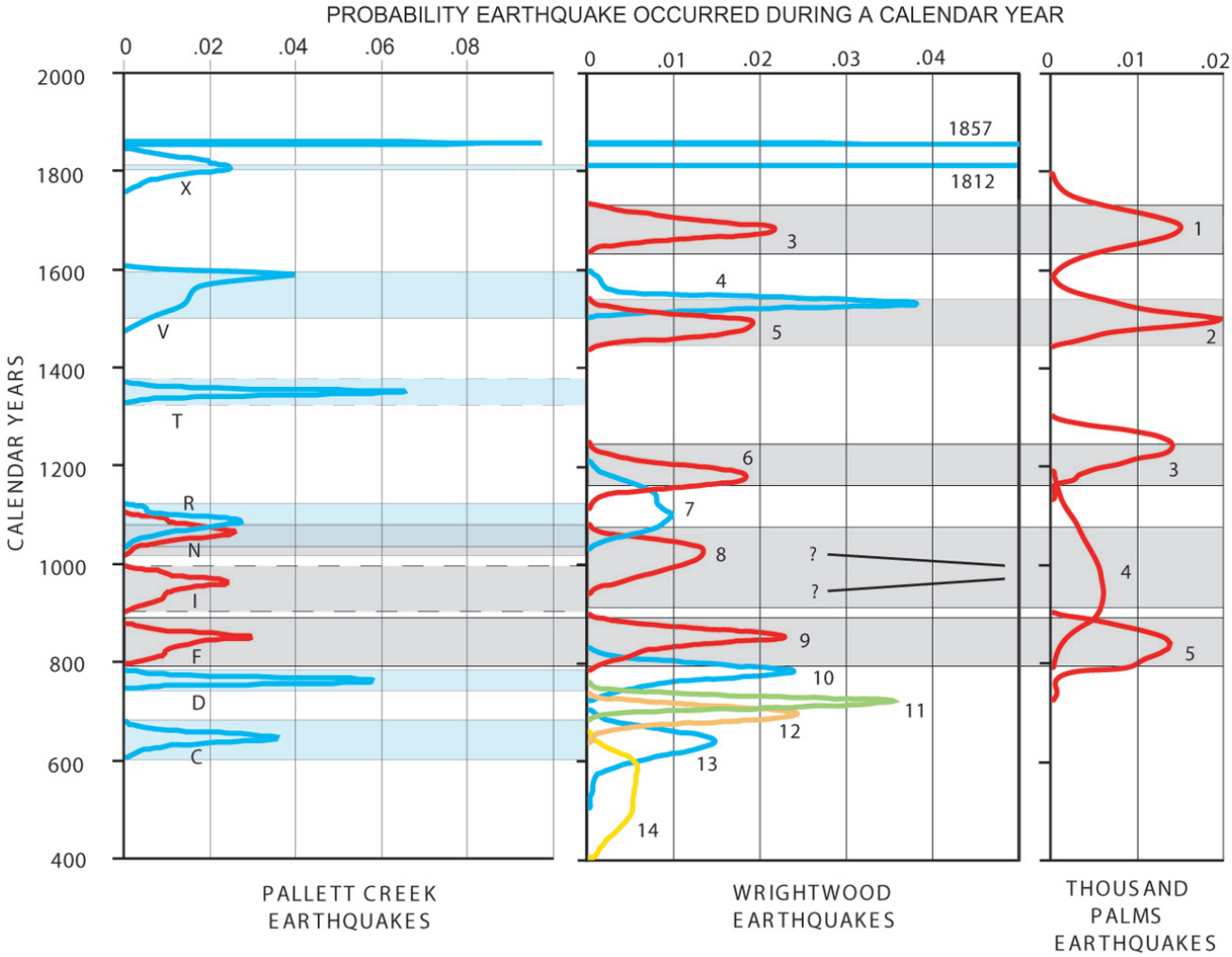

Figure 5. Probability density functions for earthquake ages constrained by stratigraphic ordering and peat accumulation rate for Wrightwood (WW) and Pallett Creek (PC) and by stratigraphic ordering alone at Thousand Palms Oasis (TP). Earthquakes that may correlate between TP and WW or among TP, WW and PC are shown in red; other earthquakes that may correlate between WW and PC shown in blue. Light blue and gray shading indicates range of overlap of probability distributions. TP event 5 may correlate with either PC event N and WW event 8 or with PC event I. Either or both PC events T and I may have ruptured through WW. [Figure 18 from Fumal et al. (2002).]

Summary

The Wrightwood paleoseismic site is characterized by 38 trenchs and natural exposures across the San Andreas fault zone (Weldon et al., 2002). The site is very significant for several reasons. It provides an uncommonly thick, relatively young, datable stratigraphic section and has widely distributed deformation that provides evidence for numerous earthquakes (Weldon et al., 2002). Paleoseismic observations indicate that the earthquakes recorded here were large-magnitude events with surface rupture lengths on the order of tens to hundreds of kilometers (Fumal et al., 2002).

A total of 14 events have been documented for the past ~1600 years in the upper 12 m of section (Weldon et al., 2002). These 14 events have a cumulative slip of 30-60 m, suggesting a mean displacement of 2-4 m per event and a slip rate of 2-4 cm/year (given a mean recurrence interval of approximately 100 years) for the San Andreas fault north of its junction with the San Jacinto fault (Biasi et al., 2002; Fumal et al., 2002; Weldon et al., 2002).

These data suggest that the southernmost 200 km of the San Andreas fault is near failure (Fumal et al., 2002). More specifically, there is a 25% probability of a ground-rupturing event in the next 30 years based on the Poisson model at the Wrightwood site (Biasi et al., 2002).

References

Biasi, G.P., R.J. Weldon II, T.E. Fumal, and G.G. Seitz, Paleoseismic event dating and the conditional probability of large earthquakes on the southern San Andreas fault, California. *Bulletin of the Seismological Society of America*, 92, 7, 2761-2781, 2002.

Fumal, T.E., R.J. Weldon II, G.P. Biasi, T.E. Dawson, G.G. Seitz, W.T. Frost, and D.P. Schwartz. Evidence for large earthquakes on the San Andreas fault at the Wrightwood, California, Paleoseismic site: A.D. 500 to present. *Bulletin of the Seismological Society of America*, 92, 7, 2726-2760, 2002.

Weldon, R.J. II, T.E. Fumal, T.J. Powers, S.K. Pezzopane, K.M. Scharer, and J.C. Hamilton. Structure and earthquake offsets on the San Andreas fault at the Wrightwood, California, Paleoseismic site. *Bulletin of the Seismological Society of America*, 92, 7, 2704-2725, 2002.

Chapter 4: Silverwood Lake Area

Introduction

Extensive fault and rock mechanics-oriented research on large-displacement faults of the San Andreas system, as well as other large-displacement faults, have defined the structure and composition of fault zones and related these to fault processes (Chester et al., 1993; Evans and Chester, 1995; Schulz and Evans, 2000; Wilson et al., 2003). However, much less work of this nature has been performed on smaller-displacement faults even though they are critical in order to understand the scaling relationships between faults of various sizes.

If the mechanical and chemical processes of small faults can be used as analogs for larger faults, then a much larger data set is available to us to study fault growth and earthquake processes. The study of small faults is important in order to understand how faults grow because small-displacement faults represent relatively young faults, as opposed to mature faults that have accumulated much slip. Using the amount of slip as a proxy for time, we are able to examine faults at different stages of development. The Silverwood Lake area, in the western portion of the San Bernardino Mountains, is a key area to examine relatively small-scale faults (Figure 1).

The San Bernardino Mountains are part of the Transverse Ranges in southern California, which formed by clockwise rotation of the western and easternmost Transverse Ranges in association with dextral shear along the Pacific-North American plate boundary (Garfunkel, 1974; Kamerling and Luyendyk, 1979, 1985; Luyendyk et al., 1980, 1985; Dickinson, 1996). The San Bernardino Mountains reflect a complex history of rapid uplift in the Late Cenozoic in association with transpressive deformation (Dibblee, 1975; Meisling and Weldon, 1982; Spotila and Sieh, 2000; Blythe et al., 2000) that generated both the highest elevations and most extensive upland plateau within the Transverse Ranges (Sadler, 1982). This broad upland plateau, called the Big Bear plateau, has been uplifted by two east-west striking thrust faults with opposing dips: the North Frontal thrust system and the Santa Ana thrust (Spotila and Sieh, 2000). Spotila and Sieh (2000) have used a deeply weathered erosion surface in the crystalline bedrock as a structural datum to constrain the amounts of displacement along these thrust fault systems to 1-2 km. Thus, the fault exposures analyzed in this work formed at depths of 1-2 km and have subsequently been exhumed due to uplift on the Santa Ana and North Frontal thrusts.

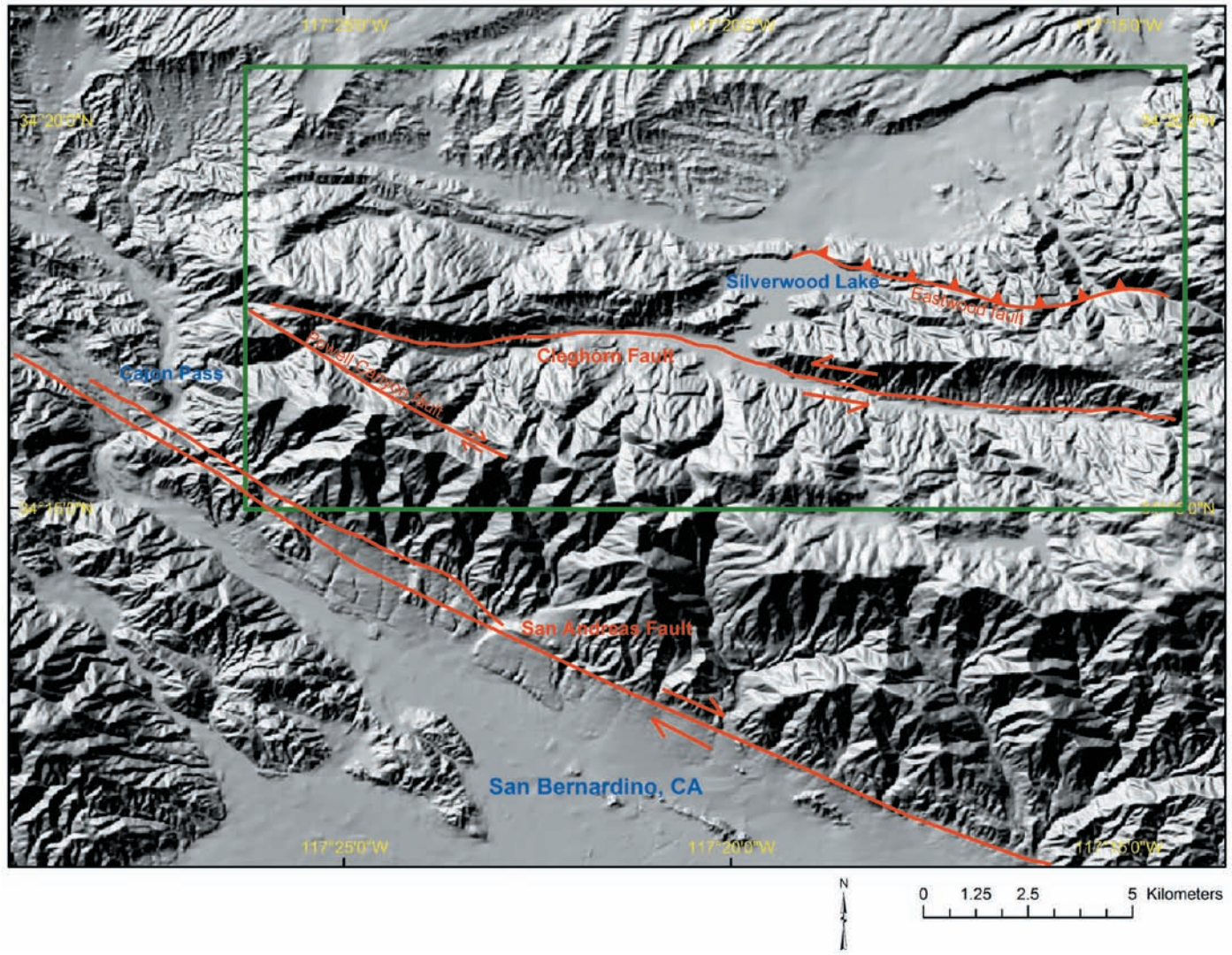

Figure 1. Shaded relief map of the western San Bernardino Mountains. Geographic locations are shown in blue and faults in red. The green box shows extent of the field area from the work of Jacobs (2005).

References

Blythe, A.E., D.W. Burbank, K.A. Farley, and E.J. Fielding, Structural and topographic evolution of the central Transverse Ranges, California, from apatite fission-track (U-Th)/He and digital evolution model analyses. *Basin Research*, 12, 97-114, 2000.

Chester, F.M., J.P. Evans, and R.L. Biegel, Internal structure and weakening mechanisms of the San Andreas fault. *Journal of Geophysical Research*, 98, B1, 771-786, 1993.

Dibblee, T.W., Jr., Late Quaternary uplift of the San Bernardino Mountains on the San Andreas and related faults, in San Andreas Fault in southern California; A guide to San Andreas fault from Mexico to Carrizo Plain, *California Division of Mines and Geology*, Spec. Rep., 118, edited by J.C. Crowell, 127-135, Sacramento, CA., 1975.

Dickinson, W.R., Kinematics of transrotational tectonism in the California Transverse Ranges and its contribution to cumulative slip along the San Andreas transform fault system. *Geological Society of America*, 305, 46, 1996.

Evans, J.P. and F.M. Chester. Fluid-rock interaction in faults of the San Andreas system: Inferences form San Gabriel fault rock geochemistry and microstructures. *Journal of Geophysical Research*, 100, B7, 13,007-13,020, 1995.

Garfunkel, Z., Model for the late Cenozoic tectonic history of the Mojave Desert, California, and for its relation to adjacent regions. *Geological Society of America Bulletin*, 86, 1931-1944, 1974.

Jacobs, J.R., Examination of exhumed faults in the western San Bernardino Mountains, California: Implications for fault growth and earthquake rupture. M.S. Thesis, *Utah State University*, 2005.

Kamerling, M. J., and B. P. Luyendyk, Tectonic rotations of the Santa Monica Mountains region, western Transverse Ranges, California, suggested by paleo-magnetic vectors. *Geological Society of America Bulletin*, 90, 331-337, 1979.

Kamerling, M. J., and B. P. Luyendyk, Paleomagnetism and Neogene tectonics of the northern Channel Islands, California. *Journal of Geophysical Research*, 90, 12485-12502, 1985.

Luyendyk, B. P., M. J. Kamerling, and R. R. Terres, Geometric model for Neogene crustal rotations in southern California. *Geological Society of America Bulletin*, 91, 211-217, 1980.

Luyendyk, B. P., M. J. Kamerling, R. R. Terres, and J. S. Hornafius, Simple shear of southern California during Neogene time suggested by paleomagnetic declinations *Journal of Geophysical Research*, 90, 12454-12466, 1985.

Meisling, K.E. and R.J. Weldon, The Late-Cenozoic structure and Stratigraphy of the western San Bernardino Mountains, in Geologic excursions in the Transverse Ranges, Cooper, J.D. (editor), *Geological Society of America Annual Meeting Guidebook*, 75-81, California State University, Fullerton, 1982.

Sadler, P.M., Later Cenozoic stratigraphy and structure of the San Bernardino Mountains, in Geologic Excursions in the Transverse Ranges. In: Cooper, J.D. (editor), *Geological Society of America Annual Meeting Guidebook*, 55-106, Cal. St. Univ., Fullerton, 1982.

Schulz S.E., and J.P. Evans., Mesoscopic structure of the Punchbowl fault, southern California, and the geologic and geophysical structure of active strike slip faults. *Journal of Structural Geology*, 22, 913-930, 2000.

Spotila, J.A. and K. Sieh, Architecture of transpressional thrust faulting in the San Bernardino Mountains, southern California, from deformation of deeply weathered surfaces. *Tectonics*, 19, 589-615, 2000.

Wilson, J.E., J.S. Chester, and F.M. Chester, Microfracture analysis of fault growth and wear processes, Punchbowl Fault, San Andreas system, California. *Journal of Structural Geology*, 25, 1855-1873, 2003.

Chapter 4: Silverwood Lake Area

Site 1—Eastwood Fault

Directions

1. Take US Hwy 138 east from I-15 at Cajon Junction.
2. Continue for roughly 10 miles and turn left (east) onto SR 173.
3. Continue for 2.4 miles past the dam spillway and turn right (south) towards Cedar Springs Dam day use area.
4. Just before the parking lot, turn left (southeast) onto jeep road.
5. Continue for ~ 1 mile and park on the right side of jeep road near the side trail with the "Restricted Area" sign.
6. The fault is ~ 15 m north of this spot on the east side of the jeep road (Figure 1).

   UTM (WGS 84): 3795358 N, 0472471 E
   Elevation: 3480 feet

Geologic Setting

The Silverwood Lake area is in the western portion of the San Bernardino Mountains, which were rapidly uplifted in the Late Cenozoic in association with transpressive deformation that generated an extensive upland plateau, called the Big Bear plateau (Dibblee, 1975; Meisling and Weldon, 1982; Sadler, 1982; Spotila and Sieh, 2000; Blythe et al., 2000). This broad upland plateau has been uplifted by two east-west striking thrust faults with opposing dips: the North Frontal thrust system and the Santa Ana thrust (Spotila and Sieh, 2000). Spotila and Sieh (2000) have used a deeply weathered erosional surface in the crystalline bedrock as a structural datum to constrain the amounts of vertical displacement along these thrust fault systems to 1-2 km. Thus, the Eastwood fault has been exhumed from at least 1-2 km depth.

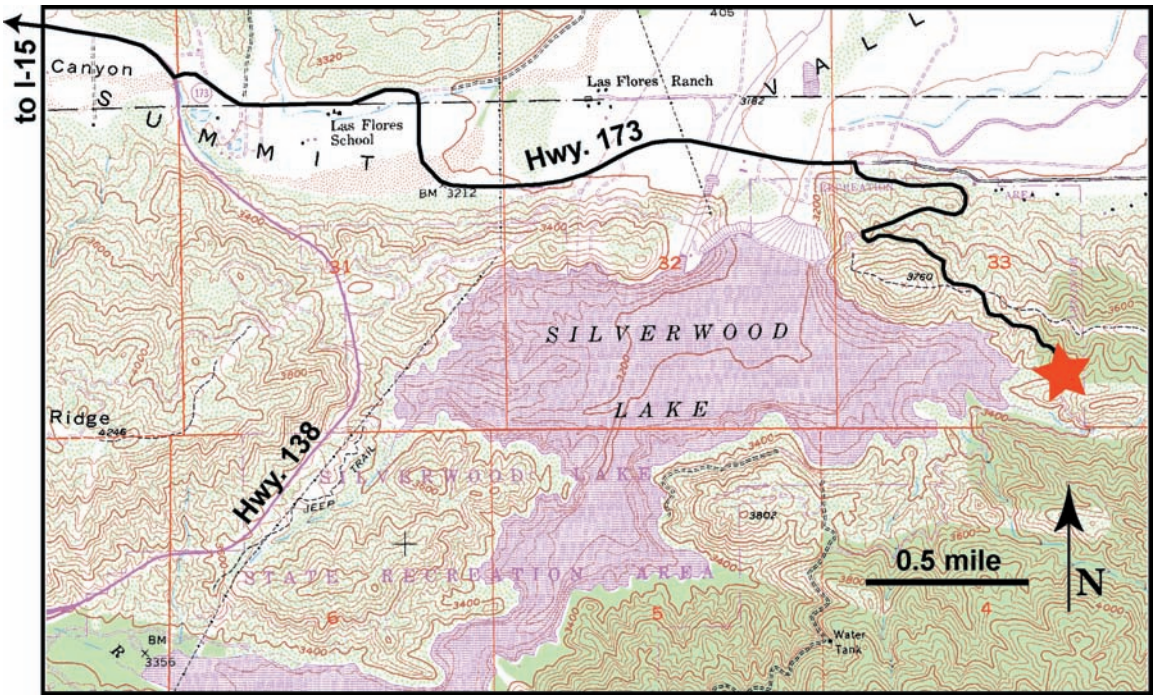

Figure 1. Topographic map of the Silverwood Lake area. Highway 138 is the purple line and Highway 173 is outlined in black. The red star marks the approximate location of the Eastwood fault exposure from the Silverwood Lake Quadrangle.

Faults exposed in the Silverwood Lake area are predominantly late Miocene (9.5-4.1 Ma) high-angle reverse faults with displacements ranging from centimeters to hundreds of meters (Meisling and Weldon, 1989). Their formation is attributed to the obliquity between the San Andreas fault system in southern California (i.e., the "Big Bend") and the plate motion vectors, thus causing oblique convergence and transpressional deformation (Spotila and Sieh, 2000).

These south-southwest vergent contractional structures are collectively called the Cedar Springs fault system, which is composed of northwest to east-west striking arcuate faults. East-west striking fault segments typically exhibit a pure north-side-up dip-slip motion, whereas northwest striking segments often have a component of strike-slip, thus making them right-oblique slip faults (Meisling and Weldon, 1989). It is important to point out that the present fault geometry of north-dipping faults has been steepened by 20-30° (decrease in dip for south-dipping faults) by the Pleistocene Western San Bernardino arch (Meisling and Weldon, 1989).

Description

The Eastwood fault exposure is located near the northeast corner of Silverwood Lake and has an orientation of 316/58° NE (Figure 2). This is a pure dip-slip reverse fault with a minimum slip constraint of ~ 180 m and a fault core thickness of 2-5 cm. The Eastwood fault places granite and granodiorite on top of the Miocene Crowder Formation, a non-marine arkosic sandstone and conglomerate. A foliated clay gouge layer was observed along the Crowder Formation fault wall and may record slip localized on the footwall side of the fault zone.

Damage elements are mostly fractures, with some subsidiary faults and minor veins, indicating the presence of fluids. The hanging wall is characterized by an altered, light pink fault breccia that extends 5 m away from the fault core. This defines the "primary damage zone". Outside of the primary damage zone is the "secondary damage zone" that lacks the pink chemically altered appearance and brecciation and is characterized by a decreasing density of damage elements away from the main fault (Figure 3). Damage element densities reach background levels at approximately 12 m from the fault core (Figure 4).

Compartmentalization of the fault zone into fault core, primary damage zone, and secondary damage zone is seen at the microscopic and geochemical level in the Eastwood fault. The primary damage zone microstructures are characterized by many fractures (open and clay, microbreccia, and/or iron oxide filled), grain comminution, and feldspar alteration. This damage decreases towards the secondary damage zone, which only has minor grain cracking with few through-going fractures and little grain comminution and alteration.

Results of X-ray diffraction indicate that alteration products in the Eastwood fault zone are smectite, laumontite, palygorskite (a fibrous clay mineral), and epidote. However, clay minerals are entirely confined to the fault core. Whole-rock geochemical analysis indicates that the fault core and primary damage zone are depleted in mobile elements relative to the host rock, which suggests increased fluid-rock interactions nearest to the fault. See Jacobs (2005) for a more detailed mesoscopic, microscopic, and geochemical characterization of the Eastwood fault.

Seismological Implications

The soft, non-cohesive fault core from the Eastwood fault is different than what has been observed from previous work on the North Branch San Gabriel and Punchbowl faults (Chester et al., 1993). These strike-slip faults are characterized by a relatively narrow and localized cataclasite and ultracataclasite fault core (Chester and Logan, 1986; Chester et al., 1993). The ultracataclasites are different than the gouge and breccia-dominated fault core of the Eastwood fault core in that they have primary cohesion (e.g., Sibson 1977). The non-cohesive fault core observed at the Eastwood fault formed at a depth of 1-2 km, whereas the North Branch San Gabriel and Punchbowl faults were formed between 2-5 km and 2-4 km, respectively (Chester and Logan, 1986; Evans and Chester, 1995). Chester et al.

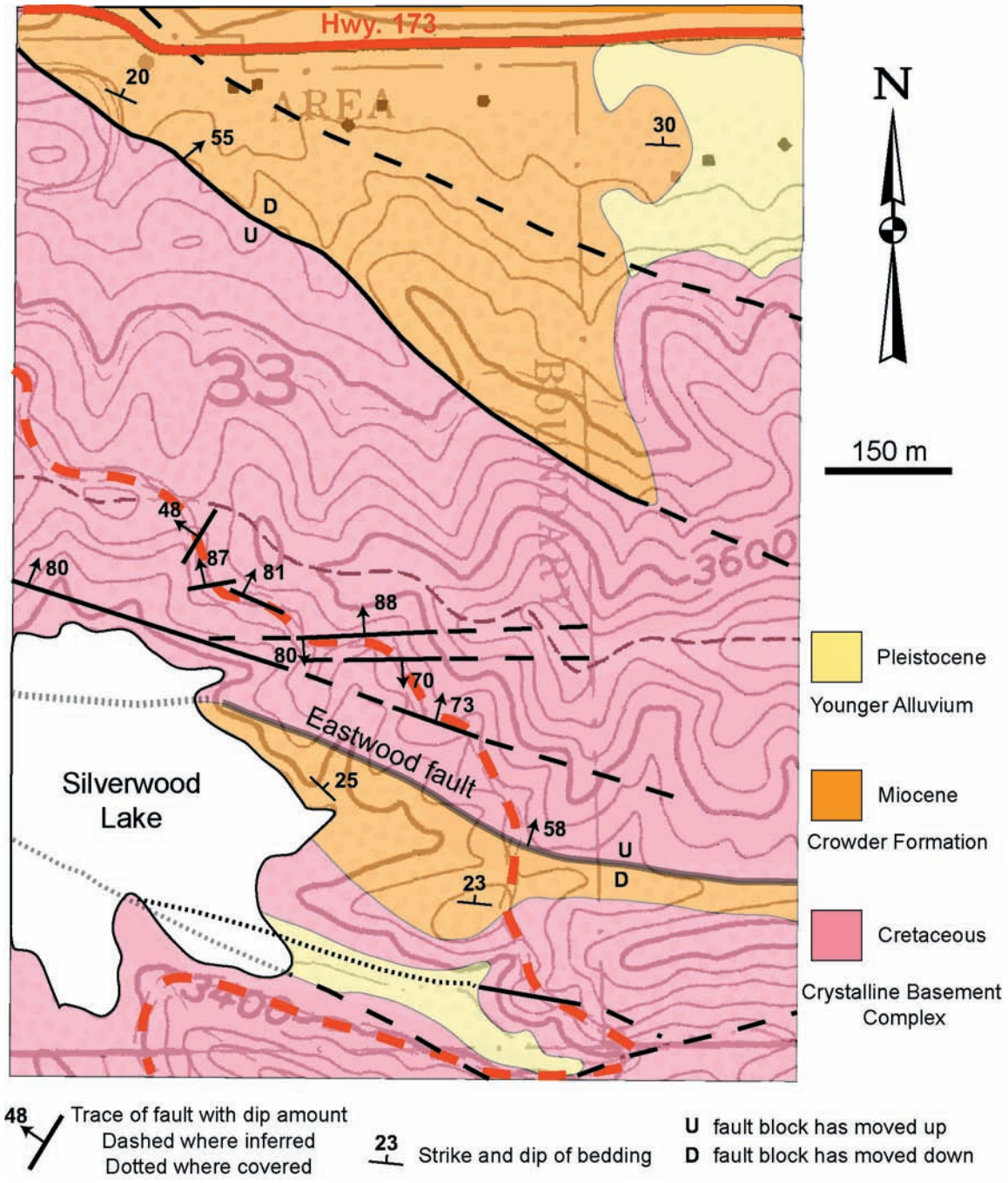

Figure 2. Geologic map of the Eastwood fault area showing US Highway 173 in solid red and the jeep road in dashed red. There is much deformation to observe in the hanging wall of the Eastwood fault while driving south on the jeep road.

(2004) explain that the progression from the non-cohesive breccia-gouge series to the cohesive cataclasites and mylonites corresponds to increasing depth of formation, causing different deformation and recovery mechanisms (e.g., Christie, 1960; Reed, 1964). Thus, the non-cohesive breccia-gouge fault cores observed in the Eastwood fault core are likely a function of the shallow depth of formation.

An asymmetry in the fault core was observed at the Eastwood fault in that the principle slip surface appears to be offset to the footwall side of the fault core. This slip preference is manifested as a

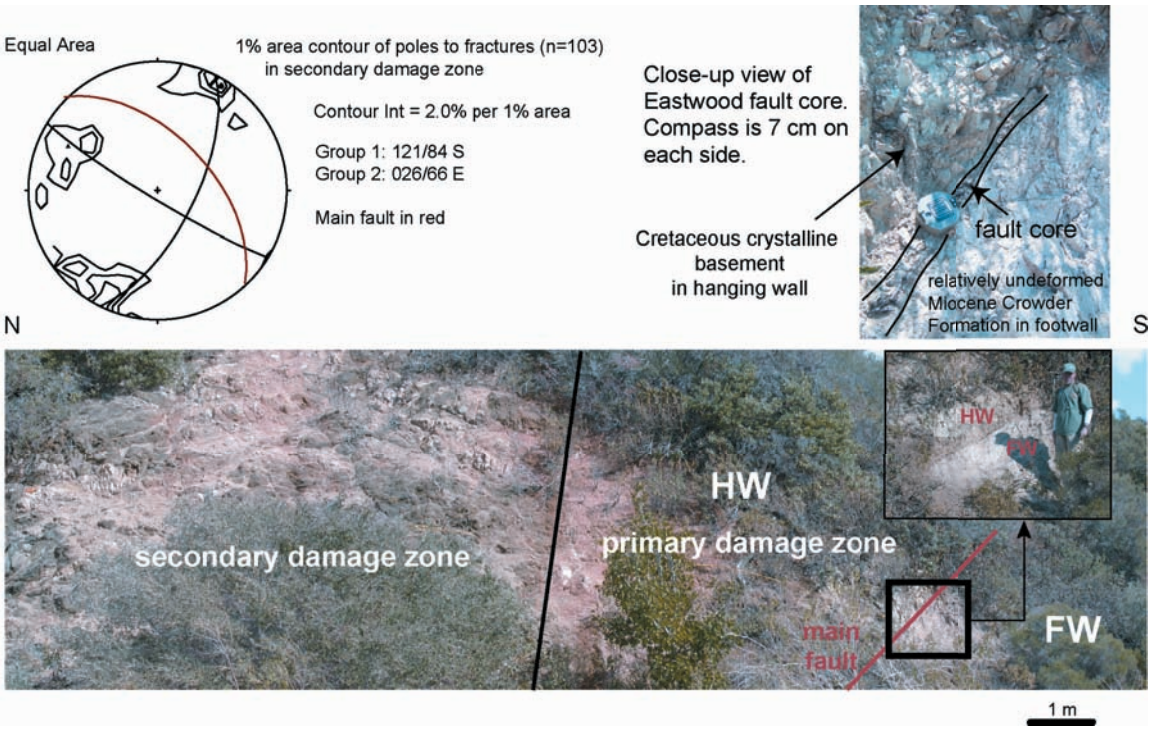

Figure 3. Photomosaic and simplified sketch of the Eastwood fault with view to the east. The lower hemisphere equal area projection is of all the fractures in the secondary damage zone (n=103) and shows contours of poles to the planes and the best fit great circles. HW: hanging wall; FW: footwall.

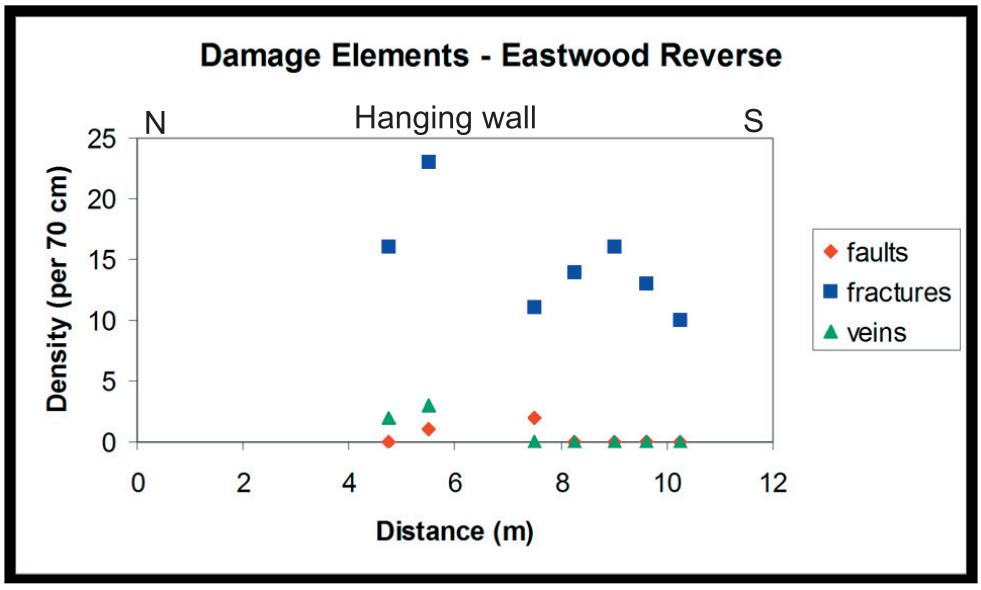

Figure 4. Transect data from the Eastwood reverse fault hanging wall showing density of subsidiary faults, fractures, and veins. The dominant damage element is the fractures. Distances are perpendicular to the main fault.

strongly foliated, clay gouge layer up against the fault wall that is typically more sheared than the rest of the fault core. This asymmetry may be due to the contrasting lithologies, with a slip preference to the softer sedimentary rocks. Alternatively, Ben-Zion and Andrews (1998) believe that "… rupture may tend to migrate from within the fault zone to an interface between the fault zone and the surrounding

rock," causing a change in rupture character from a crack-like mode to a wrinkle-like pulse.

The Eastwood fault can be used as a "model" fault to determine how much energy may be consumed by chemical alteration over the history of the fault. Jacobs (2005) proposes that most clay formation is syntectonic because: (1) Clay is exclusively found in the fault core, (2) The clay gouge exhibits a sheared texture in both outcrop and thin section, and (3) Clay occurs in other very small faults (< 1 m of slip) in the area, which indicates early clay formation by using slip as a proxy for fault maturity.

The external energy source for these alteration reactions may be the earthquakes that created the faults. At the instant of slip, large amounts of energy are released, with typically less than a third of the near-fault energy (McGarr and Fletcher, 2002) consumed as far-field radiated energy. The non-radiated energy is "deposited in a relatively small fault zone over a time scale of less than a minute" (Kanamori and Heaton, 2000). This energy would therefore be available in the hypocentral region as heat that would dissipate and be consumed by alteration reactions. The total energy associated with alteration over the life of the Eastwood fault is estimated at 4.6×10^{11} kJ (see Jacobs, 2005 for calculations). A total energy release of 2×10^{12} kJ is estimated for the history of the Eastwood fault based on the Gutenburg-Richter law (Main et al., 1999) and the fact that there is a linear relationship between magnitude and source dimension (Abercrombie, 1995). A maximum magnitude of 5.0 was assumed for the 7 km long Eastwood fault. Our calculations suggest that syntectonic alteration in the fault core may consume approximately 20% of the total earthquake energy.

References

Abercrombie, R.E., Earthquake source scaling relationships from -1 to 5 ML using seismograms recorded at 2.5-km depth. *Journal of Geophysical Research*, 100, 24,015-24,036, 1995.

Ben-Zion, Y., and D.J. Andrews, Properties and implications of dynamic rupture along a material interface. *Bulletin of the Seismological Society of America*, 88, 1085–1094, 1998.

Blythe, A.E., D.W. Burbank, K.A. Farley, and E.J. Fielding, Structural and topographic evolution of the central Transverse Ranges, California, from apatite fission-track (U-Th)/He and digital evolution model analyses. *Basin Research*, 12, 97-114, 2000.

Chester F.M. and J.M. Logan, Implications for mechanical properties of brittle faults from observations of the Punchbowl fault zone, California, USA. *Pure and Applied Geophysics*, 124, 79-106, 1986.

Chester, F.M., J.P. Evans, and R.L. Biegel, Internal structure and weakening mechanisms of the San Andreas fault. *Journal of Geophysical Research*, 98, 771-786, 1993.

Chester, F.M., J.M. Chester, D.L. Kirschner, S.E. Schulz, and J.P. Evans, Structure of large-displacement, strike-slip fault zones in the brittle continental crust. In: G.D. Karner, J.D. Morris, N.W. Driscoll, and E.A. Silver (editors), *Rheology and deformation of the lithosphere at continental margins*, 223-260, Columbia University Press, New York, NY, 2004.

Christie, J.M., Mylonitic rocks of the Moine thrust-zone in the Assynt region, north-west Scotland, *Trans. Edinburgh Geological Society*, 18, 79-93, 1960.

Dibblee, T.W., Jr., Late Quaternary uplift of the San Bernardino Mountains on the San Andreas and related faults, in San Andreas Fault in southern California; A guide to San Andreas fault from Mexico to Carrizo Plain, *California Division of Mines and Geology*, Spec. Rep. 118, edited by J.C. Crowell, 127-135, Sacramento, CA., 1975.

Evans, J.P. and F.M. Chester, Fluid-Rock interaction in faults of the San Andreas system: Inferences form San Gabriel fault rock geochemistry and microstructures. *Journal of Geophysical Research*, 100, B7, 13,007-13,020, 1995.

Jacobs, J.R., Examination of exhumed faults in the western San Bernardino Mountains, California: Implications for fault growth and earthquake rupture. M.S. Thesis, *Utah State University*, 2005.

Kanamori, H. and T.H. Heaton, Microscopic and macroscopic physics of earthquakes. *American Geophysical Union Monographs*, 120, 147-161, 2000.

Main, I., D. Irving, R. Musson, and A. Reading, Constraints on the frequency-magnitude relation and maximum magnitudes in the UK from observed seismicity and glacio-isostatic recovery rates. *Geophysical Journal International*, 137, 535-550, 1999.

McGarr, A. and J.B. Fletcher, Mapping apparent stress and energy radiation over fault zones of major earthquakes. *The Seismological Society of America Bulletin*, 92, 1633-1646, 2002.

Meisling, K.E. and R.J. Weldon, The Late-Cenozoic structure and Stratigraphy of the western San Bernardino Moun-

tains, in Geologic excursions in the Transverse Ranges, Cooper, J.D. (editor), *Geological Society of America Annual Meeting Guidebook*, 75-81, California State University, Fullerton, 1982.

Meisling, K.E. and R.J. Weldon, Late Cenozoic tectonics of the northwestern San Bernardino Mountains, southern California. *Geological Society of America Bulletin*, 101, 106-128, 1989.

Reed, J.J., Mylonites, cataclasites, and associated rocks along the Alpine fault, South Island, New Zealand. *New Zealand Journal Geology and Geophysics*, 7, 645-684, 1964.

Sadler, P.M., Later Cenozoic stratigraphy and structure of the San Bernardino Mountains, in Geologic Excursions in the Transverse Ranges. In: Cooper, J.D. (editor), *Geological Society of America Annual Meeting Guidebook*, 55-106, Cal. St. Univ., Fullerton, 1982.

Sibson, R.H., Fault rocks and fault mechanisms. *Journal of the Geological Society of London*, 133, 191-213, 1977.

Spotila, J.A. and K. Sieh, Architecture of transpressional thrust faulting in the San Bernardino Mountains, southern California, from deformation of deeply weathered surfaces. *Tectonics*, 19, 589-615, 2000.

Chapter 4: Silverwood Lake Area

Site 2—Grass Valley Fault Zone

Directions

1. Take US Highway 138 east from I-15 at Cajon Junction.
2. Continue for roughly 10 miles and turn left (east) onto SR 173.
3. Continue for 4.7 miles past the dam spillway and turn right (south) onto a gravel road.
4. Park immediately after reaching this road and hike ~ ¼ mile up the road to the east. The fault is exposed on the right (south) side of the jeep road before the dead end (Figure 1).

   UTM (WGS 84): 3796779 N, 0475200 E
   Elevation: 3600 feet

Geologic Setting

The Silverwood Lake area is in the western portion of the San Bernardino Mountains, which have been rapidly uplifted in the Late Cenozoic in association with transpressive deformation that generated an extensive upland plateau, called the Big Bear plateau (Dibblee, 1975; Meisling and Weldon, 1982; Sadler, 1982; Spotila and Sieh, 2000; Blythe et al., 2000). This broad upland plateau has been uplifted by two east-west striking thrust faults with opposing dips: the North Frontal thrust system and the Santa Ana thrust (Spotila and Sieh, 2000). Spotila and Sieh (2000) have used a deeply weathered erosion surface in the crystalline bedrock as a structural datum to constrain the amounts of vertical displacement along these thrust fault systems to 1-2 km. Thus, the Grass Valley fault zone has been exhumed from at least 1-2 km depth.

Faults exposed in the Silverwood Lake area are predominantly late Miocene (9.5-4.1 Ma) high-angle reverse faults with displacements ranging from centimeters to hundreds of meters (Meisling and Weldon, 1989). Their formation is attributed to the obliquity between the San Andreas fault system in southern California (i.e., the "Big Bend") and the plate motion vectors, thus causing oblique convergence and transpressional deformation (Spotila and Sieh, 2000).

These south-southwest vergent contractional structures are collectively called the Cedar Springs

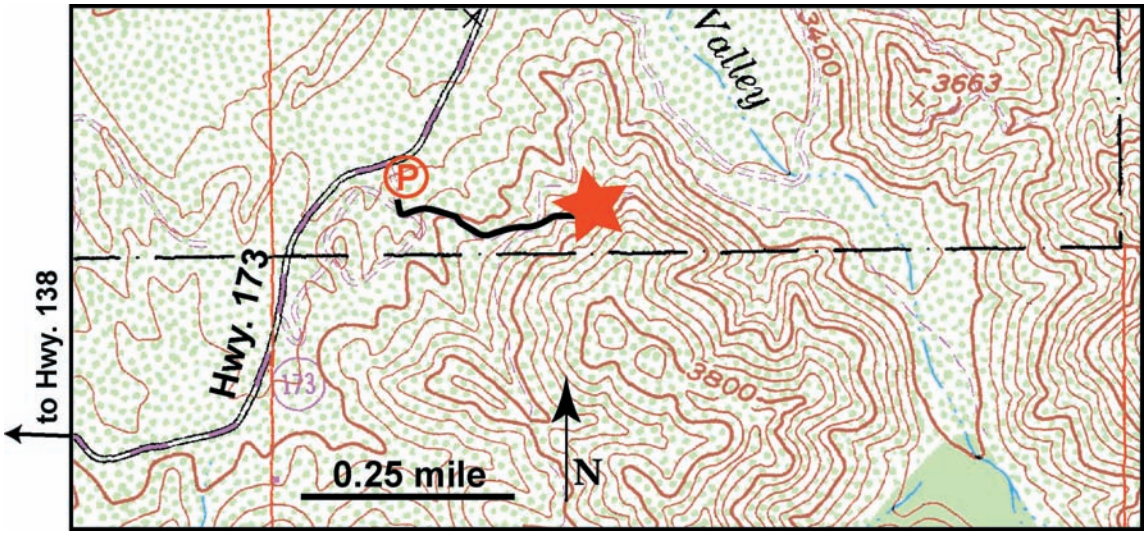

Figure 1. Topographic map from the Silverwood Lake Quadrangle of the Grass Valley fault zone area. The circled "P" shows the parking location and the red star marks the fault zone exposure.

fault system, which is composed of northwest to east-west striking arcuate faults. East-west striking fault segments typically exhibit a pure north-side-up dip-slip motion, whereas northwest striking segments often have a component of strike-slip, thus making them right-oblique slip faults (Meisling and Weldon, 1989). It is important to point out that the present fault geometry of north-dipping faults has been steepened by 20-30° (decrease in dip for south-dipping faults) by the Pleistocene Western San Bernardino arch (Meisling and Weldon, 1989).

Description

The Grass Valley fault has an orientation of 105/45° S and has accumulated ~ 40 m of oblique-reverse slip (rake on the fault plane is 55° from the east). Thickness of the fault core ranges from 2-12 cm. Multiple sub-parallel faults lie in the hanging wall; the footwall is not as damaged, but has more variability of subsidiary fault orientation (Figure 2). The damage zone is characterized by many fractures with some subsidiary faults (Figure 3a). There are approximately 50 damage elements per 70 cm scans near the main fault and the density drops off abruptly within a few meters (Figure 3b).

Fracture exhibit two preferred orientations, one sub-parallel to the main fault and the other at a high angle to the main fault. Two types of lithologies exist within this fault zone: a weathered, grus-like granodiorite host rock cut by competent granite pegmatite dikes, which serve as excellent offset markers. Faults through the more competent granite dikes are manifested as a zone of dense fractures and faults with no gouge, whereas a well-defined clay gouge fault core characterizes the granodiorite. This shows the control lithology has on fault geometry.

Except for the main fault, there is relatively little microstructural damage in the Grass Valley fault zone. Fractures are mostly open, but some are partially filled with iron oxide and chlorite. Minor alteration of feldspar grains is common. Thin section analysis from the main fault reveals intense comminution and clay development. A primary slip surface with surrounding shear fabric is present in the fault core of the main fault (Figure 4). This intense microstructural damage is absent 1 m into the hanging wall (Figure 5), showing the concentration of shear in the fault core. Results of X-ray diffraction indicate the presence of smectite, palygorskite (a fibrous clay mineral), and laumontite within 0.5 m of the central gouge and breccia layer.

Whole-rock geochemical analysis indicates that the fault core is reduced in many mobile elements relative to both the hanging wall and footwall host rock. The reduction of Na2O, CaO, and K2O is consistent with the alteration of feldspars to clays as shown by X-ray diffraction. However, MgO, MnO, and Fe2O3 show an increase in the fault core relative to the host rock. This is also consistent with the mineralogic changes in the fault core. Nontronite (a smectite mineral) and palygorskite contain Fe and Mg, respectively, which would increase the relative abundance of these elements in the fault core.

Seismological Implications

As proposed by previous workers (Chester et al., 1993; Evans and Chester, 1995; Heermance et al., 2003), the data presented here show that the fault core appears to accommodate the majority of the slip within the fault zone, as documented by transect work and microstructural analysis. The thickness of the co-seismic slip zone has significant effects on the physics of earthquakes (Kanamori and Heaton, 2000; Sibson, 2003). For example, reduction of shear resistance via friction-melting and fluid pressurization requires slip to be restricted to a few centimeters or tens of centimeters, respectively (Sibson, 2003).

Due to the lack of pseudotachylyte in the Grass Valley fault (as well as all other faults in the Silverwood Lake area), we propose that fluid pressurization is the dominant process in reducing shear resistance. Fluids are most likely allowed into the fault core during rupture, when there is opening along the fault plane. The fluids are then trapped there due to the impermeable nature of the clay-rich gouge and become pressurized during future slip events, thus reducing shear resistance.

The thickness of the co-seismic slip zone also affects the characteristic displacement, Dc, (Biegel

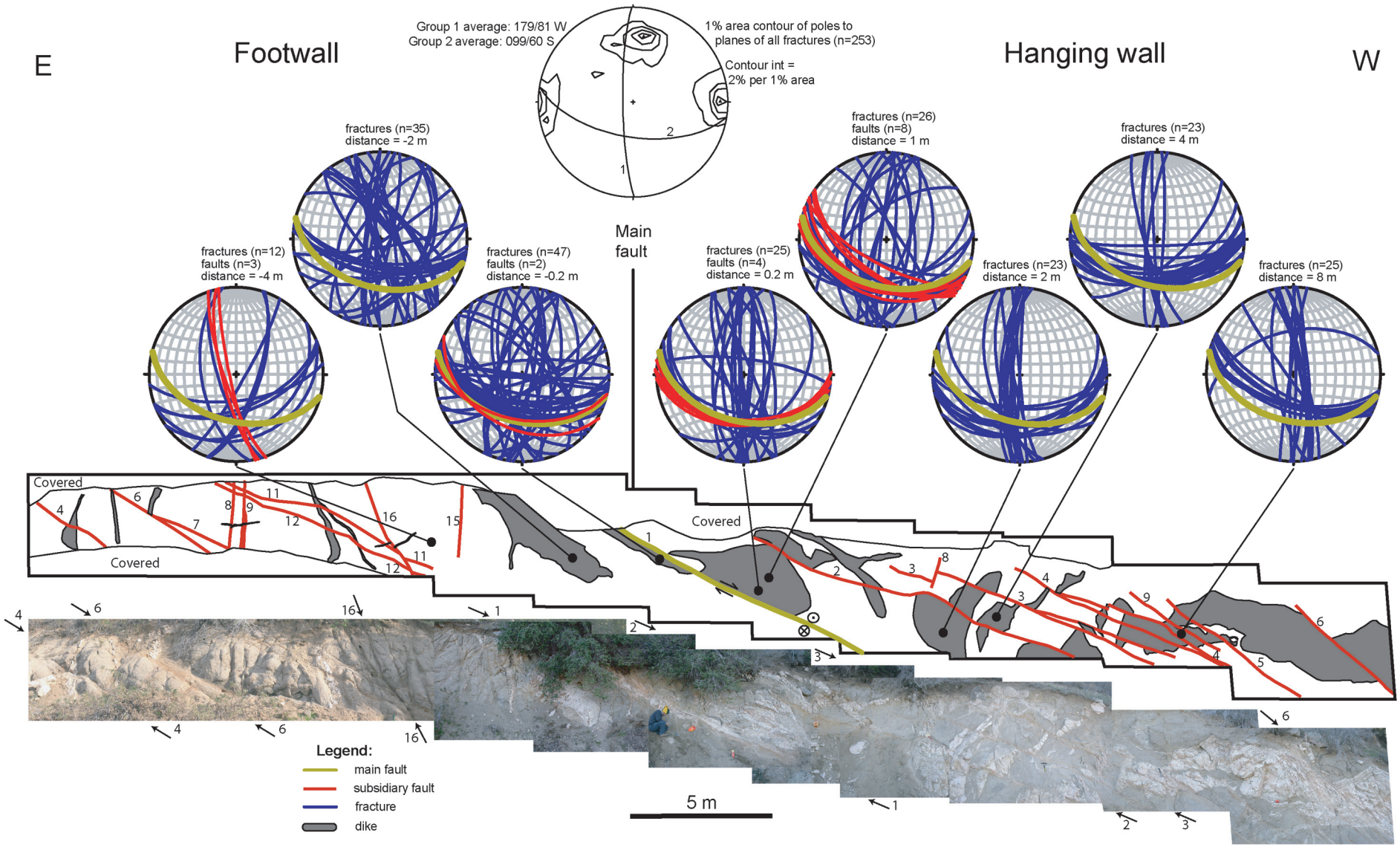

Figure 2. Photomosaic and simplified sketch of the Grass Valley fault zone with view to the south. Stereonets are lower hemisphere equal area projections. Each stereonet shows the main fault in yellow, number of planes, and distance perpendicular from the main fault core. The contoured stereonet shows poles to all fractures across the entire fault zone with best fit great circles. Note the preferred orientations of fractures, particularly in the 2, 4, and 8 m stereonets.

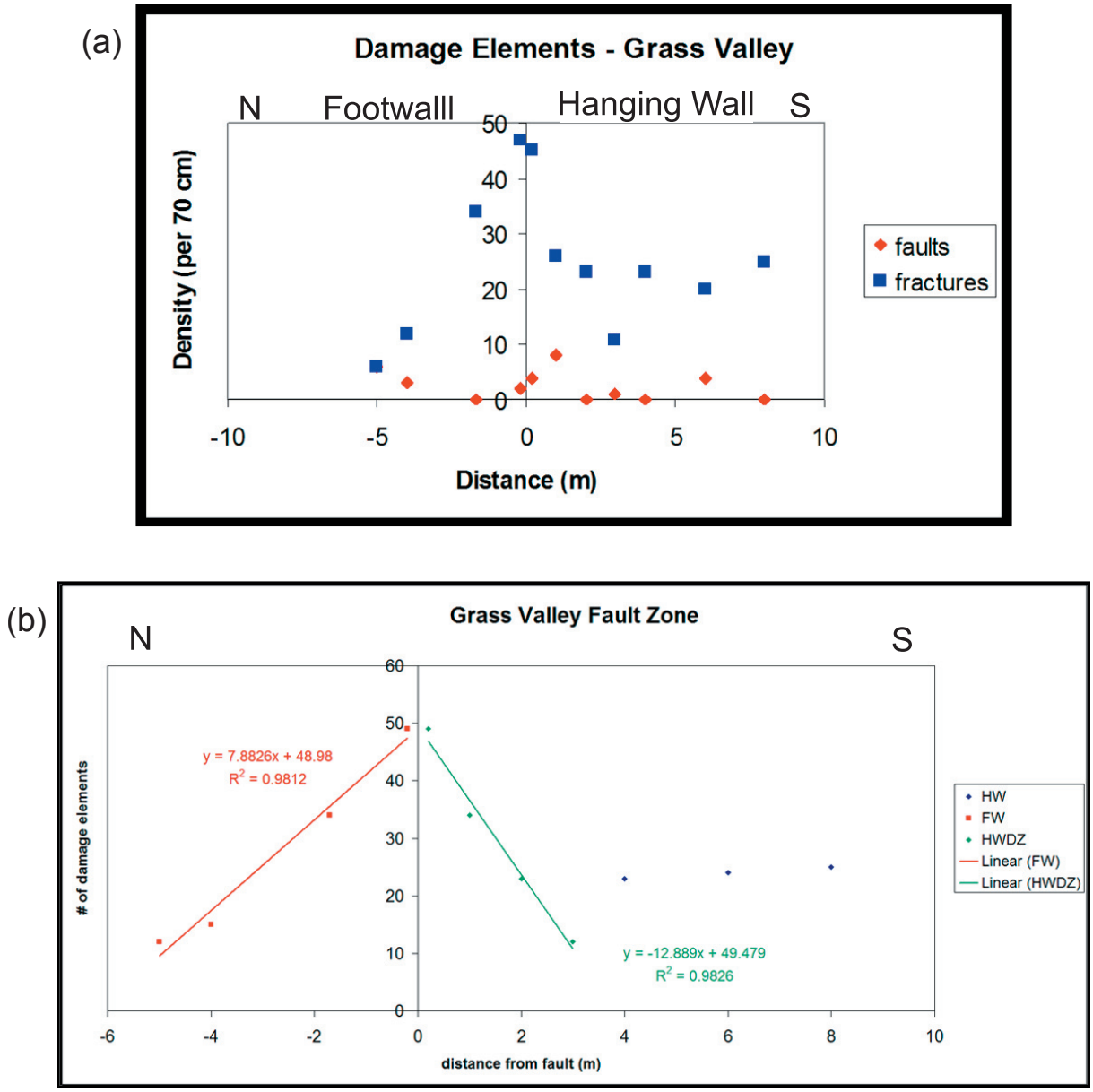

Figure 3. Transect data from the Grass Valley reverse right-lateral fault. Distances are perpendicular to the main fault. (a) Graph of subsidiary faults and fractures plotted separately. Main fault is at 0 m; hanging wall is positive distance and footwall is negative distance. The majority of damage elements are fractures. No veins were observed at this fault zone. (b) Plot of combined damage elements (subsidiary faults and fractures) per 70 cm scans across the fault zone. Note the linear decrease in density away from the main fault. Increase in damage element density from 4 to 8 m in the hanging wall is attributed to subsidiary faults. Thus, the green trendline represents the hanging wall damage zone. HW: hanging wall, FW: footwall, HWDZ: hanging wall damage zone.

and Sammis, 2005) which is defined as the displacement over which the frictional strength of a fault drops from a static value to a lower dynamic value (Dieterich, 1978a, b; Dieterich, 1979a, b), thus causing earthquake nucleation as a stick-slip friction instability (Dieterich, 1972, 1974; Rice, 1980). The thicker the co-seismic slip zone (i.e., involves much of the fault core), the larger Dc will be (Biegel and Sammis, 2005). Although there appears to be a general increase in fault core thickness with slip, there is not a significant correlation when analyzing 26 faults from the Silverwood Lake area, including the Grass

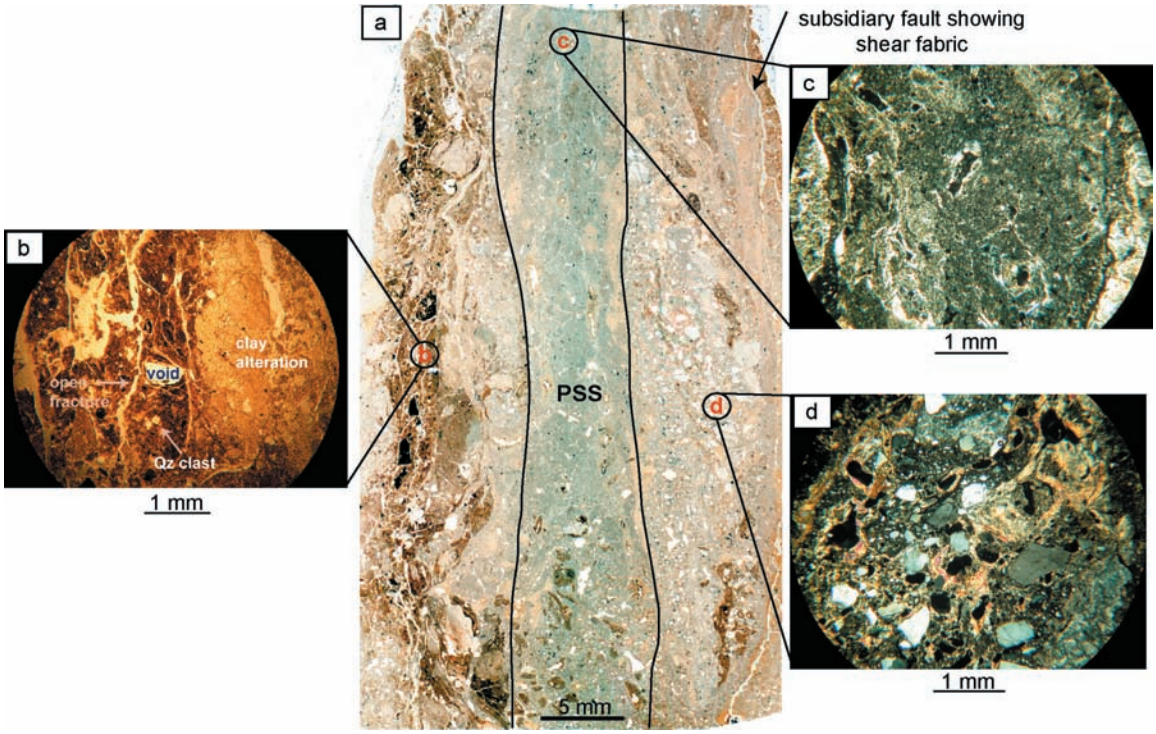

Figure 4. Microstructure of the Grass Valley fault. (a) Scan of thin section from fault core. PSS = primary slip surface. (b) Photomicrograph of fault core in PPL showing open fractures and alteration. (c) Photomicrograph in CPL of PSS. (d) Photomicrograph in CPL of brittle damage surrounding the PSS. CPL = cross polarized light; PPL = plane polarized light.

Valley fault. However, the damage zone does appear to thicken with increased slip.

The presence of expanding clays in the fault cores explains the typical increase in loss on ignition relative to the damage zone, due to the trapped fluids in the impermeable clay-rich gouge. Frictional heating during rupture may produce thermal pressurization of these trapped fluids causing fault weakening as proposed by several workers (Byerlee, 1990; Rice, 1992; Chester et al., 1993; Sibson, 2003). The enrichment of the fault core with smectite is consistent with previous work on the Punchbowl fault (Chester and Logan, 1986; Solum et al., 2003). The low coefficient of friction of smectite, particularly montmorillonite, may help to further weaken the fault.

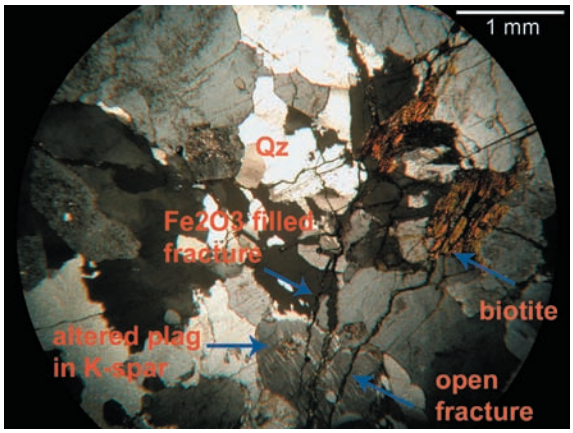

Figure 5. Photomicrograph in cross polarized light of the Grass Valley fault zone hanging wall 1 m from the fault core. Note the pronounced decrease in damage from Figure 4 (Jacobs, 2005).

References

Biegel, R.L. and C.G. Sammis, Relating fault mechanics to fault zone structure. *Advances in Geophysics*, 47, 2005.

Blythe, A.E., D.W. Burbank, K.A. Farley, and E.J. Fielding, Structural and topographic evolution of the central Transverse Ranges, California, from apatite fission-track (U-Th)/He and digital evolution model analyses. *Basin Research*, 12, 97-114, 2000.

Byerlee, J., Friction, overpressure, and fault normal compression. *Geophysical Research Letters*, 17, 2109-2112, 1990.

Chester, F.M., J.P. Evans, and R.L. Biegel, Internal structure and weakening mechanisms of the San Andreas fault. *Journal of Geophysical Research*, 98, 771-786, 1993.

Chester F.M. and J.M. Logan, Implications for mechanical properties of brittle faults from observations of the Punchbowl fault zone, California, USA. *Pure and Applied Geophysics*, 124, 79-106, 1986.

Dibblee, T.W., Jr., Late Quaternary uplift of the San Bernardino Mountains on the San Andreas and related faults, in San Andreas Fault in southern California; A guide to San Andreas fault from Mexico to Carrizo Plain, *California Division of Mines and Geology*, Spec. Rep. 118, edited by J.C. Crowell, 127-135, Sacramento, CA., 1975.

Dieterich, J.H., Time-dependent friction in rocks. *Journal of Geophysical Research*, 77, 3690-3697, 1972.

Dieterich, J.H., Earthquake mechanisms and modeling. Annual *Review of Earth Planetary Sciences*, 2, 275-301, 1974.

Dieterich, J.H., Preseismic fault slip and earthquake prediction. *Journal of Geophysical Research*, 83, 3940-3947, 1978a.

Dieterich, J.H., Time-dependent friction and the mechanics of stick-slip. *Pure Applied Geophysics*, 116, 790-806, 1978b.

Dieterich, J.H., Modeling of rock friction, 1, Experimental results and constituitive equations. *Journal of Geophysical Research*, 84, 2161-2168, 1979a.

Dieterich, J.H., Modeling of rock friction, 2, Simulation of pre-seismic slip. *Journal of Geophysical Research*, 84, 2169-2175, 1979b.

Evans, J.P. and F.M. Chester, Fluid-Rock interaction in faults of the San Andreas system: Inferences form San Gabriel fault rock geochemistry and microstructures. *Journal of Geophysical Research*, 100, B7, 13,007-13,020, 1995.

Heermance, R., Z.K. Shipton, and J.P. Evans, Fault structure control on fault slip and ground motion during the 1999 rupture of the Chelungpu fault, Taiwan. *The Seismological Society of America Bulletin*, 93, 1034-1050, 2003.

Jacobs, J.R., Examination of exhumed faults in the western San Bernardino Mountains, California: Implications for fault growth and earthquake rupture. M.S. Thesis, *Utah State University*, 2005.

Kanamori, H. and T.H. Heaton, Microscopic and macroscopic physics of earthquakes. *American Geophysical Union Monographs*, 120, 147-161, 2000.

Meisling, K.E. and R.J. Weldon, The Late-Cenozoic structure and Stratigraphy of the western San Bernardino Mountains, in Geologic excursions in the Transverse Ranges, Cooper, J.D. (editor), *Geological Society of America Annual Meeting Guidebook*, 75-81, California State University, Fullerton, 1982.

Meisling, K.E. and R.J. Weldon, Late Cenozoic tectonics of the northwestern San Bernardino Mountains, southern California. *Geological Society of America Bulletin*, 101, 106-128, 1989.

Rice, J.R., Elastic Wave Emission from Damage Processes. *Journal of Nondestructive Evaluation*, 1, 215-224, 1980.

Rice, J.R., Fault stress states, pore pressure distributions, and the weakness of the San Andreas fault. In: Evans, B. and T. F. Wong (editors), *Fault Mechanics and Transport Properties in Rocks*, 475-503, Academic, San Diego, Calif., 1992.

Sadler, P.M., Later Cenozoic stratigraphy and structure of the San Bernardino Mountains, in Geologic Excursions in the Transverse Ranges. In: Cooper, J.D. (editor), *Geological Society of America Annual Meeting Guidebook*, 55-106, Cal. St. Univ., Fullerton, 1982.

Spotila, J.A. and K. Sieh, Architecture of transpressional thrust faulting in the San Bernardino Mountains, southern California, from deformation of deeply weathered surfaces. *Tectonics*, 19, 589-615, 2000.

Sibson, R.H., Thickness of the seismic slip zone. *The Seismological Society of America Bulletin*, 93, 1169-1178, 2003.

Solum, J.G., B.A. van der Pluijm, and D.R. Peacor, Influence of phyllosilicate mineral assemblages, fabrics, and fluids on the behavior of the Punchbowl fault, southern California. *Journal of Geophysical Research*, 108, B5, 2233, doi: 10.1029/2002 JB001858, 2003.

Chapter 5: San Jacinto Fault

Site 1—Ramona Indian Reservation

Directions

The exposure is part of a road cut on the eastern boundary of the Ramona Indian Reservation. Access requires permission and coordination with the Tribal office at Anza (Phone: 951-763-0371/4105; address: P.O. Box 391372 Anza, CA 92539).

1. Exit I-15 in Temecula; go eastward on CA-79. After 18 miles CA-79 becomes CA-371, on which you need to drive 15 miles to get to Anza. Alternatively, you can get to Anza by driving from Palm Springs on CA-74 (24 miles from the junction with CA-111) and turn left into CA-371 (6 miles).
2. From here follow instructions using Figure 1. In Anza, turn north into Bautista Canyon Rd. and follow it until the junction with NF-6S18. To get to this junction, drive north 2.2 miles up Bautista Canyon Rd. to a "T" junction, turn

Figure 1. Location map of the road cut exposure (red circle) along the San Jacinto Fault. (Base map is from maps.google.com.)

left and continue west and then north with the road. Take the 2nd turn to the left toward the northwest and drive up to the junction.

3. Turn right from Bautista Canyon Rd. into NF-6S18. You will climb to the northeast with the forest service road until the reservation's gate. [You will need to get permission and coordinate your entrance to the reservation with the tribal office (see contact information above).] After passing the gate, continue with the road until you arrive to an elongated valley with Hog Lake on your left (dry most of the year).
4. From Hog Lake the road turns right (southeastward) and follows the fault; the fault scarp, as well as other geomorphic fault features, can be seen south of the road. Drive 2.2 miles. The road will bend sharply to the south and descend. Park your car above the bend in the road (about 70 m north of the fault scarp) and walk along and down the road.
5. After walking few tens of meters you will pass a locked car gate (the reservation's boundary). The exposure is about 5 m south of the gate on the road cut and consists of a meter wide gouge layer separating Quaternary sediments. It is located immediately below the fault scarp. Some cleaning may be needed in order to observe the delicate structural features.

   *Note: the last ½ mile or so of driving may require 4X4 vehicle; access to the exposure from the east is blocked.

   UTM (WGS 84): 3717206 N, 529900 E
   Elevation: 4560 feet

Geologic Setting

The exposure is located within the 20 km long Anza section of the San Jacinto fault (SJF) that is known as the Anza Seismicity Gap (Brune, 1968; Sanders and Kanamori, 1984). This section of the fault is well expressed by geomorphic features and the fault is relatively simple with only one major active strand, the Clark fault (Rockwell et al., 1990), that separates surficial tonalite and other leucocratic plutonic rocks on the northeast against gabbroic and more melanocratic rocks to the southwest (Sharp, 1967). These lithologies probably do not extend very deep below the surface, as the local velocity structure indicates faster basement velocities at seismogenic depths on the northeastern side of the fault (Scott et al., 1994). The total right-lateral displacement across all strands of the SJF southeast of Hemet is estimated to be 29 km (Sharp, 1967). The surface slip rate was estimated by trench studies in the Anza area, a few km southeast of the study area to be on the order of 12-18 mm/y (Rockwell et al.1990; Merifield et al., 1991).

More recently, in a new set of trenches across the SJF in Hog Lake, Rockwell et al. (2005) documented the occurrence of 15 surface ruptures during the past 3500 years, with the most recent event at approximately A.D. 1760. The last seven of these earthquakes produced an excess of 28 m of slip, indicating that these are large events. The study area is on the edge of the Ramona Indian Reservation, northeast of the Anza Valley. In the vicinity of the road cut exposure the surface expression of the fault indicates that the fault is linear and highly localized, with one narrow principal strand. The exposed gouge zone juxtaposes locally surficial middle Pleistocene alluvial deposits on the southwest against late Pleistocene alluvial deposits on the northeast.

Description

The meter-wide gouge zone includes a single Principal Slip Surface (PSS) and three distinct gouge layers. Figure 2 and the text following (a–d) describe the detailed structural analysis (Dor et al. 2005a) of the gouge exposure in the road cut and in a trench that was excavated on the side of the road 3 m below the gouge exposure (the trench is now covered).

(a) Panoramic view showing the upper and lower road cut exposures with the inferred location of the PSS (green) and the analyzed frames (black boxes) presented to the right. In the center of the panel the fault is covered with debris.

(b) A cross fault view of the gouge and adjacent wall rocks, with a division to 5 structural domains. The three gouge layers from southwest to northeast are: massive, course-grained, brittle and moderately

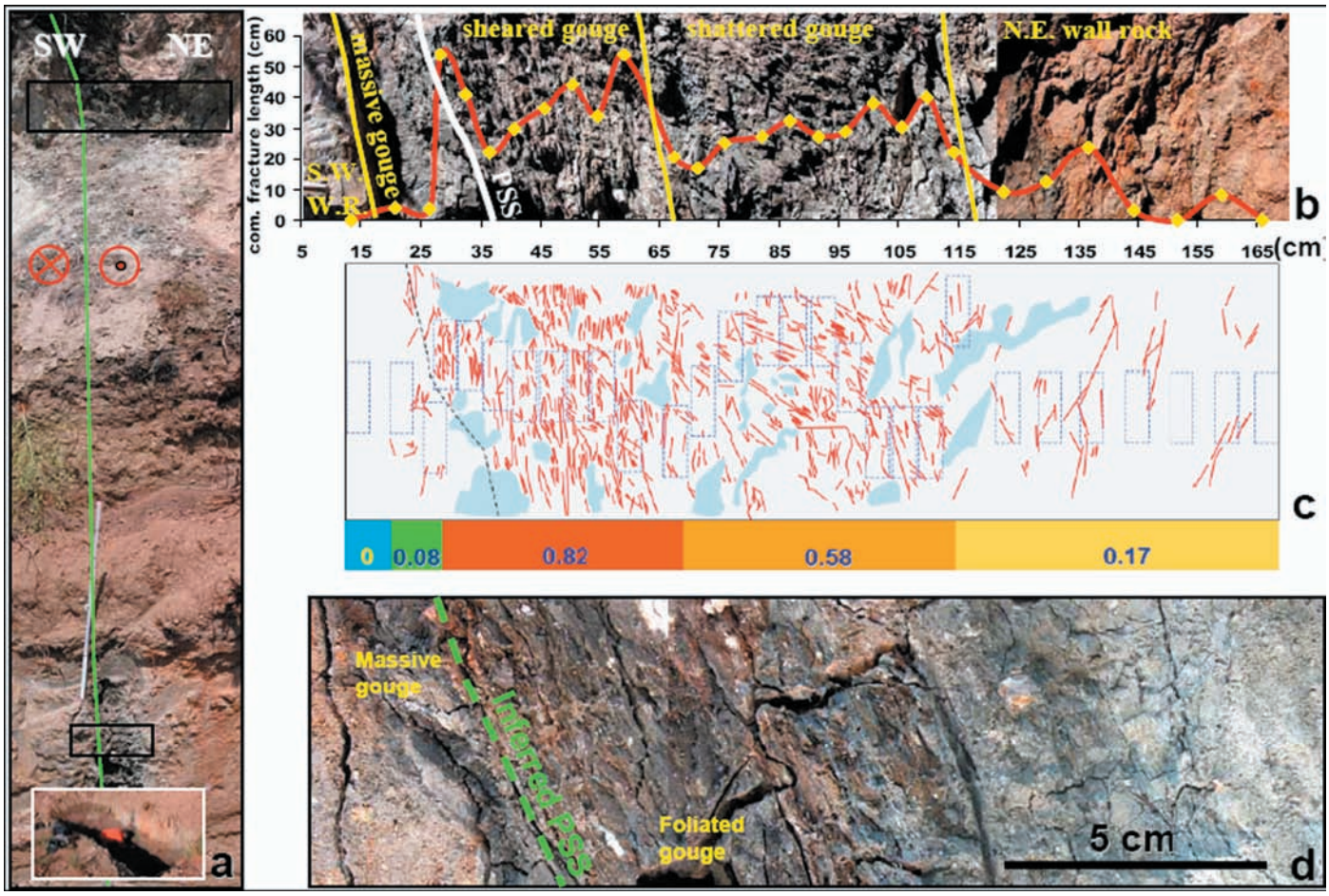

Figure 2. Upper and lower analyzed frames from the road cut exposure. See descriptions a, b, c, and d in the site description for details.

fractured layer southwest of the PSS; a gouge layer rich in clay, highly sheared and consists of numerous small slip surfaces northeast of the PSS. These slip surfaces are shiny, curved and contain low-angle slip striations.

Most of the surfaces are oriented parallel to the fault; the next gouge layer provides a gradual transition from the sheared gouge on the southwest to the northeastern wall rock. This clay-rich gouge layer has a mixed-mode fracture population dominated by mode I fractures (joints); it therefore appears to be mostly shattered, and we observed little evidence of shearing. The fracture orientation is more diverse with respect to the sheared gouge layer. The southwestern boundary of the gouge zone is sharp and smooth while the northeast boundary is more diffuse and gradual.

The red graph shows the trend of fracturing intensity across the fault. Each yellow dot indicates the cumulative fracture length (CFL) in cm measured in the rectangular frame right below it in the middle panel.

(c) A digitized fracture map of the upper panel. Light blue spots mark zones with insufficient visibility for detailed mapping. Dashed line marks the PSS. The rectangles are samples of CFL. The numbers on the lower horizontal bar give fracture density (FD) calculated for each of the structural domains from the upper panel by dividing the CFL from all the samples in the domain with the cumulative area of the used samples. A sharp contrast exists between the FD of the sheared and massive gouge. Note also that the FD of the NE wall rock is higher than the FD of the massive gouge. The fracture density

analysis highlights and confirms the apparent structural division and the sense of asymmetry in the qualitative damage pattern.

(d) The gouge 3 m below the upper road cut narrows down to 15 cm but maintains its structural division. Massive, gray, 1 cm wide gouge appears on the SW and highly foliated (sheared) gouge appears on the NE.

Similar gouge fabric with the same sense of asymmetry in damage distribution can be observed on the walls of the next creek to the southeast, in two additional exposures of the fault, 100 and 140 m away from the road.

Seismological Implications

The sense of damage asymmetry in the structure of the meter scale gouge is consistent with high resolution seismic imaging by Lewis et al. (2005), based on fault zone trapped waves recorded across the three branches of the SJF south of Anza. Their inversion results indicate the existence of ~100 m wide fault zone trapping structures at the different branches. These waveguides extend to a depth of about 3.5 km. The inversion results show further that the trapping structure at each of the branches is not centered on the surface expression of the fault, but is offset by 50-100 m to the northeast, implying more low velocity damaged fault zone material on the northeast side of the three branches of the fault.

The asymmetry in damage distribution across the gouge zone and in the structure of the waveguides reflects short and long term asymmetric damage accumulation (respectively) that can result from a preferred rupture direction on this fault section. The sense of asymmetry suggests that the preferred direction is from southeast to northwest as damage is expected to develop primarily in the tensional quadrant of the radiated seismic field.

The theory of rupture along a material interface predicts that ruptures on a fault that separates two different elastic solids will evolve with sufficient propagation distance to narrow wrinkle-like pulses, propagating preferentially in the direction of slip of the material with slower seismic velocities (Ben-Zion, 2001 and references therein; figure 3a). The theory farther predicts that more damage is expected

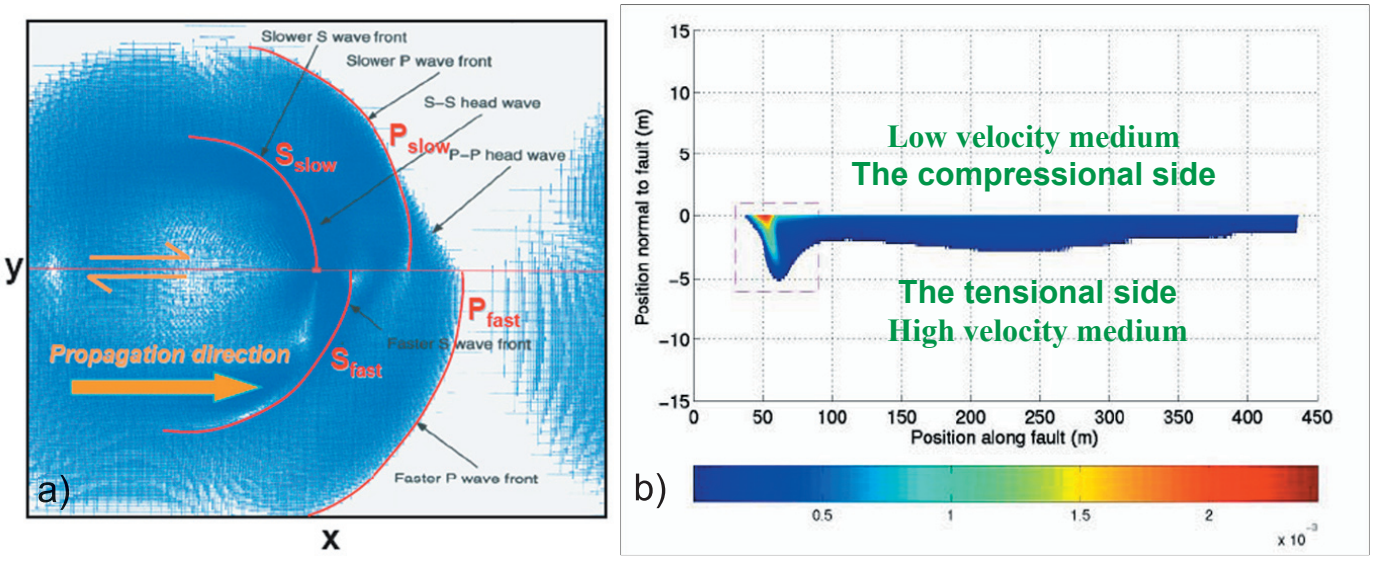

Figure 3. a) Particle velocities at a given time generated by a wrinkle-like rupture pulse (small red bar within the white box) propagating to the right along a right-lateral strike-slip fault between different elastic solids (thin red horizontal line). The slower velocity block is above the fault as manifested by the fronts of the radiated seismic waves (from Ben-Zion, 2001). b) Plastic strain (color scale) generated by a wrinkle-like rupture pulse propagating to the right on a fault separating a compliant material at $y > 0$ from stiffer material at $y < 0$. The stiffer side of the fault is in the tensional quadrant of the radiation pattern for the preferred propagation direction of the wrinkle-like pulse. [From Ben-Zion and Shi (2005).]

on the side of the fault with higher seismic velocity, which for the preferred propagation direction is the side that is persistently in the tensional quadrant of the radiated seismic field (Shi and Ben-Zion, 2005; figure 3b). Local tomography results of Scott et al. (1994) show that in seismogenic depth the more damaged northeast side of the fault has higher seismic velocities. This correlation is therefore compatible with propagation of wrinkle-like rupture pulses on the San Jacinto Fault in this area preferentially toward the northwest.

References

Ben-Zion, Y., Dynamic rupture in recent models of earthquake faults. *Journal of Mechanics and Physics in Solids*, 49, 2209-2244, 2001.

Ben-Zion, Y. and Z. Shi, Dynamic rupture on a material interface with spontaneous generation of plastic strain in the bulk. *Earth and Planetary Science Letters*, in press, 2005.

Brune, J.N., Seismic moment, seismicity, and rate of slip along major fault zones. *Journal of Geophysical Research*, 73, 777-784, 1968.

Dor, O., T.K. Rockwell, and Y. Ben-Zion, Geologic observations of damage asymmetry in the structure of the San Jacinto, San Andreas and Punchbowl faults in southern California: A possible indicator for preferred rupture propagation direction. Submitted to *Pure and Applied Geophysics*, 2005a.

Lewis, M., Z. Peng, Y. Ben-Zion, and F. Vernon, Shallow seismic trapping structure in the San Jacinto fault zone near Anza, California. *Geophysical Journal International*, in press, 2005.

Merifield, P.M., T.K. Rockwell, and C.C. Loughman, A slip rate based on trenching studies, San Jacinto fault zone near Anza, California. In: James McCalpin (editor), *Engineering Geology and Geotechnical Engineering*, no. 27, 28-1--28-21, 1991.

Rockwell, T.K., C. Loughman, and P. Merifield, Late Quaternary rate of slip along the San Jacinto fault zone, Southern California. *Journal of Geophysical Research*, 95, 6, 8593-8605, 1990.

Rockwell, T., G. Seitz, D. Ragona, T. Dawson, Geoff Faneros1, Danielle Verdugo, and O. Altangerel1, Investigation of segment controls on the rupture history of the southern San Jacinto fault. *Seismological Research Letters*, 76, 254, 2005.

Sanders, C.O. and H. Kanamori, A seismotectonic analysis of the Anza seismic gap, San Jacinto fault zone, southern California. *Journal of Geophysical Research*, 89, 5873-5890, 1984.

Scott, J.S., T.G. Masters, and F.L. Vernon, 3-D velocity structure of the San Jacinto fault zone near Anza, California – I. P waves. *Geophysical Journal International*, 119, 611-626, 1994.

Sharp, R., The San Jacinto fault in southern California. *Geological Society of America Bulletin*, 78, 705-730, 1967.

Shi, Z. and Y. Ben-Zion, A parameter-space study of conditions favoring unidirectional wrinkle-like rupture pulses on a material interface. M.S. Thesis, in prep., 2005.

All References

Abercrombie, R.E., Earthquake source scaling relationships from -1 to 5 ML using seismograms recorded at 2.5-km depth. *Journal of Geophysical Research*, 100, 24,015-24,036, 1995.

Agnew, D.C. and K.E. Sieh, A documentary study of the felt effects of the great California earthquake of 1857. *Bulletin of the Seismological Society of America*, 68, 1717-1729, 1978.

Anderson, J.L., R.H. Osborne, and D.F. Palmer, Petrogenesis of cataclastic rocks within the San Andreas fault zone of southern California, USA. *Tectonophysics*, 67, 221-249, 1980.

Anderson, J.L., R.H. Osborne, and D.F. Palmer, Cataclastic rocks of the San Gabriel fault—An expression of deformation at deeper crustal levels in the San Andreas fault. *Tectonophysics*, 98, 209-251, 1983.

Andrews, D. J. and Y. Ben-Zion, Wrinkle-like pulse on a fault between different materials. *Journal of Geophysical Research*, 102, 553– 5571, 1997.

Ashby, M.F. and R.A. Verrall, Deformation maps for olivine. *Eos, Transactions, American Geophysical Union*, 58, 512, 1977.

Barrows, A.G., J.E. Kahle, and D.J. Beeby, Earthquake hazard and tectonic history of the San Andreas Fault Zone, Los Angeles County, California. *Open file report 85-10 LA*, California Department of Conservation, Division of Mines and Geology, 1985.

Ben-Zion, Y., Dynamic rupture in recent models of earthquake faults. *Journal of the Mechanics and Physics of Solids*, 49, 2209-2244, 2001.

Ben-Zion, Y., and D.J. Andrews, Properties and implications of dynamic rupture along a material interface. *Bulletin of the Seismological Society of America*, 88, 1085–1094, 1998.

Ben-Zion, Y. and Z. Shi, Dynamic rupture on a material interface with spontaneous generation of plastic strain in the bulk. *Earth and Planetary Science Letters*, in press, 2005.

Biasi, G.P., R.J. Weldon II, T.E. Fumal, and G.G. Seitz, Paleoseismic event dating and the conditional probability of large earthquakes on the southern San Andreas fault, California. *Bulletin of the Seismological Society of America*, 92, 7, 2761-2781, 2002.

Biegel, R.L. and C.G. Sammis, Relating fault mechanics to fault zone structure. *Advances in Geophysics*, 47, 2005.

Blythe, A.E., D.W. Burbank, K.A. Farley, and E.J. Fielding, Structural and topographic evolution of the central Transverse Ranges, California, from apatite fission-track (U-Th)/He and digital evolution model analyses. *Basin Research*, 12, 97-114, 2000.

Borg, I.Y., M. Friedman, J.W. Handin, D.V. Higgs, Experimental deformation of Saint Peter sand: A study of cataclastic flow. In: D.T. Griggs (Editor), *Rock deformation—A symposium, Memoir Geological Society of America*, 133-191, Boulder, Colorado, 1960.

Borradaile, G.J., Particulate flow of rock and the formation of rock cleavage. *Tectonophysics*, 72, 305-321, 1981.

Bowen, W., Electronic Map Library. Department of Geography, California State University, Northridge, 2003. <http://130.166.124.2/library.html>

Brodsky, E.E. and H. Kanamori, Elastohydrodynamic lubrication of faults. *Journal of Geophysical Research*, 106, B8, 16,357-16,374, 2001.

Brune, J.N., Seismic moment, seismicity, and rate of slip along major fault zones. *Journal of Geophysical Research*, 73, 777-784, 1968.

Brune, J.N., Seismic source dynamics, radiation and stress. *Reviews of Geophysics*, 29, 688-699, 1991.

Brune, J.N., T.L. Henyey, and R.F. Roy, Heat flow, stress and rate of slip along the San Andreas fault, California. *Journal of Geophysical Research*, 74, 3821-3827, 1969.

Byerlee, J., Friction, overpressure, and fault normal compression. *Geophysical Research Letters*, 17, 2109-2112, 1990.

Chester, F.M., Field Guide to the Punchbowl Fault Zone at Devil's Punchbowl Los Angeles County Park, California. *Texas A&M University*, Texas, vol. 2.1, 1999.

Chester, F.M. and J.S. Chester, Ultracataclasite structure and friction processes of the Punchbowl fault, San Andreas system, California. *Tectonophysics*, 295, 199-221, 1998.

Chester F.M. and J.M. Logan, Implications for mechanical properties of brittle faults from observations of the Punchbowl fault zone, California, USA. *Pure and Applied Geophysics*, 124, 79-106, 1986.

Chester F.M. and J.M. Logan, Composite planar fabric of gouge from the Punchbowl fault, California. *Journal of Structural Geology*, 9, 621-634, 1987.

Chester, F.M., J.M. Chester, D.L. Kirschner, S.E. Schulz, and J.P. Evans, Structure of large-displacement, strike-slip fault zones in the brittle continental crust. In: G.D. Karner, J.D. Morris, N.W. Driscoll, and E.A. Silver (editors), *Rheology and deformation of the lithosphere at continental margins*, 223-260, Columbia University Press, New York, NY, 2004.

Chester, F.M., J.P. Evans, and R.L. Biegel, Internal structure and weakening mechanisms of the San Andreas fault. *Journal of Geophysical Research*, 98, B1, 771-786, 1993.

Christie, J.M., Mylonitic rocks of the Moine thrust-zone in the Assynt region, north-west Scotland, *Trans. Edinburgh Geological Society*, 18, 79-93, 1960.

Cox, B.F., R.E. Powell, M.E. Hinkle, and D.A. Lipton, Mineral resource potential map of the Pleasant View Roadless Area, Los Angeles county, California. *U.S. Geological survey Miscellaneous Field Studies Map*, MF-1649-A, scale 1:62,500, 1983.

Dibblee, T.W. Jr., Displacements on the San Andreas fault system in the San Gabriel, San Bernardino, and san Jacinto Mountains, southern California. In: *Proc. Conf. on Geologic Problems of San Andreas Fault System*. Stanford University Publications of Geological Science, 11, 260-276, 1968.

Dibblee, T.W., Jr., Late Quaternary uplift of the San Bernardino Mountains on the San Andreas and related faults, in San Andreas Fault in southern California; A guide to San Andreas fault from Mexico to Carrizo Plain, *California Division of Mines and Geology*, Spec. Rep., 118, edited by J.C. Crowell, 127-135, Sacramento, CA., 1975.

Dibblee, T.W. Jr., Geology of the Devil's Punchbowl, Los Angeles County Park, California. *Geological Society of America Centennial Field guide—Cordilleran Section*, Published by the Geological Society of America, Inc., California, vol. 1, 193-198, 1987.

Dickinson, W.R., Kinematics of transrotational tectonism in the California Transverse Ranges and its contribution to cumulative slip along the San Andreas transform fault system. *Geological Society of America*, 305, 46, 1996.

Dieterich, J.H., Time-dependent friction in rocks. *Journal of Geophysical Research*, 77, 3690-3697, 1972.

Dieterich, J.H., Earthquake mechanisms and modeling. *Annual Review of Earth Planetary Sciences*, 2, 275-301, 1974.

Dieterich, J.H., Preseismic fault slip and earthquake prediction. *Journal of Geophysical Research*, 83, 3940-3947, 1978a.

Dieterich, J.H., Time-dependent friction and the mechanics of stick-slip. *Pure Applied Geophysics*, 116, 790-806, 1978b.

Dieterich, J.H., Modeling of rock friction, 1, Experimental results and constituitive equations. *Journal of Geophysical Research*, 84, 2161-2168, 1979a.

Dieterich, J.H., Modeling of rock friction, 2, Simulation of pre-seismic slip. *Journal of Geophysical Research*, 84, 2169-2175, 1979b.

Dor, O., T.K. Rockwell, and Y. Ben-Zion, Geologic observations of damage asymmetry in the structure of the San Jacinto, San Andreas and Punchbowl faults in southern California: A possible indicator for preferred rupture propagation direction. Submitted to *Pure application of Geophysics*, 2005a.

Dor, O., Y. Ben-Zion, T.K. Rockwell, and J.N. Brune, Pulverized fault zone rocks along the Mojave section of the San Andreas fault. Submitted to *EPSL*, 2005b.

Edington, J.W., K.N. Melton, and C.P. Cutler, *Superplasticity. Progress in Materials Science*, 21, 63-170, 1976.

Ehlig, P.L., Pre-Cenozoic geology of the San Gabriel Mountains, southern California. *Geological Society of America*, 3, 116, 1971.

Ehlig, P.L., History, seismicity, and engineering geology of the San Gabriel fault, In: *Geology, Seismicity and Environmental Impact*, 247-251, Association of Engineering Geologists, Sudbury, Mass., 1973.

Ehlig, P.L., Origin and tectonic history of the basement terrain of the San Gabriel Mountains, central Transverse Ranges. In: W.G. Ernst (editor), *The Geotectonic Development of California*, Rubey vol. 1, pp. 584-600, Prentice-Hall, Englewood Cliffs, N.J., 1981.

Engelder, J.T., Cataclasisand the geration of fault gouge. *Geological Society of America Bulletin*, 85, 1515-1522, 1974.

Evans, J.P. and F.M. Chester. Fluid-rock interaction in faults of the San Andreas system: Inferences form San Gabriel fault rock geochemistry and microstructures. *Journal of Geophysical Research*, 100, B7, 13,007-13,020, 1995.

Fuis, G.S., R.W. Clayton, P.M. Davis, T. Ryberg, W.J. Lutter, D.A. Okaya, E. Hauksson, C. Prodehl., J.M., Murphy, M.L. Benthien, S.A. Baher, M.D. Kohler, K. Thygesen, G. Simila, and G.R. Keller, Fault systems of the 1971 San Fernando and 1994 Northridge earthquakes, southern California: Relocated aftershocks and seismic images from LARSE II. *Geology*, 31, 171-174, 2003.

Fumal, T.E., R.J. Weldon II, G.P. Biasi, T.E. Dawson, G.G. Seitz, W.T. Frost, and D.P. Schwartz. Evidence for large earthquakes on the San Andreas fault at the Wrightwood, California, Paleoseismic site: A.D. 500 to present. *Bulletin of the Seismological Society of America*, 92, no. 7, 2726-2760, 2002.

Garfunkel, Z., Model for the late Cenozoic tectonic history of the Mojave Desert, California, and for its relation to adjacent regions. *Geological Society of America Bulletin*, 86, 1931-1944, 1974.

Harris, R.A., and S.M. Day, Dynamic 3D simulations of earthquakes on en echelon faults, *Geophysical Research Letters*, 26, 2089-2092, 1999.

Hazlett, R., Field Guide To the Geology of the Eastern San Gabriel Mountains & San Andreas Fault in the Cajon Pass Area, Southern California. California, 1995.

Heaton, T.H., Evidence for and implication of self-healing pulses of slip in earthquake rupture. *Physics of The Earth and Planetary Interiors*, 64, 1-20, 1990.

Heermance, R., Z.K. Shipton, and J.P. Evans, Fault structure control on fault slip and ground motion during the 1999 rupture of the Chelungpu fault, Taiwan. *The Seismological Society of America Bulletin*, 93, 1034-1050, 2003.

Hickman, S.H., Stress in the lithosphere and the strength of active faults. U.S. Natl. Rep. Int. Union Geod. Geophys., 1987-1990, *Reviews of Geophysics*, 29, 759-775, 1991.

Jacobs, J.R., Examination of exhumed faults in the western San Bernardino Mountains, California: Implications for fault growth and earthquake rupture. M.S. Thesis, *Utah State University*, 2005.

Jennings, C.W., and R.G. Strand, Los Angeles sheet, Geological map of California, scale 1:250,000. *California Division of Mines and Geology*, Sacramento, 1969.

Jones, L.M., Focal mechanisms and the state of stress on the San Andreas fault in southern California. *Journal Geophysical Research*, 93, 11,883-11844, 1988.

Kamerling, M. J., and B. P. Luyendyk, Tectonic rotations of the Santa Monica Mountains region, western Transverse Ranges, California, suggested by paleo-magnetic vectors. *Geological Society of America Bulletin*, 90, 331-337, 1979.

Kamerling, M. J., and B. P. Luyendyk, Paleomagnetism and Neogene tectonics of the northern Channel Islands, California. *Journal of Geophysical Research*, 90, 12485-12502, 1985.

Kanamori, H. and T.H. Heaton, Microscopic and macroscopic physics of earthquakes. *American Geophysical Union Monographs*, 120, 147-161, 2000.

Lachenbruch, A.H. and J.H. Sass, Heat flow and energetics of the San Andreas fault zone. *Journal of Geophysical Research*, 85, 6185-6222, 1980.

Lewis, M., Z. Peng, Y. Ben-Zion, and F. Vernon, Shallow seismic trapping structure in the San Jacinto fault zone near Anza, California. *Geophysical Journal International*, in press, 2005.

Logan, J.M., Creep, stable sliding and premonitory slip. In: *Proceedings of Conference II; experimental studies of rock friction with application to earthquake prediction*, U.S. Geological Survey, Menlo Park, California, 1977.

Logan, J.M., Creep, stable sliding and premonitory slip. In: Rock friction and earthquake prediction, *Pure and Applied Geophysics*, 116, 773-789, 1978a.

Logan, J.M., Experimental studies of fold and thrust faults. *Abstracts with Programs–Geological Society of America*, 10, 21, 1978b.

Luyendyk, B. P., M. J. Kamerling, and R. R. Terres, Geometric model for Neogene crustal rotations in southern California. *Geological Society of America Bulletin*, 91, 211-217, 1980.

Luyendyk, B. P., M. J. Kamerling, R. R. Terres, and J. S. Hornafius, Simple shear of southern California during Neogene time suggested by paleomagnetic declinations *Journal of Geophysical Research*, 90, 12454-12466, 1985.

Main, I., D. Irving, R. Musson, and A. Reading, Constraints on the frequency-magnitude relation and maximum magnitudes in the UK from observed seismicity and glacio-isostatic recovery rates. *Geophysical Journal International*, 137, 535-550, 1999.

Matti, J.C. and D.M. Morton, Paleogeographic evolution of the San Andreas fault in southern California: A reconstruction based on a new cross-fault correlation. In: Powell, R.E., Weldon II, R.J., Matti, J.C. (editors), The San Andreas Fault System: Displacement, Palinspastic Reconstruction, and Geologic Evolution. *The Geological Society of America Memoirs*, 178, 107-160, 1993.

McGarr, A. and J.B. Fletcher, Mapping apparent stress and energy radiation over fault zones of major earthquakes. *The Seismological Society of America Bulletin*, 92, 1633-1646, 2002.

Meisling, K.E. and R.J. Weldon, The Late-Cenozoic structure and Stratigraphy of the western San Bernardino Mountains, in Geologic excursions in the Transverse Ranges, Cooper, J.D. (editor), *Geological Society of America Annual Meeting Guidebook*, 75-81, California State University, Fullerton, 1982.

Meisling, K.E. and R.J. Weldon, Late Cenozoic tectonics of the northwestern San Bernardino Mountains, southern California. *Geological Society of America Bulletin*, 101, 106-128, 1989.

Melosh, H.J., Acoustic fluidization: A new geologic process? *Journal of Geophysical Research*, 84, 7513-7520, 1979.

Merifield, P.M., T.K. Rockwell, and C.C. Loughman, A slip rate based on trenching studies, San Jacinto fault zone near Anza, California. In: James McCalpin (editor), *Engineering Geology and Geotechnical Engineering*, no. 27, 28-1--28-21, 1991.

Morton, D.M. and A.K. Baird, The Paloma Valley ring-complex, southern California Batholith. *Geological Society of America*, 3, 167, 1971.

Noble, L.F., Geology of the Valyermo Quadrangle and vicinity. *USGS*, Map GQ-50, 1954.

Oakeshott, G.B., Geology of the epicentral area. *California Division of Mines and Geology Bulletin*, 196, 19-30, 1971.

Pachell, M. A., and Evans, J. P., Structural analysis of the Gemini strike-slip fault zone, Central Sierra Nevada, California. *Journal of Structural Geology*, 24, 1903-1924, 2002.

Powell, R.E., Balanced palinspastic reconstruction of pre-Late Cenozoic paleogeology, southern California: Geologic and kinematic constraints on evolution of the San Andreas fault system. In: R.E. Powell, R.J. Weldon, and J.C. Matti (editors), The San Andreas Fault System: Displacement, Palinspastic Reconstruction, and Geologic Evolution, *The Geological Society of America Memoirs*, 178, 1-107, 1993.

Powell, R.E. and R.J. Weldon, Evolution of the San Andreas Fault. *Annual Review of Earth Planetary Sciences*, 20, 431-468, 1992.

Reed, J.J., Mylonites, cataclasites, and associated rocks along the Alpine fault, South Island, New Zealand. New Zealand *Journal Geology and Geophysics*, 7, 645-684, 1964.

Rice, J.R., Elastic Wave Emission from Damage Processes. *Journal of Nondestructive Evaluation*, 1, 215-224, 1980.

Rice, J.R., Fault stress states, pore pressure distributions, and the weakness of the San Andreas fault. In: Evans, B. and T. F. Wong (editors), *Fault Mechanics and Transport Properties in Rocks*, 475-503, Academic, San Diego, Calif., 1992.

Rockwell, T.K., C. Loughman, and P. Merifield, Late Quaternary rate of slip along the San Jacinto fault zone, Southern California. *Journal of Geophysical Research*, 95, 6, 8593-8605, 1990.

Rockwell, T., G. Seitz, D. Ragona, T. Dawson, Geoff Faneros1, Danielle Verdugo, and O. Altangerel1, Investigation of segment controls on the rupture history of the southern San Jacinto fault. *Seismological Research Letters*, 76, 254, 2005.

Rubin, C.M., S. Thompson, K. Abdrakhmatov, R.J. Weldon, Thrust fault paleoseismology in an intercontinental tectonic setting, Kyrgyz Tien Shan, central Asia. *Geological Society of America 1999 Annual Meeting*, 31, 376, 1999.

Sadler, P.M., Later Cenozoic stratigraphy and structure of the San Bernardino Mountains, in Geologic Excursions in the Transverse Ranges. In: Cooper, J.D. (editor), *Geological Society of America Annual Meeting Guidebook*, 55-106, Cal. St. Univ., Fullerton, 1982.

Sammis, C.G., R.H. Osborne, J.L. Anderson, and M. Banerdt, Reading stress from cataclastic rocks. *Eos, Transactions, American Geophysical Union*, 61, 1118, 1980

Sanders, C.O. and H. Kanamori, A seismotectonic analysis of the Anza seismic gap, San Jacinto fault zone, southern California. *Journal of Geophysical Research*, 89, 5873-5890, 1984.

Scholz, C., P. Molnar, and T. Johnson, Detaile studies of frictional sliding of granite and implications for the earthquake mechanism. *Journal of Geophysical Research*, 77, 6392-6406, 1972.

Schulz, S.E., Geochemical, petrologic, and structural characterization at multiple scales of deformation associated with the Punchbowl fault, southern California. M.S Thesis, *Utah State University*, Utah, 1997.

Schulz S.E., and J.P. Evans, Spatial variability in microscopic deformation and composition of the Punchbowl fault, southern California: Implications for mechanisms, fluid-rock interaction, and fault morphology. *Tectononphysics*, 295, 223-244, 1998.

Schulz S.E., and J.P. Evans., Mesoscopic structure of the Punchbowl fault, southern California, and the geologic and geophysical structure of active strike slip faults. *Journal of Structural Geology*, 22, 913-930, 2000.

Scott, J.S., T.G. Masters, and F.L. Vernon, 3-D velocity structure of the San Jacinto fault zone near Anza, California – I. P waves. *Geophysical Journal International*, 119, 611-626, 1994.

Shapiro, N.M., M. Campillo, L. Stehly, and M.H. Ritzwoller, High resolution surface wave tomography from ambient seismic noise. *Science*, 307, 1615-1618, 2005.

Sharp, R., The San Jacinto fault in southern California. *Geological Society of America Bulletin*, 78, 705-730, 1967.

Shi, Z. and Y. Ben-Zion, A parameter-space study of conditions favoring unidirectional wrinkle-like rupture pulses on a material interface. M.S. Thesis, in prep., 2005.

Sibson, R.H., Interactions between temperature and fluid pressure during earthquake faulting, a mechanism for partial or total stress relief. *Nature*, 243, 66-68, 1973.

Sibson, R.H., Fault rocks and fault mechanisms. *Journal of the Geological Society of London*, 133, 191-213, 1977.

Sibson, R.H., Thickness of the seismic slip zone. *The Seismological Society of America Bulletin*, 93, 1169-1178, 2003.

Solum, J.G., B.A. van der Pluijm, D.R. Pecor, and L.N. Warr, Influence of phyllosilicate mineral assemblages, fabrics, and fluids on the behavior of the Punchbowl fault, southern California. *Journal of Geophysical Research*, 108, B5, 2233, doi: 10.1029/2002JB001858, 2003.

Spotila, J.A. and K. Sieh, Architecture of transpressional thrust faulting in the San Bernardino Mountains, southern California, from deformation of deeply weathered surfaces. *Tectonics*, 19, 589-615, 2000.

Stesky, R.M. and W.F. Brace, Estimation of frictional stress on the San Andreas Fault from laboratory measurements. Stanford University Publications, *Geological Sciences*, 13, 206-214, 1973.

Taplin, D.M.R., G.L. Dunlop, and T.G. Langdon, Flow and failure of superplastic materials. *Annual Review of Material Sciences*, 9, 151-189, 1979.

Weldon, R. J., San Andreas fault, Cajon Pass, southern California. *Geological Society of America Centennial Field Guide—Cordilleran Section*. Published by the Geological Society of America, Inc., California, vol. 1, 193-198, 1987.

Weldon, R.J. and K.E. Sieh, Holocene rate of slip and tentative recurrence interval for large earthquakes on the San Andreas Fault, Cajon Pass, Southern California. *Geological Society of America Bulletin*, 96, 793-812, 1985.

Weldon, R.J. II, K.E. Meisling, and J. Alexander, A speculative history of the San Andreas fault in the central Transverse Ranges, California. In: R.E. Powell, R.J. Weldon, II and J.C. Matti (editors), The San Andreas Fault System: Displacement, Palinspastic Reconstruction, and Geologic Evolution. *Geological Society of America Memoir*, 178, 161-198, 1993.

Weldon, R.J. II, T.E. Fumal, T.J. Powers, S.K. Pezzopane, K.M. Scharer, and J.C. Hamilton. Structure and earthquake offsets on the San Andreas fault at the Wrightwood, California, Paleoseismic site. *Bulletin of the Seismological Society of America*, 92, no. 7, 2704-2725, 2002.

Wilson, J., Microfracture fabric of the Punchbowl fault zone, San Andreas system, California, M.S. Thesis, *Texas A&M University*, in prep., 1998.

Wilson, J.E., J.S. Chester, and F.M. Chester, Microfracture analysis of fault growth and wear processes, Punchbowl Fault, San Andreas system, California. *Journal of Structural Geology*, 25, 1855-1873, 2003.

Zoback, M.D. and J.H. Healy, In situ stress measurements to 3.5 km depth in the Cajon Pass scientific borehole: Implications for the mechanics of crustal faulting. *Journal of Geophysical Research*, 97, 5039-5057, 1992.